

UNCLASSIFIED

AD NUMBER: AD0811579

LIMITATION CHANGES

TO:

Approved for public release; distribution is unlimited.

FROM:

Distribution authorized to U.S. Gov't. agencies and their contractors; Administrative/Operational Use; 12 Apr 1972. Other requests shall be referred to Air Force Aero Propulsion Lab., Wright-Patterson AFB, OH

AUTHORITY

AFAPL ltr 12 Apr 1972

THIS PAGE IS UNCLASSIFIED

Dynatech Corporation Report No. 692

AFAPL-TR-67-20



DEVELOPMENT OF A 50 KVA LABORATORY PROTOTYPE  
SUPERCONDUCTING AC GENERATOR

H. W. Mooncal  
C. J. Oberhauser  
H. A. Robinson  
J. M. Reynolds

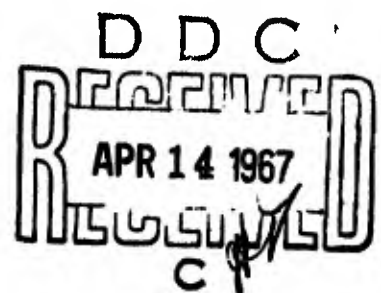
Dynatech Corporation

TECHNICAL REPORT AFAPL-TR-67-20

February 1967

"This document is subject to special export controls and each transmittal to foreign governments or foreign nationals may be made only with prior approval of the Aerospace Power Division (APD), Air Force Aero Propulsion Laboratory, Wright-Patterson Air Force Base, Ohio 45433."

Air Force Aero Propulsion Laboratory  
Research and Technology Division  
Air Force Systems Command  
Wright-Patterson Air Force Base, Ohio



DDC FILE COPY 811579

### SPECIAL NOTICES

"Foreign announcement and distribution of this report is not authorized.

The distribution of this report is limited because it contains technology identifiable with items on the strategic embargo lists excluded from export or re-export under U.S. Export Control Act of 1949 (63STAT. 7), as amended (50 U.S.C. App. 2020-2031), as implemented by AFR 400-10."

"Qualified requesters may obtain copies of this report from DDC."

ACCESSION FOR		
CPSTI	WHITE SECTION <input type="checkbox"/>	
DDC	LOFF SECTION <input checked="" type="checkbox"/>	
UNANNOUNCED	<i>for statement</i>	
JUSTIFICATION	<i>on Dec</i>	
CY	<i>Ln</i>	
DISTRIBUTION/AVAILABILITY CODES		
DIST.	AVAIL.	END/1/2 SPECIAL
<i>2</i>		

Dynatech Corporation Report No. 692

*See from 14/12*

DEVELOPMENT OF A 50 KVA LABORATORY PROTOTYPE  
SUPERCONDUCTING AC GENERATOR

H. W. Mooncai  
C. J. Oberhauser  
H. A. Robinson  
J. M. Reynolds

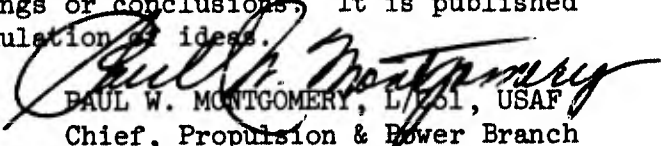
"This document is subject to special export controls and each transmittal to foreign governments or foreign nationals may be made only with prior approval of the Aerospace Power Division (APD), Air Force Aero Propulsion Laboratory, Wright-Patterson Air Force Base, Ohio 45433."

## FOREWORD

This is the final report of a program conducted by Dynatech Corporation, Cambridge, Massachusetts, under Contract No. AF 33(615)-2687. The contract was initiated under BPSN 5(63-8128-62405214) entitled, "Development of a 50 KVA Laboratory Prototype Superconducting AC Generator." Mr. Henry W. Mooncai is the principal investigator for Dynatech Corporation. The work is administered under the direction of the Aero Propulsion Laboratory (APIE-3), Research and Technology Division, Lt. A. L. Parrillo, Project Engineer. This report covers work conducted from March 15, 1965 through October 31, 1966.

This report was submitted by the authors February 1967.

Publication of this report does not constitute Air Force approval of the report's findings or conclusions. It is published only for the exchange and stimulation of ideas.

  
PAUL W. MONTGOMERY, L/Col, USAF  
Chief, Propulsion & Power Branch  
Aerospace Power Division

## ABSTRACT

The objective of this exploratory development program was the completion of the superconducting generator investigations initiated under previous contracts,\* and culminating with the fabrication and evaluation of a 50 kva laboratory model to verify the generator performance potential predicted by such investigations. The design and fabrication effort of the laboratory model superconducting generator was divided into three major areas. First, an electrical phase provided for the field and armature components from an electrical viewpoint. Second, a heat transfer phase provided for the removal of heat generated by the loss mechanisms of the generator. Third, a mechanical phase provided and maintained the environment package required by the superconductors. The completed generator was tested to demonstrate a capability of power generation. A one megawatt generator design is presented based on the experience gained on the design and test of the 50 kva generator.

---

\* Contract AF 33(547)-11062  
Contract AF 33(615)-1574

## TABLE OF CONTENTS

<u>Section</u>	<u>Page</u>
1 INTRODUCTION	1
2 SUMMARY AND CONCLUSIONS	2
3 DESIGN	5
3.1 Electrical Design	5
3.1.1 Field Design	6
3.1.1.1 Magnetic Circuit	6
3.1.1.2 Electric Circuit	9
3.1.1.3 Thermal Circuit	9
3.1.1.4 Winding Configuration and Materials	12
3.1.1.4.1 Choice of Nb <sub>3</sub> Sn Superconductor for the Field Winding	14
3.1.1.4.2 Superconducting Winding Construction	14
3.1.1.5 Preliminary Tests of the Superconducting Field Winding	17
3.1.1.5.1 Field Winding Test	17
3.1.1.5.2 Field Winding and Joint Test	17
3.1.1.5.3 The Field Winding and Joint Assembly Encapsulated in the Shaft	17
3.1.2 Armature Design	19
3.1.2.1 Choice of Superconductors for the Armature	20
3.1.2.2 Design and Armature Voltage Wave-shape	21
3.1.3 Liquid Metal Brushes	24
3.2 Thermal Design	26
3.2.1 Field and Armature Electrical Leads	27

# TABLE OF CONTENTS (continued)

<u>Section</u>	<u>Page</u>
3.2.2 Field and Armature Lead Heat Exchangers	33
3.2.3 Windage	33
3.2.4 Investigation of Candidate Armature Frame Materials	35
3.2.5 Investigation of Heat Transfer in the Generator Armature	37
3.2.5.1 Purpose	37
3.2.5.2 Summary	37
3.2.5.3 Nomenclature and Geometry	38
3.2.5.4 Heat Transfer Correlation Between Two Concentric Cylinders with the Inner Rotating	41
3.2.5.5 Heat Transfer Analysis of the Armature Windings	43
3.2.5.6 Heat Transfer Away from the Sides and Outer Diameter of the Armature	47
3.2.5.7 Numerical Evaluation	49
3.2.5.8 Extension of Analysis to Investigate the Effect of Potting Adhesive Between the Conductors and the Armature Frame	49
3.2.5.9 Armature Conductor Cooling Tests	56
3.2.5.10 Armature Cooling Test	56
3.2.6 Other Sources of Heat Transfer Into the Intermediate Stage Structure	59
3.2.6.1 Radiation From the Outer Casing	59
3.2.6.2 Convection From Outer Chamber	59
3.2.6.3 Conduction From Connecting Tubes and Convection From Shaft	61
3.2.6.4 Boiling Heat Transfer Between Liquid Nitrogen and Iron Return Path	61
3.2.7 Other Sources of Heat Transfer Into the 10° K Region	61
3.2.7.1 Radiation From Intermediate Temperature Structure	61
3.2.7.2 Convection From Intermediate Temperature Structure	61
3.2.7.3 Conduction Along Shaft and Connecting Tubes (Shaft Closures)	61



## TABLE OF CONTENTS (continued)

<u>Section</u>	<u>Page</u>
3.2.7.4 Conduction and Radiation From Iron Return Path Enclosure	61
3.3 Mechanical Design	61
3.3.1 Environmental Chamber	61
4 TESTS AND RESULTS	70
4.1 Experimental Test Setup	70
4.1.1 Instrumentation	70
4.2 Experimental Tests	73
4.2.1 Preliminary Cooldown Test	73
4.2.2 First Exploratory Test	76
4.2.3 Second Exploratory	79
5 1-MEGAWATT GENERATOR	84
 <u>Appendices</u>	
I FIELD WINDING TESTS	88
II ARMATURE WAVEFORM TESTS	92
LIST OF REFERENCES	102

## LIST OF ILLUSTRATIONS

<u>Figure</u>		<u>Page</u>
1	Cut-Away View of the Laboratory Model Superconducting Generator	3
2	Comparison of Field Diameters for a 50 kva Generator Utilizing Iron and Without Iron	8
3	Electrical Circuit of Field	10
4	Field Electric Circuit Current Flow Schematic	11
5	Thermal Path Schematic	13
6	Partial Cross-Section of Niobium-Tin Type Superconducting Ribbon	15
7	A Layer of Superconductor Ribbon is Shown Wound on the Field Winding Core During Fabrication	16
8	An interlayer material of mylar coated copper foil is shown applied over each layer of superconductor. This interlayer is bonded to the superconductor layer with an epoxy potting.	16
9	Superconducting Joint Resistance	18
10	The Armature Gramme Ring Winding During Fabrication	20
11	AC Loss Comparison of Various Nb <sub>3</sub> Sn Superconductors for 50 kva Generator Armature Application	22
12	Flux Distribution of a Typical Field Winding Acting Alone	23
13	Liquid Metal Brush	26
14	Heat Flow per Lead vs. Current	29
15	q/I per Lead vs. Normalized Current	30
16	Upper Stage Heat Flow vs. Current	31
17	Upper Stage Lead Electrothermal Characteristics	32
18	Field-Lead Heat Exchanger Temperature Differential vs. Power Input	34
19	Thermal Conductivity of Ceramics vs. Temperature	36
20	Schematic of Armature and Shaft Assembly	39

# LIST OF ILLUSTRATIONS (continued)

<u>Figure</u>		<u>Page</u>
21	Schematic Representation of Different Regions of Flow in an Annulus	41
22	Vortex Pattern in a Rotating Annulus	42
23	Geometry Used for Calculating Gap Film Coefficients	43
24	Armature Model	44
25	One Winding Model	44
26	Local Nusselt Number in a Bend	48
27	Helium Inlet Temperature vs. Thermal Conductivity of Armature Frame Material	50
28	Helium Temperature Rise vs. Helium Flow Rate	51
29	Helium Inlet Temperature vs. Total Heat Load	52
30	One Winding Model	53
31	Effect of Armature Parameters on Helium Inlet Temperature	55
32	Armature Conductor Cooling Test Apparatus	57
33	$\Delta T$ vs. Power Loss Density	58
34	Ducting Schematic	59
35	Armature Cooling Test Results	60
36	General Assembly of 50 kva Laboratory Model Superconducting Generator	62
37	Rotor Assembly	65
38	Drive End Shaft Assembly	68
39	Liquid Metal Brush End Shaft Assembly	69
40	Experimental Test Setup for Prototype Model Superconducting Generator	71
41	Electrical Interconnection and Instrumentation Schematic Diagram	72

# LIST OF ILLUSTRATIONS (continued)

<u>Figure</u>		<u>Page</u>
42	Thermal Instrumentation Schematic Diagram	74
43	Thermocouple Location Schematic Diagram	75
44	Vacuum vs. Temperature (during preliminary cooldown)	77
45	Sinusoidal Output Voltage Waveshapes	78
46	Phase Voltage vs. Field Excitation	80
47	Power Output vs. Field Excitation	81
48	Resistance of Superconductor Armature vs. Temperature	82
49	1-Megawatt Superconducting Generator	85
50	Test Apparatus	89
51	Test Instrumentation and Power Supply Block Diagram for Superconducting Field Winding	90
52	Armature Waveshape Test Apparatus	93
53	Brush and Slip Ring Assembly	93
54	Instrumentation and Power Supply Schematic Diagram of Armature Waveshape Test Apparatus	94
55	Field Strength vs. Exciting Current of Copper Field Magnet	95
56	Field Intensity Waveshape of Copper Field Magnet	96
57	One Turn (or a bundle of turns) with no Distribution Armature Waveshape	97
58	Twenty-two Turns Distributed Over a 60° Span Armature Waveshape	97
59	Fourty-four Turns Distributed Over a 120° Span Armature Waveshape	99
60	Two Twenty-two Turn Winding Distributed Over a 60° Span With No Chording (full pitch or spaced 180° apart)	100

LIST OF ILLUSTRATIONS (continued)

<u>Figure</u>		<u>Page</u>
61	Two Twenty-two Turn Winding Distributed Over a $60^\circ$ Span With $30^\circ$ Chording ( $5/6$ pitch or spaced $150^\circ$ apart)	100
62	Two Twenty-two Turn Winding Distributed Over a $60^\circ$ Span With $60^\circ$ Chording ( $2/3$ pitch or spaced $120^\circ$ apart)	101

## Section 1

### INTRODUCTION

Under sponsorship of the Air Force Aeropropulsion Laboratory\* of the Research and Technology Division of the Air Force Systems Command, Dynatech has been studying the application of superconductor technology to rotating electrical generators. Under the first year's program, design characteristics of a superconductor generator were defined, and supporting experiments were performed to demonstrate the level of the thermal and electrical losses which form the basis of the cooling system which must be provided to maintain the conductors at superconducting temperatures. A report describing the first year's work was issued (Ref. 1). The second year's program consisted primarily of applied research demonstrating electrical, thermal, and magnetic effects in a superconductor under conditions which occur in superconductor generators, and provided design data. A report describing the second year's work was issued (Ref. 2).

The objective of the current phase of the program was the completion of the superconducting generator investigations culminating with the fabrication and evaluation of a 50 kva laboratory model to verify the generator performance potential predicted by the previous investigations.

The design and fabrication of a practical superconducting generator focused on the various losses which occur in the system. This approach was necessary because the refrigerator applies a very large multiplier on energy lost at low temperatures (10°K) if this energy is to be rejected at ambient conditions (300°K). The design requirement was that these losses be kept at an absolute minimum. An effective means must be provided to maintain the environment necessary for superconductivity. This effort was divided into three major areas. First, an electrical phase which provided for the field and armature components from an electrical viewpoint. Second, a heat transfer phase which provided for the removal of heat generated by the loss mechanisms of the generator. Third, a mechanical design phase which provided and maintained the environment package required by the superconductors. Also, the main drive system for the generator was provided.

---

\*Air Force Project Engineer: Lt. A.L. Parrillo, Wright-Patterson Air Force Base, Ohio.

## Section 2

### SUMMARY AND CONCLUSIONS

The objective of this exploratory development program was the completion of the superconducting generator investigation initiated under Contract AF 33(657)-11062, culminating with the fabrication and evaluation of a 50 kva laboratory model to verify the predicted generator performance potential.

Parametric and design studies were conducted to refine the design of the generator. Supporting experiments on the structural, thermal, and electrical properties of materials were conducted to determine their feasibility in the cryogenic environment. Each component part was extensively investigated and further supported experimentally before fabricating, testing and installing in the generator. These included the field coil and shaft assembly, armature windings and support structure, magnetic path, electrical leads and joints, lead heat exchangers, coolant ducting, and the environmental chambers. Also, auxiliary systems were constructed or installed. These include: the drive vacuum, coolant, and instrumentation systems.

The completed generator is shown in Figure 1.

Exploratory tests at 6,000 rpm shaft speed were conducted with the prototype model superconducting generator and showed that:

1. The generator could withstand cooldown to its operating temperature level while maintaining structural integrity.
2. The pressure in the vacuum spaces could be maintained low enough to provide effective insulation against heat input from the ambient environment during operation.
3. The rotating superconducting field coil could maintain its superconductivity during rotation and against the armature reaction when the generator is loaded.
4. The thermal circuit of the shaft was effective in isolating the field from the external thermal environment.
5. Generation of power in a superconducting armature is possible. A power output of 6.1 kilowatts was generated during the low-speed test.
6. The armature exhibited apparent quenching without noticeable adverse effects.
7. The phase voltages and power as a function of field excitation behave in the same manner as a conventional generator.

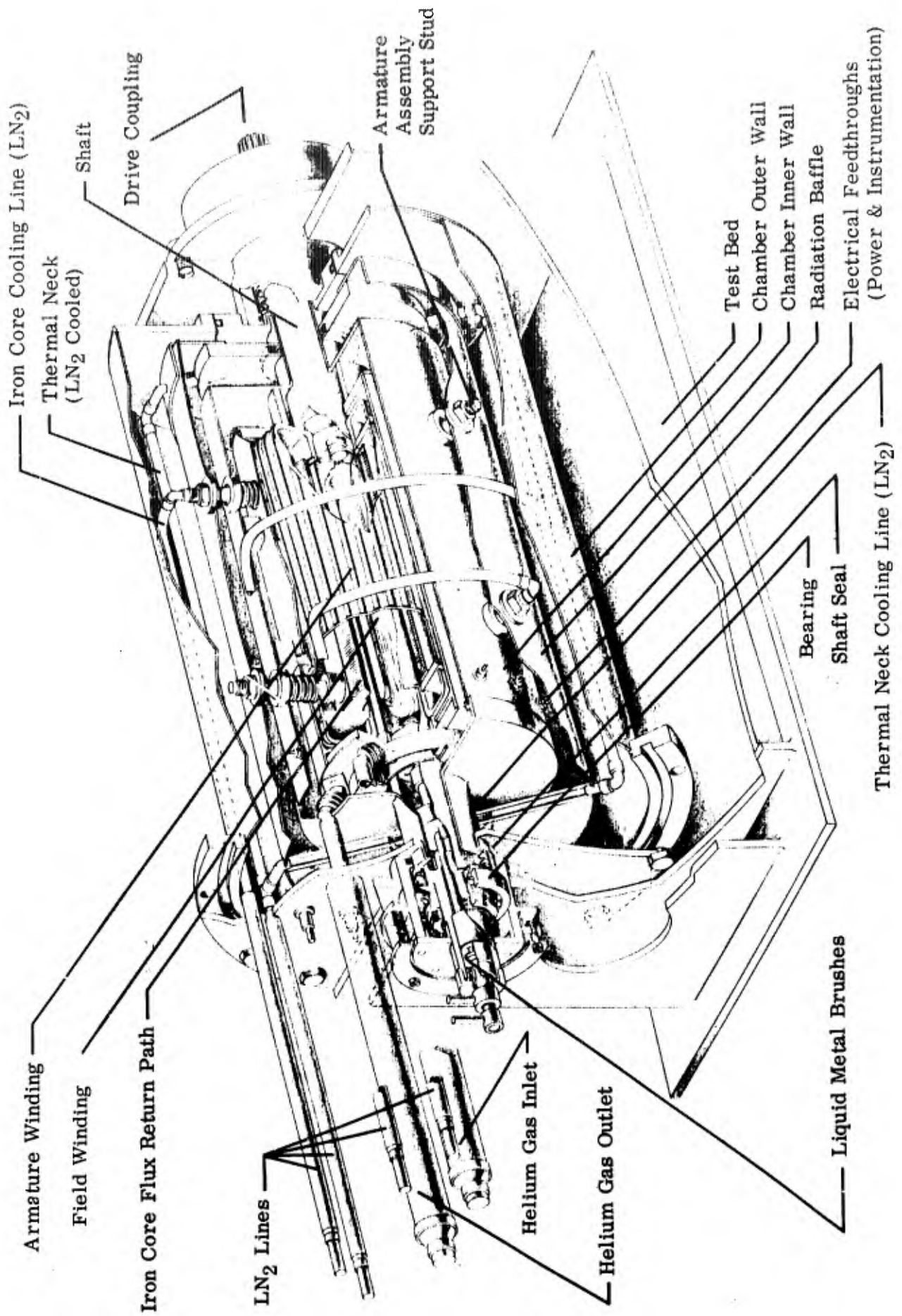


Figure 1. Cutaway View of the Laboratory Model Superconducting Generator



## Section 3

### DESIGN

The objective of the design phase was to design a 50 kva laboratory model generator which would verify the performance potential predicted by previous investigations (Refs. 1 and 2). This machine was not intended to be a minimum weight and volume package. In essence, this generator was to:

1. Demonstrate that 50 kva can be generated in an entirely superconducting generator.
2. Demonstrate that effective cooling can be attained with gaseous helium at 10°K as in the original Dynatech generator design (Ref. 1).
3. Demonstrate that non-catastrophic failures of the machine will occur when portions of a functioning winding go normal.

Since this machine was to be a "proof of principle" device, the design was based on achieving maximum simplicity and reliability consistent with the requirement that the general configuration be a prototype of the 1 MW operational machine. For this reason, all materials and components were standard items which could be purchased on an off-the-shelf basis.

The design effort was divided into three major areas:

1. An electrical phase in which the field and armature configurations were determined.
2. A heat transfer phase which provided for the efficient removal of heat generated in and heat conduction into the generator.
3. A mechanical design phase which provided the structural package required by the generator.

#### 3.1 Electrical Design

The basic electrical components of the laboratory model superconducting ac generator consist of a field winding and an armature winding plus auxiliary parts. The required rotating magnetic field is produced by physically rotating the field winding structure. This rotating magnetic field induces an alternating voltage in the stationary three-phase windings of the armature at the frequency of rotation.

The electrical characteristics of this generator are shown in Table I.

The design of the field and armature are the most sensitive portions of the program. The ultimate details of the machine construction are so intimately connected to the field and armature configuration that it is really not proper to divorce the electrical design phase from the overall design problem. Consequently, we have included the machine conceptual and parametric design under the heading of "electrical design."

The design of the machine is completely dominated by the necessity of reducing losses in the active region to a minimum. This requirement stems from the fact that the heat rejection system (refrigerator and radiator) are the heaviest components in the generator system. Moreover, 400 watts of power are required by the refrigerator to reject 1 watt from 10°K to ambient conditions at 300°K. Therefore, both system weight and efficiency are strong functions of the level of losses incurred in the active (10°K) region of the machine.

Table I

Power rating (kva)	50
Voltage line to line (rms volts)	1000
Line current (amperes)	29
Phases	3
Connection of armature phases	Wye
Frequency (hertz)	400
Superconductor operating temperature range	10-12°K

### 3.1.1 Field Design

The design of the field was based upon three considerations of equal importance. They were, first, the electric and magnetic circuits; second, the thermal aspects; and third, the mechanical integrity.

#### 3.1.1.1 Magnetic Circuit

The most important operation in the design of a practical superconducting generator system is the minimization of the low-temperature heat load. This is true because every watt of heat removed from the low-temperature regions requires many watts of power input to the refrigerator. At the present state of the art, the refrigerator and its space radiator are larger and heavier than the generator itself. Therefore, the system weight, volume, and overall efficiency are strongly dependent on the capacity of the refrigerator, which is directly dependent on the generator heat load. Obviously, then, design compromises must be strongly weighted towards minimizing this heat load.

In conventional generators, losses in the armature iron are at least 1% of the generator output. If such a machine were rewound (field and armature) with superconducting wire and run as a superconducting generator, the power input to the refrigerator to remove just the iron losses would be greater than the total power output of the generator. For this reason, early Dynatech systems studies concluded that iron must be completely excluded from the armature of any superconducting machine.

The deletion of the iron return path carries a penalty: the magnetomotive force of the field coil must be increased significantly to prevent a large decrease in flux density at the armature. This does not directly cause a high refrigeration penalty, since the power input and heat load attributable to a superconducting field coil is primarily

due to dissipation in the field lead-in wires. However, a higher magnetomotive force does require a larger field coil, resulting in a larger diameter shaft. Shaft windage power increases approximately as the 3.75 power of shaft diameter. In all Dynatech generator designs to date, windage power has constituted a significant portion of the total refrigerator heat load. Therefore, although it is not desirable to have iron in the armature of a superconducting generator, the elimination of the iron results in an increase in the windage.

It is characteristic of heat pumps (refrigerators) that their required power input per unit of refrigeration decreases as the difference between the heat removal temperature and the heat rejection temperature decreases. With a fixed rejection temperature then, required power input to the refrigerator will decrease if the heat removal temperature can be raised.

In a heat pump operating on an ideal Carnot cycle:

$$\frac{\text{refrigerator power input}}{\text{refrigeration produced}} = \frac{T_{\text{rejection}} - T_{\text{removal}}}{T_{\text{removal}}}$$

This is the inverse of the coefficient of performance (COP). In a heat pump operating between 10°K and 300°K, 1/COP can be no smaller than 20. At a heat removal temperature of 80°K and the same rejection temperature, 1/COP can be no smaller than 2.75. In practice, refrigerators operate at much higher inverse COP's. This factor is often called out as "percentage of ideal Carnot cycle operation." The actual 1/COP is then found by dividing (1/COP) by this percentage. Typically the percentage decreases as (T<sub>rejection</sub> - T<sub>removal</sub>) increases, due to component inefficiencies, departure from the idealized cycle, and heat leaks.

From a practical viewpoint, the characteristics mean that an iron core operated at 80°K will result in less weight and power than one which is operated at 10°K. This concept was investigated in detail and found to be not only feasible but also advantageous for two reasons:

1. The use of the iron return path allowed a reduction in the required coil size (and shaft diameter), reducing the total heat load at 10°K; and
2. The iron heat load would be taken out at 80°K, where the refrigerator had excess cooling capacity, so no additional upper-stage refrigeration penalty was incurred.

Figure 2 shows required field diameter versus desired armature flux density for fields with and without iron return paths. For an armature flux density of 10 kilogauss, the field with an iron return path must be 2.0 inches diameter. Without iron, the field must be 3.0 inches in diameter. Including the thickness of the shaft required to support these field coils results in windage diameters of 2.14 inches and 3.20 inches, respectively. Although the larger coil can have a shorter windage length for the same output voltage (due to higher rotational velocity), the windage goes approximately as the 3.75 power of shaft diameter. Obviously, the larger shaft has much higher windage losses.

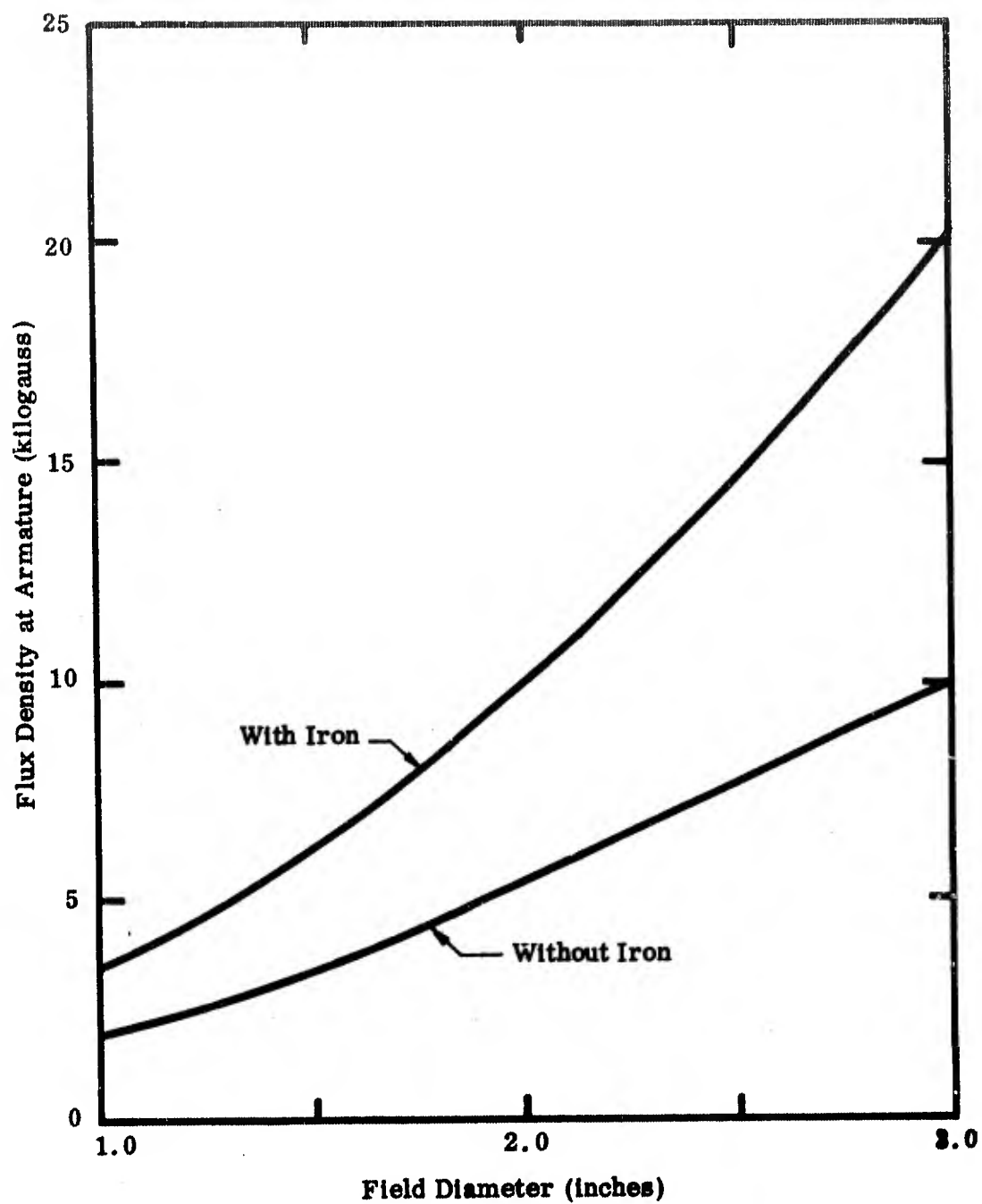


**Fig. 2. Comparison of Field Diameters for a 50 KVA Generator Utilizing Iron and Without Iron**

Let us now examine this generator with iron return path in comparison to the original system design (Ref. 1) to determine what the differences are. Windage in the original design was calculated to be 58 Btu/hr. Detailed calculations during the course of this contract have revealed that the original coil design is not feasible with the superconducting wires currently available. A practical coil for this original design would have to be twice as long and perhaps slightly larger in diameter at the present state of the art. Therefore, the windage would be at least twice as great as the given windage (58 Btu/hr).

By comparison, the windage for the coil with iron return path is 74 Btu/hr. This represents a nominal increase of 16 Btu/hr over the original design. However, the use of the iron return path allows the elimination of the stray flux shield originally used. Since this flux shield dissipated about 7 Btu/hr, the net increase is only 9 Btu/hr. The total lower-stage (10°K) losses in the original design were 203.3 Btu/hr. The total weight of the refrigerator package, including space radiator and startup allowance was 460 lbs. Therefore, the additional weight due to the additional 9 Btu/hr heat load can be no more than  $9/203.3 (460) = 20.4$  lbs. This is conservative, since a significant fraction of the total refrigerator weight is connected with the upper-stage (80°K) refrigeration. The only additional weight penalty is that of the iron core itself and the enclosure required to isolate it from the 10°K region. From actual weight measurements on prototype generator components, this is 25 lbs. Therefore, the total system weight increase is about 45 lbs., which is much less than the additional refrigerator weight required to remove the windage of a presently feasible field coil operating without an iron return path.

#### 3.1.1.2 Electric Circuit

The electric circuit for the field winding is a simple series circuit with the field winding being energized through two terminals as shown in Figure 3. Liquid metal slip rings are used to provide an electrical connection between the rotating and the stationary portions of the field circuit (Section 3.1.3). As shown in Figure 4, the shaft is used as one lead while the other connection is provided by a central conductor which runs down the axis of the shaft to the field winding. The normal and superconducting leads are joined at a relatively massive copper junction which functions as a heat path through which the lead and junction losses are conducted to the surface of the shaft.

#### 3.1.1.3 Thermal Circuit

There are four sources of heat in the field system:

1. Conduction of heat down the shaft and the leads.
2. Heat generation in the leads and at the normal-to-superconducting joints.
3. Heat generation in the stainless steel shaft due to armature reaction.
4. Heat generation in the field winding due to quench and release of field-stored energy.

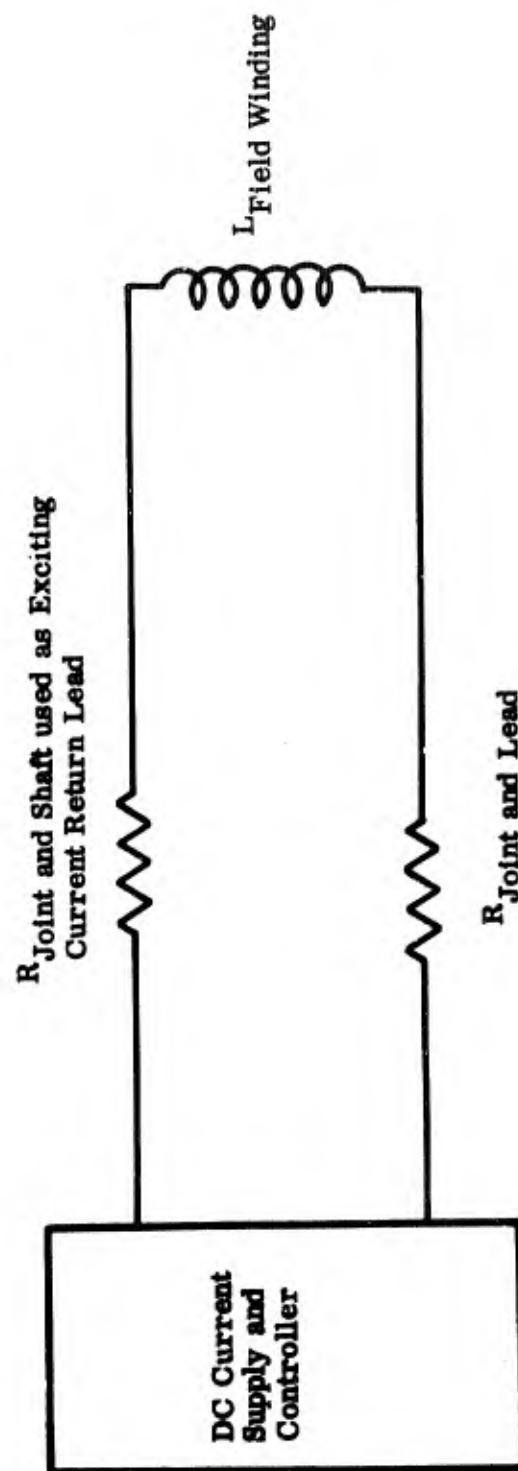


Fig. 3. Electrical Circuit of Field

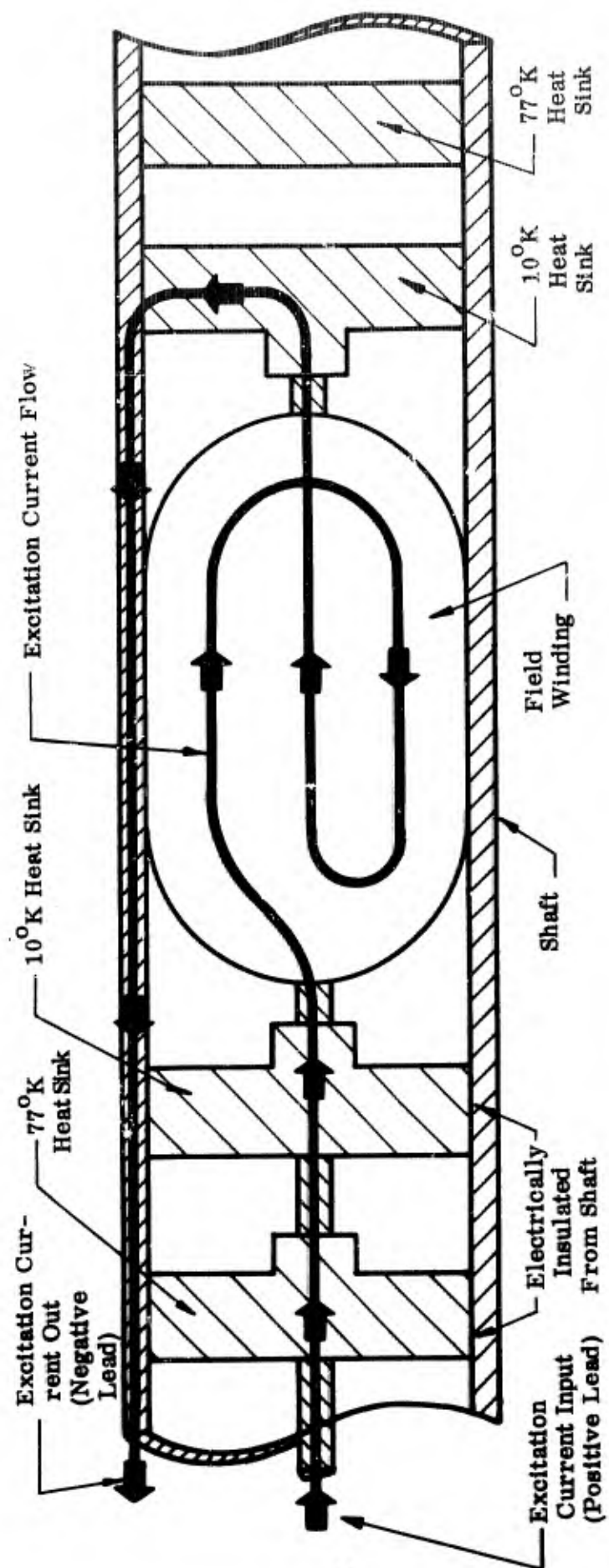


Fig. 4. Field Electric Circuit Current Flow Schematic

These thermal inputs are rejected through the shaft to the cold helium environment. Each point of heat generation is provided with a relatively large cross section of copper by which to reach the surface of the shaft. The high speed of rotation of the shaft assures that an adequate heat transfer coefficient exists at the shaft surface to remove all the heat with a small temperature difference between the shaft surface and the helium. The paths of heat flow are shown schematically in Figure 5.

Heat generated in the field winding due to the release of its stored energy in the event of a quench is carried out to the shaft via the iron core and the relatively high thermal conducting potting material.

#### 3.1.1.4 Winding Configuration and Materials

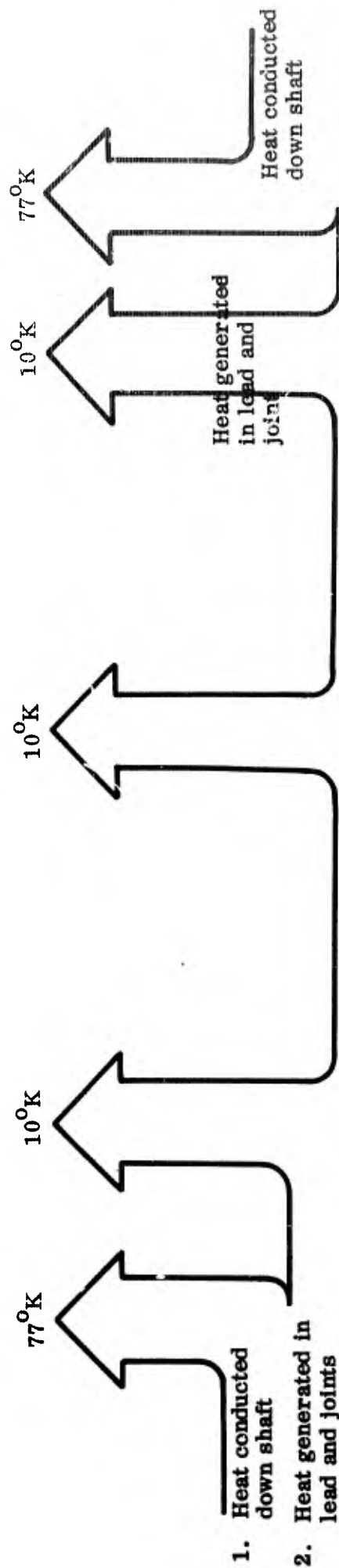
After adoption of the ferromagnetic circuit concept, consideration was focused first on the physical and electrical characteristics of the commercially available superconductors; secondly, on the protection of the field in the event of a transition to the normal state; and thirdly, on the structural features of the field system to withstand the stresses of rotation at 24,000 rpm.

System considerations dictate that the superconductor should operate at the highest possible temperature in order to reduce the refrigeration loss. This limits the choice to a niobium-tin type superconductor wire since this is the only "high" temperature superconductor commercially available in wire form. This material tends to be brittle; and so a wire with a high strength-supporting substrate is required to protect against the stresses experienced during rotation and/or a "quench".

A characteristic of most niobium-tin superconductors when wound into a coil is a certain degree of instability which causes the superconductor to revert to its normal state at a current lower than its maximum critical field. This instability is at a maximum in the low magnetic field region and decreases as the intensity of the magnetic field increases (Ref. 3). Since certain regions of the field coil will be subject to such a low magnetic field, some means must be provided to reduce the degree of instability. Metal plating the superconductor with a high electrical and thermal conductivity metal such as copper or silver can significantly improve the degree of stability (Ref. 4). Also, magnetic flux movements in the field coil create an adverse magnetic environment increasing the instability. Additional stability in the low field region can be obtained by the use of an insulated high-conductivity copper foil between layers of windings to electromagnetically damp out flux movements thus isolating local instabilities to within its own layer. During a transition to a normal state of the field, the interlayer of copper foil and plating on the superconductor provide protection of the field coil windings. Inductive protection is provided by the interlayer copper foils which act as shorted turns and thus limit the rate of change of flux during a transition to the normal state. The time constant of the closed copper turns are longer than the coil current decay time constant so that a larger fraction of the field energy is dissipated in the copper. The high thermal conductivity of copper readily carries the heat away from the coil to prevent any large temperature gradients within the coil resulting in hot spots. This also helps to reduce temperature gradients and shocks during thermal cycling.

The iron core should have a high saturation induction in order to prevent limitation of the magnetic circuit due to saturation. Also, a high magnetic permeability at the high inductions is essential. Iron-cobalt alloys meet these requirements and are available commercially. The alloy used for the field core is an alloy of iron and cobalt in equal proportions with about 2% vanadium.





Heat Generated due to

1. Current flow down shaft
2. Armature reaction on shaft
3. Windage
4. Field winding quench

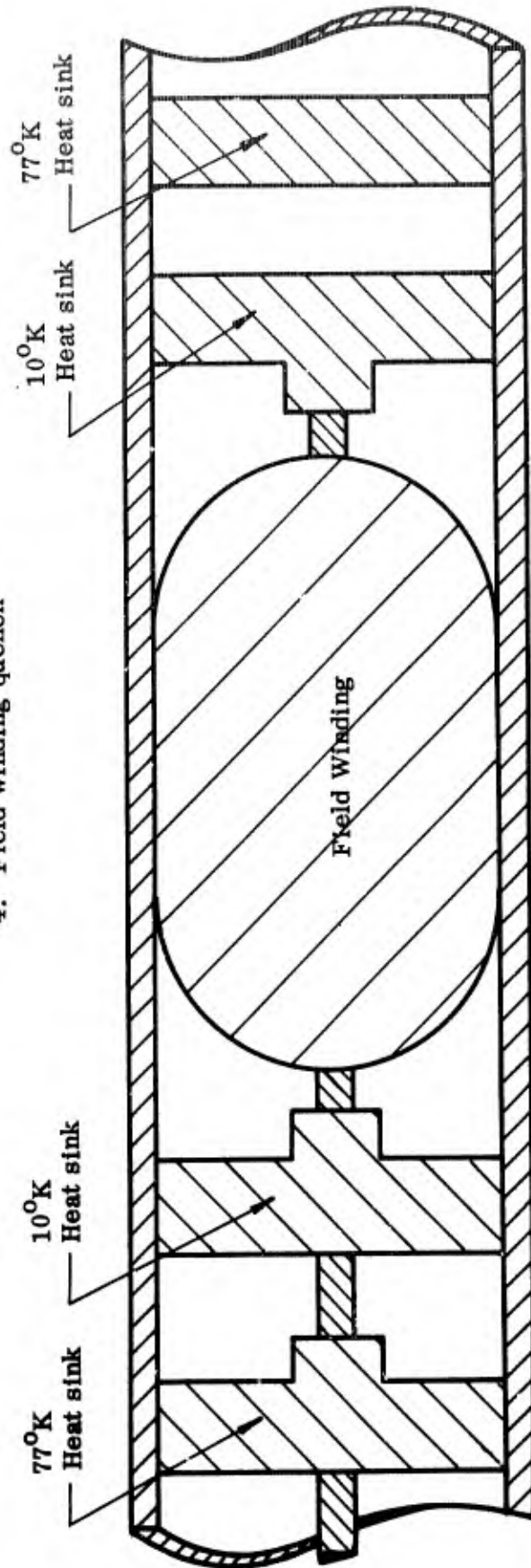


Fig. 5. Thermal Path Schematic

#### 3.1.1.4.1 Choice of Nb<sub>3</sub>Sn Superconductor for the Field Winding

Nb<sub>3</sub>Sn has been widely studied and is made by a variety of techniques and in several wire forms. Fabrication techniques of currently available Nb<sub>3</sub>Sn fall into two basic categories. The first category is a wire which must be wound into the desired form before reaction by heat-treating the wire at about 1000°C; and the second category is available in ribbon or tape form which requires no further heat treatment.

The wire form has the advantage of being ductile during winding and conforms more readily to the winding geometries of the generator field and armature. A disadvantage is the heat treatment required after winding into the desired form. This limits the structural material upon which the field and armature can be formed. A shell fabricated from ceramic materials such as alumina or beryllia can be used during the heat treatment and the iron core inserted afterwards. However, care must be exercised in this structural design since these ceramics tend to be brittle. Also, the protection afforded by copper cladding the wires and use of insulated copper interleaving between layers of turns cannot be used due to the high temperature requirement of the heat treatment. In addition, the wire becomes very brittle after heat treatment. Also, external protective measures must be adopted to protect against a quench of a coil wound from this type of Nb<sub>3</sub>Sn.

The ribbon or tape form has the inherent advantage of not requiring any further heat treatment and does not impose a high temperature requirement on the field structural material. The wider tape geometry is, however, a disadvantage when winding field coils in a helical form. Also, its large current capacity requires large current input requirements which is eventually reflected in the form of large slip rings and brushes (liquid metal brushes). The narrower ribbon geometry lends itself reasonably well to winding into a helical coil form as well as having a reasonable current requirement. Thus, this dc requirement was fulfilled by the pre-reacted type superconductor ribbon with a silver plating.

Centrifugal forces due to rotation of the coil system and Lorentz forces due to the excitation current with resulting field tend to push the windings out radially away from the core. The windings of the coil are restrained by encasing the coil within the shaft. The individual windings in each layer are restrained by potting each layer to the insulated copper foil with a filled epoxy as each layer is wound.

#### 3.1.1.4.2 Superconducting Winding Construction

The superconducting winding consists of superconductors in the form of ribbons wound around a ferromagnetic core. This core is composed of an alloy of iron, cobalt and vanadium which exhibits a high saturation induction in excess of 23 kilogauss. The superconductor is a commercially available niobium-tin type ribbon which does not require further heat treatment before or after winding. It is flexible and withstands a reasonable amount of handling. As shown in the cross-sectional view of the ribbon in Figure 6, the ribbon is composed of niobium-tin deposited on a stainless steel substrate and is finally electroplated with silver. This silver improves the electromagnetic characteristics and also simplifies the handling of the ribbon (Ref. 4).

Figure 7 shows the superconducting ribbon in the process of being wound on the core. Since this field winding is to rotate at 24,000 rpm, an epoxy potting was

used to pot each ribbon in place, in addition to the banding afforded by the shaft which supports the entire field winding. This epoxy potting is a specially formulated potting compound specifically used for superconducting magnets and is commercially available. It is a filled epoxy with compatible electrical, thermal and mechanical properties. Also, it is designed to withstand repeated thermal cycling between room temperature and 4.2°K.

An inherent characteristic of niobium-tin superconductors is a certain degree of instability which causes the superconductor to revert to its normal state at a current lower than its maximum critical current. This instability is at a maximum in the low magnetic field region and decreases as the magnetic field increases. The degree of stability can be significantly improved by the high electrical and thermal conductivity of the metal plating used on the ribbon. Additional stability is obtained by the use of an interlayer of insulated metal. This interlayer insulated metal is composed of a 1 mil thick sheet of annealed copper which is insulated on both sides with a bonded layer of 0.25 mil mylar sheet.

This mylar-copper-mylar interlayer material is wound between superconductor layers as shown in Figure 8 and held together with the potting compound to make it an integral part of the magnet mass. The purpose of this interlayer material is to provide electromagnetic damping of the flux movements in the superconductors. It is also a heat sink and thermal path for the heat generated during a quench of the field winding.

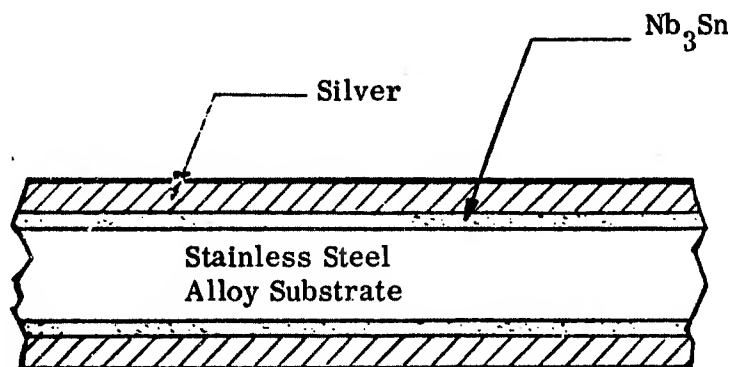
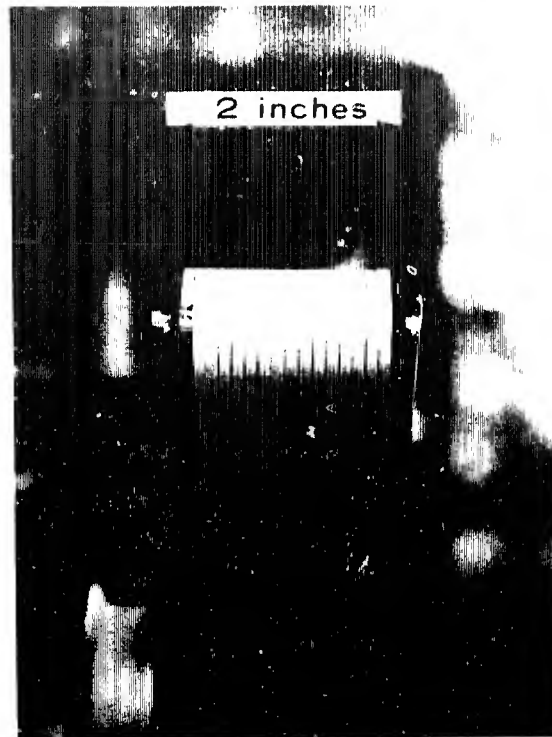
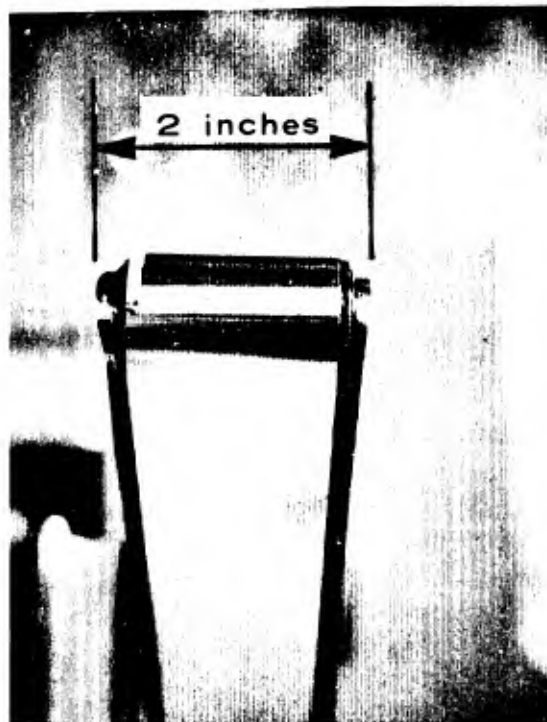


Fig. 6. Partial Cross-Section of Niobium-Tin Type Superconducting Ribbon



**Figure 7. A Layer of Superconductor Ribbon is Shown Wound On the Field Winding Core During Fabrication**



**Figure 8. An interlayer material of mylar coated copper foil is shown applied over each layer of superconductor. This interlayer is bonded to the superconductor layer with an epoxy potting.**

#### 3.1.1.5 Preliminary Tests of the Superconducting Field Winding

Three tests to determine the superconducting integrity of the field winding were conducted at various phases of its construction and assembly into the shaft.

1. After the field winding was wound but without the actual joints.
2. The field winding with the actual joints to determine the effect of joint resistance
3. The field winding and joints assembly inserted in shaft and encapsulated.

Details of these tests are presented in Appendix I.

##### 3.1.1.5.1 Field Winding Test

After the field winding was completed, the coil was initially tested in liquid helium to determine its superconducting integrity, critical current value at 4.2°K and its stability. This test showed that superconductivity was attained and that a critical current of 110 amperes was reached before quenching at an operating temperature of 4.2°K. This high value of critical current indicated a very good winding for the superconductor used. The stability tests were conducted at a maintained value of 90 amperes for various time periods of five minutes with no signs of instability or quenching either during the energizing period, the maintained period, or the de-energizing period. The energizing current was increased and decreased at a steady rate of about 100 amperes per minute. Observation of the superconducting field winding after this test showed that it withstood the thermal cycling without any visible physical changes. Details of this and the following tests are shown in Appendix I.

##### 3.1.1.5.2 Field Winding and Joint Test

After the field superconductor leads were joined to the copper slugs which also serve as heat sinks for the normal leads, a test was performed to determine the electrical resistance values of these joints and to recheck the superconducting integrity of the field winding.

Figure 9 shows the joint resistances as the slopes of the given curves. Both joints are very good with resistance values less than one-third of a micro-ohm. The positive joint has a slightly higher resistance than the ground-return joint. At the operating current value, these joints are 0.30 micro-ohms for the positive joint and 0.22 micro-ohms for the negative joint. The total expected heat dissipation from both joints at the operating current level is 0.64 milliwatts which is entirely negligible. No attempts to quench the field winding were made; however, current values of up to 90 amperes were maintained during this test.

##### 3.1.1.5.3 The Field Winding and Joint Assembly Encapsulated in the Shaft

After the field winding and joint assembly were inserted into the shaft and encapsulated, a test was performed to verify the integrity of the field assembly. This

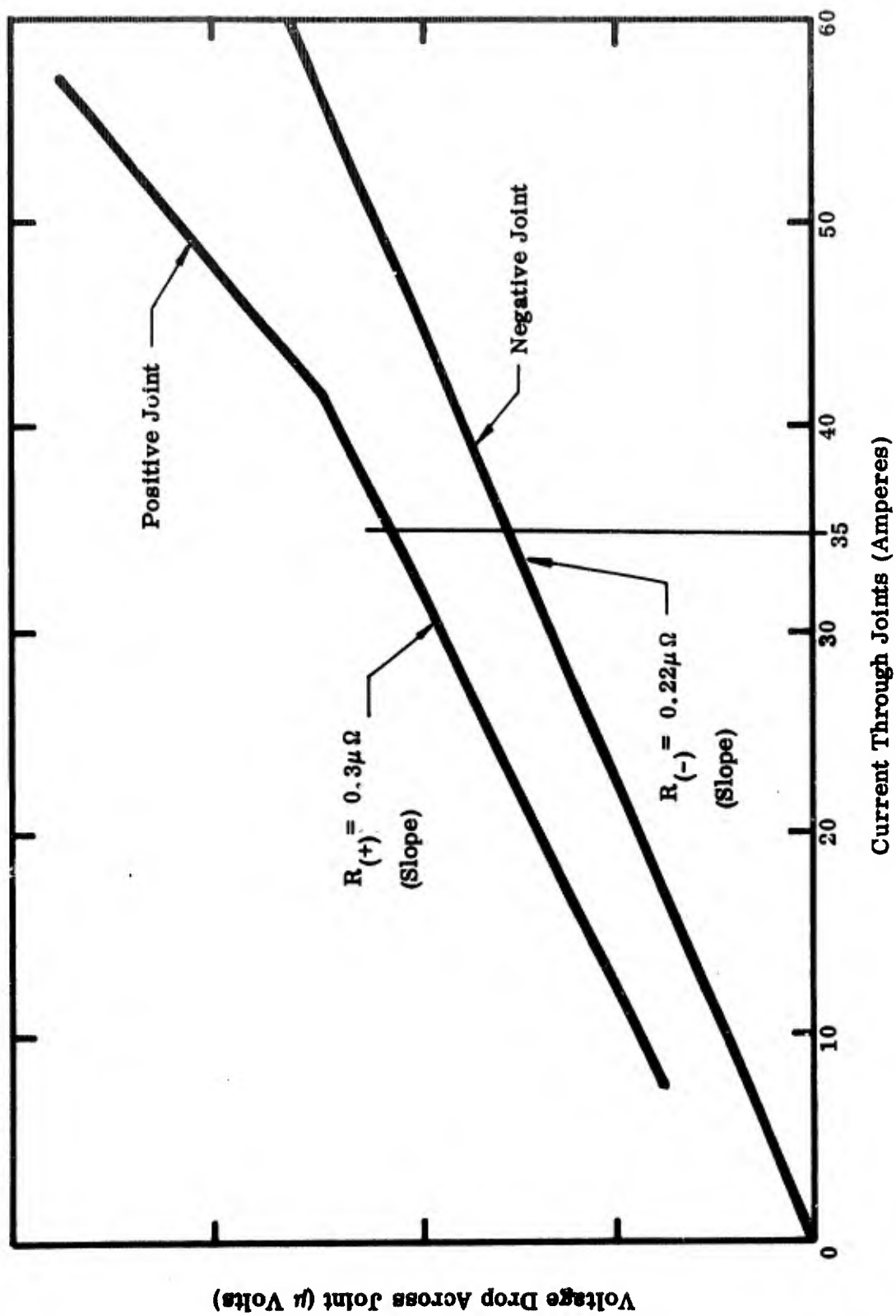


Fig. 9. Superconducting Joint Resistance

test showed that the integrity of the superconducting field was maintained. Again, no attempts were made to quench the field winding. Values of twice the operating current were consistently attained and maintained for periods of at least five minutes before reducing the current to zero and recycling many times to demonstrate the controllability and stability of the field winding.

### 3.1.2 Armature Design

The basic methods by which an ac voltage is generated in a superconducting generator is the same as in a conventional synchronous generator; i.e., in accordance with Faraday's Law, a voltage is induced in the armature conductors when the magnetic flux produced by the generator field winding is rotated. The voltage induced in the armature conductors is proportional to the flux density ( $B$ ), the active length of the conductors ( $l$ ), and the velocity of the flux passing the conductor ( $v$ ).

The superconducting generator was designed and built with the armature as the stationary member (stator) to preclude the necessity of having rotating contacts in the armature circuit and to keep the diameter of the rotating member as small as possible, minimizing windage losses and centrifugal forces at the high shaft speeds, up to 24,000 rpm.

The techniques for winding an armature with superconductors, however, differ from the techniques used for winding conventional generators with copper magnet wire because of the characteristics of superconductors. In winding a superconducting armature the following constructional requirements must be met:

1. The superconductor must be wound in one continuous length for each phase. Joints within a phase winding cannot be tolerated since a joint represents a point of heat generation within the superconductor.
2. The end windings must be supported and insulated from each other while retaining accessibility to the coolant.
3. Superconductors in ribbon form have relatively lower ac losses compared to wire forms, but they cannot be easily bent or twisted without taking up a great deal of space thus making end turns large.

Armature windings in conventional synchronous generators are usually wound with many separate loop sections to facilitate construction and are then connected together to form the entire phase winding. In order to use a continuous piece of superconductor and minimize the end loop space in the superconductor armature winding, a Gramme Ring winding configuration was used. This winding is shaped much like a toroid and minimizes the space required by the end loops. This winding type lends itself to being formed around the plastic inner chamber containing the iron flux return path as shown in Figure 10. The end windings are interleaved with mylar tape to provide insulation. Also, this winding configuration isolates the windings of each phase thus minimizing the insulation requirement.

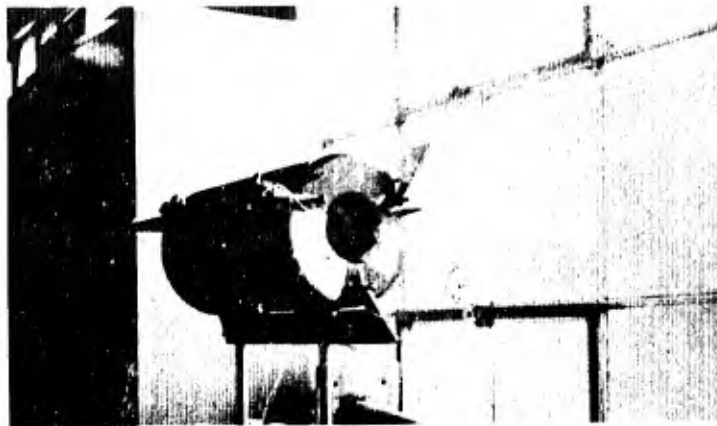


Figure 10. The Armature Gramme Ring Winding  
During Fabrication

The choice of superconductor as presented in Section 3.1.2.1 resulted in the use of a commercially-available ribbon type  $\text{Nb}_3\text{Sn}$  superconductor which is silver-plated (RCA Type 60214).

The winding distribution of the armature was experimentally confirmed as presented in Section 3.1.2.2, and showed that the distribution used yielded a sinusoidal output voltage waveshape.

#### 3.1.2.1 Choice of Superconductors for the Armature

It is important to note that at the time of the design, emphasis in the development of superconductor wires had been devoted primarily to dc applications. The principles guiding the development of dc materials are quite different from those for ac application.

There are several considerations which govern the selection of a material for the armature windings:

1. The critical temperature should be as high as possible in order to give an acceptable refrigeration system weight. Since the refrigerator weight increases rapidly as the operating temperature decreases, we were limited to relatively few hard superconductor compounds:  $\text{V}_3\text{Si}$  ( $T_c = 14\text{--}15^\circ\text{K}$ );  $\text{V}_3\text{Ga}$  ( $14\text{--}1/2^\circ\text{K}$ );  $\text{NbN}$  ( $16^\circ\text{K}$ ); and  $\text{Nb}_3\text{Sn}$



(18° K). Of these, only Nb<sub>3</sub>Sn is commercially available.

2. The material must be sufficiently flexible or ductile to wind the generator.
3. The ac heating losses in the stator must be kept to acceptable levels. The configuration of the material must exhibit a minimum of heating losses when subjected to a magnetic field. Alternatively, the current-carrying capacity should be very high. This suggests a thin film, whose thickness is of the order of the field penetration depth or less.
4. The critical field should not limit the design. Probably all of the hard alloy or compound superconductors meet the requirement are properly oriented with respect to plied magnetic field.

As discussed previously, commercially available in many forms. They fall into two basic categories.. The first category is a wire which must be wound into the desired form before reaction by heat treatment at 1000°C. Thereafter, the wire is extremely brittle and cannot be handled. The second category is a ribbon or tape form which requires no further heat treatment. Use of the Gramme Ring configuration limits the superconductor to those in the second category because the plastic inner chamber, upon which the armature was wound, cannot tolerate the heat treatment. From a geometry and handling standpoint, neither the ribbon nor the tape is entirely satisfactory; however, the ribbon geometry was chosen for our configuration.

From the viewpoint of ac losses, thin films have an advantage of lower ac losses than thicker solid-core tapes and wires. Although thin films deposited on non-conducting substrates show even smaller ac losses because there are no eddy current losses present in the substrate, the available thin films are deposited on either hastelloy or niobium substrates. Because of the high resistivity of these metals the amount of eddy heating due to the substrate is small, however, when compared to the hysteresis ac losses. A comparison of the calculated ac losses of all the available wires is shown in Figure 11.

#### 3.1.2.2 Design and Armature Voltage Waveshape

The waveshape of the armature voltage is important because a nonsinusoidal magnetic field created by the armature current can induce eddy heating in the shaft thereby adding to the heat load. Balanced sinusoidal polyphase currents in a symmetrical three phase armature winding create an armature reaction mmf wave consisting of a constant amplitude space fundamental rotating at synchronous speed which is stationary with respect to the field. However, any non-sinusoidal polyphase currents will contain harmonic components. The armature reaction mmf created by these harmonic components will rotate at greater than synchronous speeds and will no

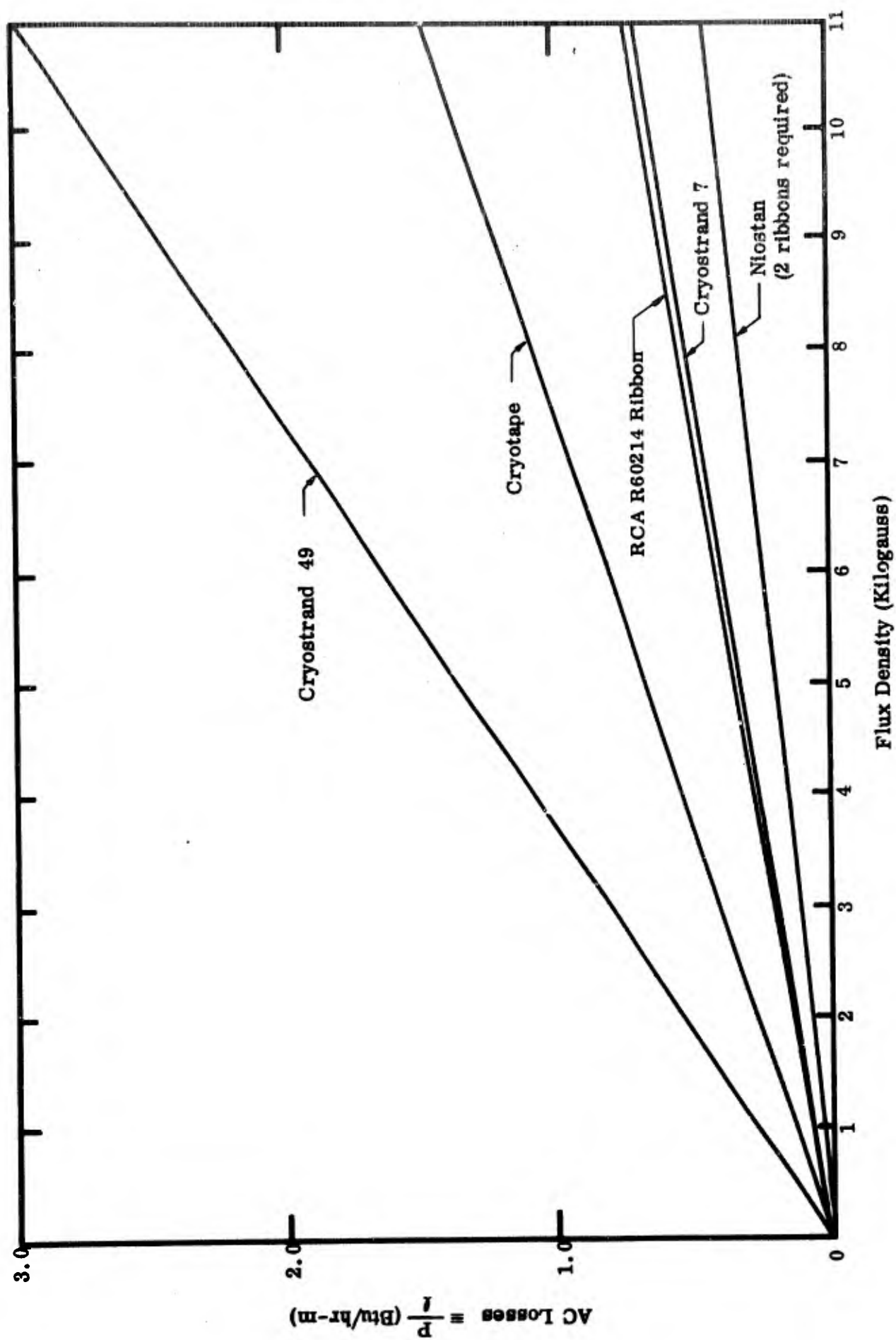
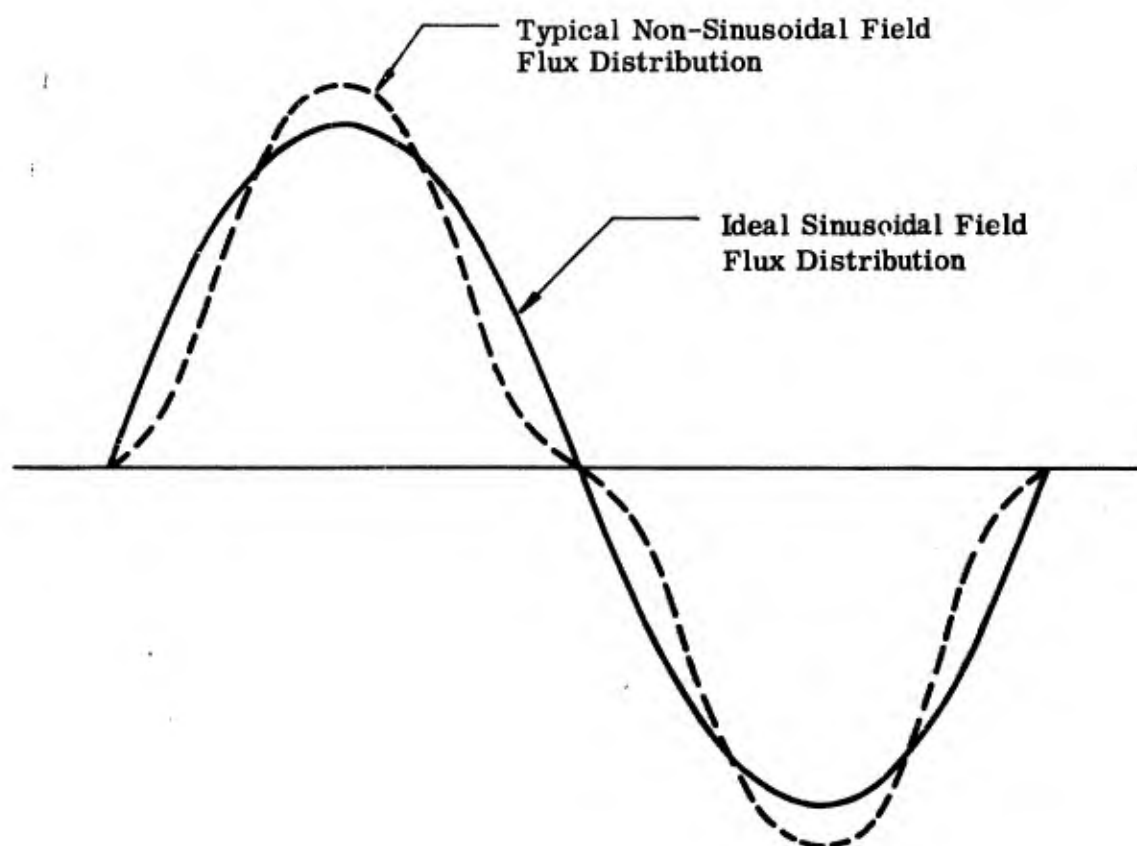


Fig. 11. AC Loss Comparison of Various  $Nb_3Sn$  Superconductors for 50 KVA Generator Armature Application

longer be stationary with respect to the field. This results in eddy heating of the shaft. Also, hot spots may be produced on the shaft which can lead to quenching of the superconducting field located within the shaft. Therefore, an effort should be made to obtain an armature output waveform which is as nearly sinusoidal as possible.

The flux distribution of a typical field winding acting alone is only approximately sinusoidal as shown in Figure 12. This non-sinusoidal field will create harmonic components in the armature voltage waveform. These harmonic components may be reduced to a low level by the techniques of distribution and fractional pitching the armature windings (Ref. 5). Calculations were performed on these factors and tests conducted for experimentally supporting these factors. Details of these tests are presented in Appendix II.



**Fig. 12 Flux Distribution of a Typical Field Winding Acting Alone**

To facilitate testing, a model using copper windings throughout was used to

simulate the superconductors in the armature and field. The field strength magnitude and distribution of the simulated field coil were measured by the use of a wire loop sensor to determine the degree of correction required. The winding factors were applied accordingly to reduce those harmonic components which could be expected to exhibit a large magnitude.

Tests were conducted to verify the degree of distribution and chording of the armature winding necessary to achieve a sinusoidal output waveshape with two different winding geometries based on a Gramme Ring configuration:

1. A 44-turn winding distributed over a  $120^\circ$  span of the armature (which is our original design winding), and
2. Two 22-turn windings each distributed over a  $60^\circ$  span of the armature and with  $60^\circ$  chording ( $2/3$  pitch or  $120^\circ$  apart).

The voltage waveshape was checked by superimposing a calculated sine wave over the measured waveshape. The measured sine wave followed the calculated sine wave extremely closely. Thus, the voltage waveshape may be considered as sinusoidal. Because of its simple geometry which provides phase voltage isolation and simplifies fabrication, the 44-turn winding distributed over a  $120^\circ$  span of the armature was used in the 50 kva laboratory model generator armature.

### 3.1.3 Liquid Metal Brushes

Past Dynatech experience has shown that it is virtually impossible to successfully energize a rotating superconducting field coil through conventional rubbing-block brushes (slip rings). Such brushes tend to "chatter" due to geometric variations and the stick-slip characteristic of sliding friction. The result is a high frequency "make-and-break" action, which tends to interrupt the current flow to the coil. Every time one of the brushes loses contact, the magnetic field in the coil starts to collapse. This results in internal heat generation which causes the coil to quench at low excitation current levels.

There are a number of possible methods to improve this situation. One is to put a filter network across the field leads between the brushes and the field coil. Another is to connect a resistor across the field leads in the same position to provide "crowbar protection". These two methods can compensate for the basically undesirable characteristics of conventional brushes at the expense of adding components on or inside the rotating shaft.

A logical alternative to the above methods is the replacement of conventional brushes with liquid metal brushes which utilize a bridge of liquid metal to carry the current between the stationary and rotating parts of the brush.

Dynatech's experience with liquid metal brushes dates back to early experimental work on the superconducting generator when a set of liquid metal brushes was designed and fabricated to overcome field quenching problems caused by conventional brushes. The design approach was simple and straightforward: the liquid metal was contained in an annular cavity in the external rotating part of the brush, making contact

with a central non-rotating member. With this configuration, the radial acceleration due to rotation contains the liquid metal in the annular cavity, once a threshold speed is passed. This assures relatively constant contact area between the liquid metals and the brush parts. In addition, it allows the brushes to operate satisfactorily in any orientation with respect to gravity (or in the complete absence of gravity) if properly designed.

The electrical operating characteristics of liquid metal brushes are strongly affected by geometry, operating speed, and current in a way that has not been explained to date. Typically, the resistance across a liquid metal brush is lower than across a conventional brush and goes down with increasing rotational speed and current. These characteristics would appear to be caused by a change in the contact resistance between the liquid metal and the brush components. In addition to these steady-state parametric variations of brush resistance, there is a periodic variation which occurs at the frequency of rotation or multiples thereof. This periodic variation goes down as the contact area is increased. Therefore, it is probably caused by waves on the free surface of the liquid metal. Such waves would be excited by an imbalance or lack of concentricity in the brushes, or could result from vibration elsewhere in the system. They are difficult to avoid and easily sustained, since liquid metals are relatively inviscid. In our experience, the magnitude of this periodic resistance is much smaller than the rms value of the total brush resistance. Our tentative hypothesis is that the surface waves cause periodic variations in the contact area between the liquid metal and the brush components. This hypothesis is empirical, based on the behavior of our two different liquid metal brush designs.

The current-carrying capability of conventional brushes feeding an inductive load is largely based on wear criteria. The make-and-break operating characteristics causes sparking which erodes the contacting surfaces. Therefore, one often uses empirical limits (e. g. , 10 amps/sq. in. of contact area) in the design of conventional brushes. Because liquid metal brushes do not exhibit this make-and-break characteristic, their electrical loading is not limited by this criterion. Instead, the design is limited by joule heating and hydraulic (drag) heating in the brushes and by mechanical (stress) considerations.

The main consideration in the design of the brushes for the 50 kw prototype generator was the high operating speed. This required a small brush diameter to keep stresses and hydraulic drag heating as low as possible. A small diameter with low contact area was feasible in this case because of the relatively low field current (about 40 amps maximum). To provide extra strength and rigidity, the brushes were mounted inside the free end of the generator shaft.

Figure 13 shows a cross-section of the liquid metal brushes used on the prototype generator. The non-rotating central members are coaxially arranged, with an insulating sleeve between them. Ball bearings at either end of the assembly locate the non-rotating elements. The rotating (outer) parts of the brushes are insulated from each other by a spacer which has a cavity to retain any liquid metal which may slosh out of the brushes. The inner brush passes current to the field through a lead which is electrically insulated from the shaft. A plastic sleeve insulates this inner brush from the shaft. The outer brush is shorted to the shaft, which is used as a return path for the field current.

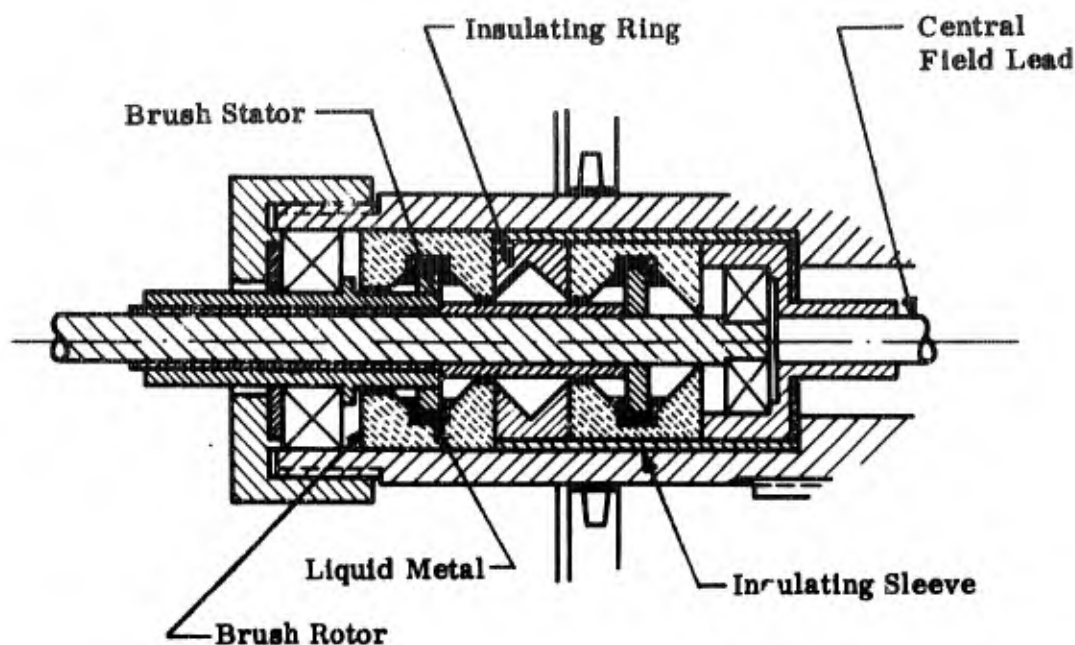


Fig. 13. Liquid Metal Brush

Our experience with these brushes during actual generator operation is limited to two tests. In the first, the brushes satisfactorily energize the field coil up to a current of 28 amps and a rotational speed of about 9500 rpm, which were the maximum values attempted in that test.

Between the first and second tests, the brushes were removed, inspected, cleaned, and reinstalled. Post-installation tests indicated satisfactory condition. However, during the second test, a high resistance developed in the brush circuit, severely limiting the amount of current which the field power supply could put into the field. The resistance fluctuated and could be temporarily reduced by tightening the screw cap which retains the brushes in the shaft end. This symptom indicated contamination between the adjoining surfaces in the current path. The brushes were removed, cleaned, checked, and reinstalled. Unfortunately, other problems prevented any further evaluation of the brushes during the second test.

### 3.2 Thermal Design

The design of the 50 kva laboratory prototype generator involved design compromises between electrical, mechanical, and thermal requirements, with additional overall constraints of reasonable cost, flexibility, and high probability of successful operation with minimum development time. Obviously, one particular requirement dominated the design of some components. For instance, the shaft design was determined solely from operating speed (mechanical) consideration, once the field coil diameter was selected from electrical considerations. The result is that

the thermal performance of some components did not involve any "thermal design" as such, but resulted wholly from electrical and/or mechanical requirements, while other components were designed purely from thermal considerations, limited only by the overall constraints mentioned above.

It is an inherent characteristic of a superconducting generator that it will not operate if the superconductive material is above some limiting temperature which is a function of current and applied magnetic field. Therefore, the design of those components which affect the temperature of the superconductive material (lead heat exchangers, cooling ducts, etc.) must meet thermal requirements, even to the total disregard of other considerations.

One other factor should be noted in evaluating the thermal performance of the prototype generator. Although the design output is 50 kva, the work statement requires that the machine be basically capable of being reworked (rewound) to produce 1000 kva. The result of this stipulation has been higher thermal loads than would be expected in a machine having the rated output of the prototype.

The thermal design of the prototype superconducting generator evolved logically from previous Dynatech conceptual designs. In common with these, the prototype generator removes heat at two temperature stages, about 10° K and 80° K. This arrangement reflects the proposed use of a two-stage cryogenic refrigerator in an integrated system. The reason for removing heat at a higher temperature is to reduce the heat load at the lower temperature. This is desirably because the weight and required input power of the refrigerator are much higher at 10° K than at 80° K. In the prototype generator, the intermediate temperature heat load is removed by vaporizing liquid nitrogen, since this is the easiest method of simulating an 80° K refrigerator stage.

Liquid nitrogen is circulated through two flanges on the shaft enclosure and through the container for the iron return path, removing heat from the shaft enclosure, the shaft and upper-stage field leads (by convection across the "air" gap between the enclosure and the rotating shaft), the iron return path, the upper-stage (power) leads for the armature and, by conduction, from the radiation shield between the outer casing and the inner chamber.

Lower-stage cooling is effected by gaseous helium produced by vaporizing liquid helium. Delivery temperature and flow rate are controllable over a large range. To prevent in-leakage of atmospheric air and for practical reasons, delivery pressure at the generator is slightly above atmospheric (0.25 to 0.50 psig), rather than the 10 psia delivered by the proposed system refrigerator. This increases windage by about the same ratio as the pressure increase (around 50%).

### 3.2.1 Field and Armature Electrical Leads

The problem of achieving optimum operation in stage-cooled electrical leads carrying current between room temperature and the generator operating temperature received extensive analytical and experimental attention in the course of the two previous Air Force superconducting generator contracts. The work was reported in detail in References 1 and 2. Our conclusions, based on this work, were



that annealed high-purity silver was the best material for both upper-and lower-stage leads. Figures 14, 15, 16 and 17 show the operating characteristics of such leads between 273° K and 77° K (upper stage) and 77° K and 4.2° K (lower stage). The lower-stage leads were tested with alternating and direct current. The upper-stage leads were tested with direct current only, since the lower-stage tests showed very little difference.

Rated output of the generator armature is about 30 amps per phase. Four leads were provided (one neutral). The lower-stage armature leads were optimized for 45 amps in order to stay below the sharp breakaway just above the optimum operating point. From Figure 15, this yields a  $\dot{q}/I$  of 0.032 Btu/hr-amp (per lead) at  $I/I_{opt} = 0.67$  (ac curve). Therefore, the three-phase leads have a total heat input to the 10° K region of  $3 \times 30 \times 0.032 = 2.9$  Btu/hr. The neutral lead, which ideally carries no current, runs at  $I/I_{opt} = 0$ . From Figure 14, this is  $\dot{q}/\dot{q}$  at  $I_{opt} = 0.80$ . Using Figure 14,  $\dot{q}/I$  at  $I/I_{opt} = 1.00$  is 0.026 Btu/hr-amp. Therefore, heat input down the lower-stage of the neutral lead is  $0.80 \times 45 \times 0.026$  or about 0.9 Btu/hr. Therefore, the total lower-stage lead heat input is 3.8 Btu/hr at rated current.

The upper stage armature leads were optimized for 30 amps. This is feasible in this case since there is no abrupt breakaway of heating above the optimum current point. From Figure 17,  $\dot{q}/I$  at  $I/I_{opt} = 1.00$  is about 0.120 Btu/hr-amp. Therefore, the three-phase leads will each transfer  $30 \times 0.120 = 3.6$  Btu/hr to the intermediate (80° K) temperature stage. From Figure 16,  $\dot{q}/\dot{q}$  at  $I_{opt} = 0$  is about 0.3, so the neutral lead will transfer about 1.1 Btu/hr.

The field coil produces a calculated 300 gauss at the armature per amp of input current with the iron return path. Tests have verified that the actual output is somewhat lower than this value. Nominal operating flux density is 10 kilogauss, requiring about 40 amps of field current. Current flows to the field coil down a staged lead located on the axis of rotation inside the shaft. The shaft itself is used as a return lead. Joule heating in the shaft is a total of about 6.8 Btu/hr. One half to one third of this must be removed at 10° K. Heat transfer is very good, since the shaft is in direct communication with the coolant stream.

The internal (staged) field lead is somewhat of a departure from previous Dynatech practice. For practical reasons, it was not feasible to use silver for the upper-stage lead material. Instead, this is a stainless steel rod, 5/16 inch in diameter, which is mechanically self-supporting and also serves to seal one end of the shaft interior. Calculated heat flow down this rod into the intermediate staging point is 9.1 Btu/hr at 40 amps input. This is only about twice the heat input of an optimum silver lead, but this compromise did not involve a large thermal penalty.

The lower-stage internal field lead is annealed high-purity silver nominally optimized for 45 amps. The upper end of the lead is certain to be higher than 77° K because the intermediate staging point rejects heat from the lead through the intermediate heat sink into the shaft, hence into the helium around the shaft, and from there to one of the liquid-nitrogen-cooled flanges. The calculated heat leak down this lead to 10° K is between 1.5 and 3.0 Btu/hr, depending on the temperature of its "hot" end.



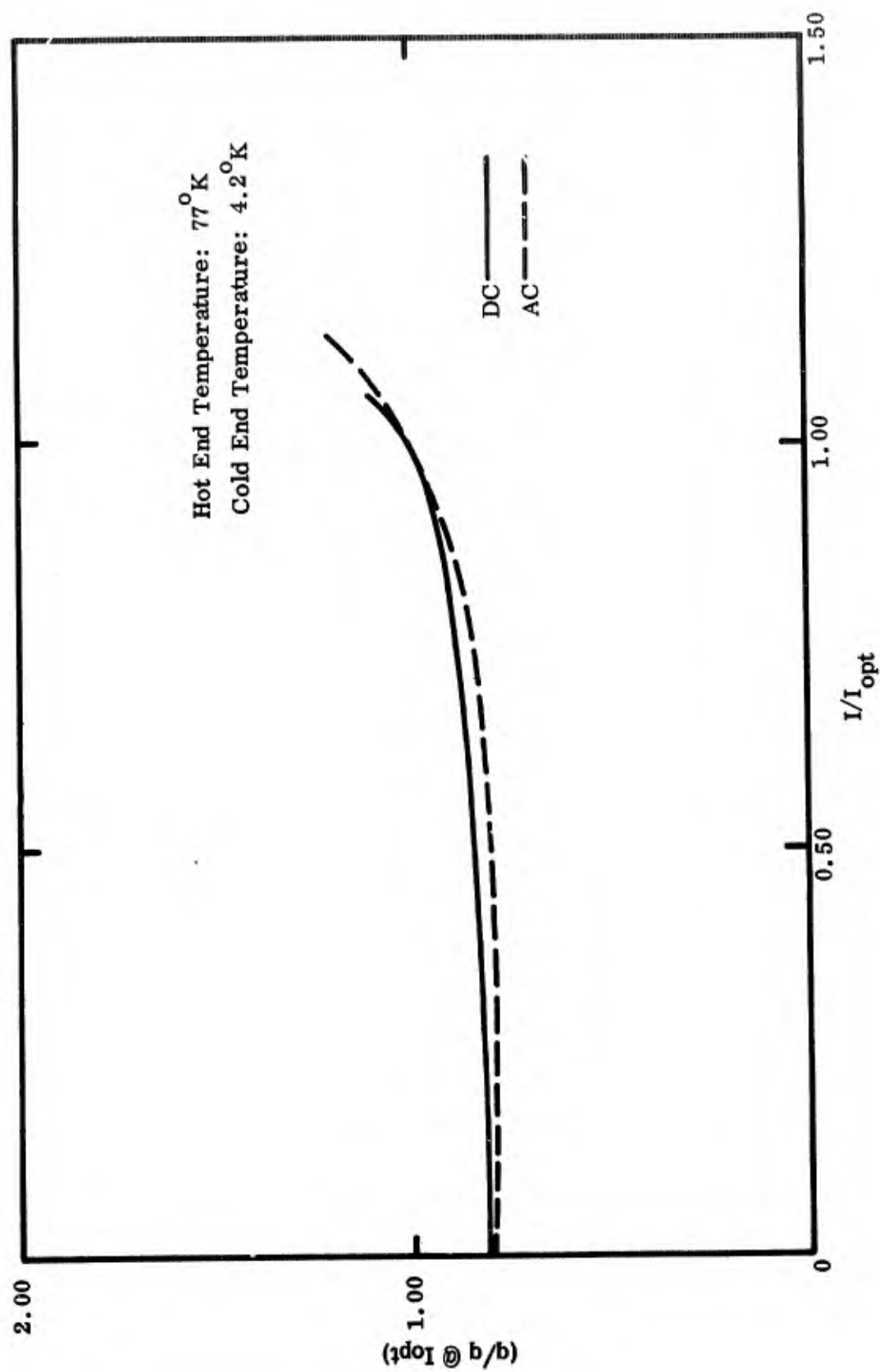


Fig. 14. Heat Flow per Lead vs. Current (Normalized):  
Alternating and Direct Current Annealed High-  
Purity Silver

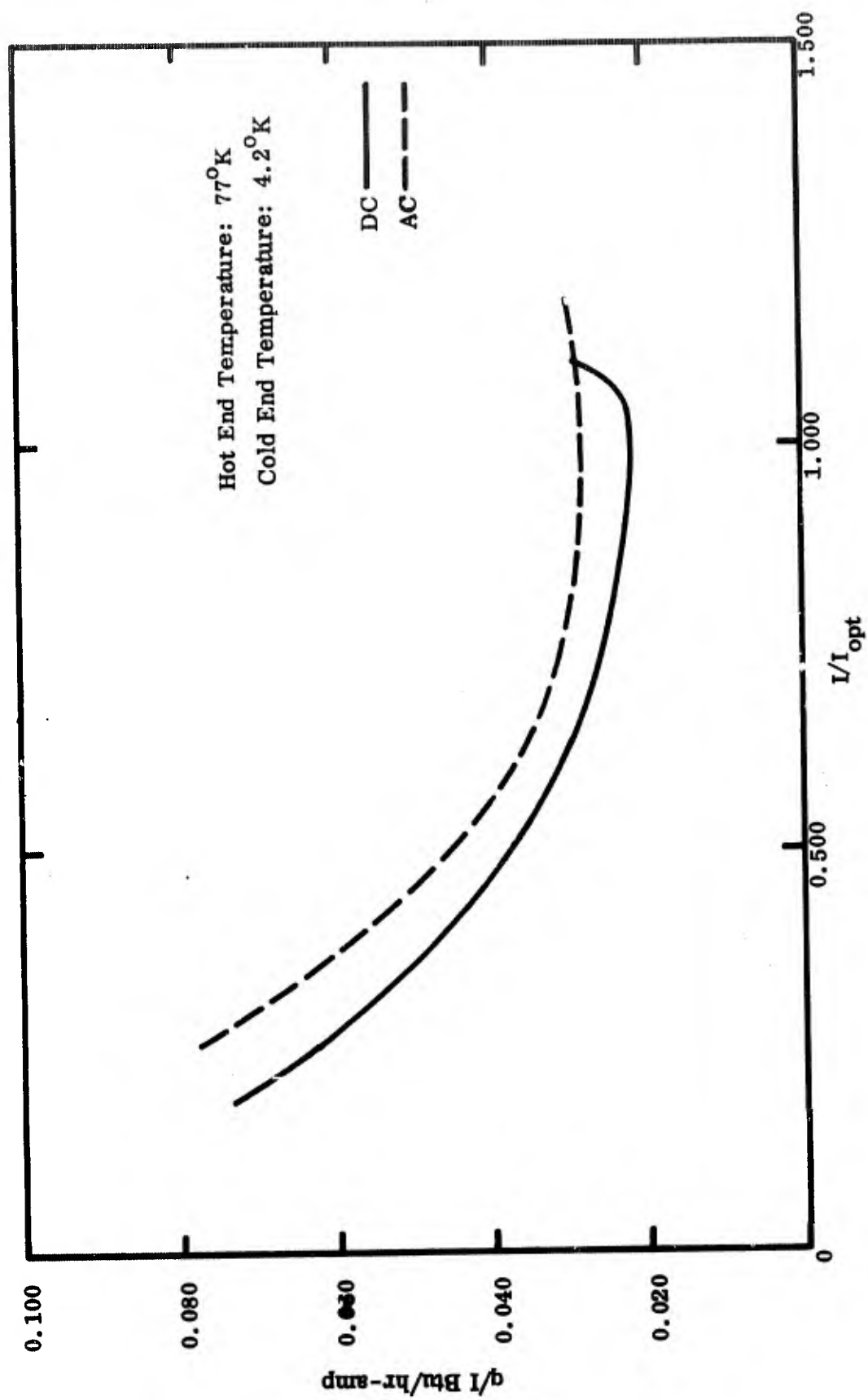


Fig. 15.  $q/I$  per Lead vs. Normalized Current:  
Alternating and Direct Current Annealed  
High-Purity Silver

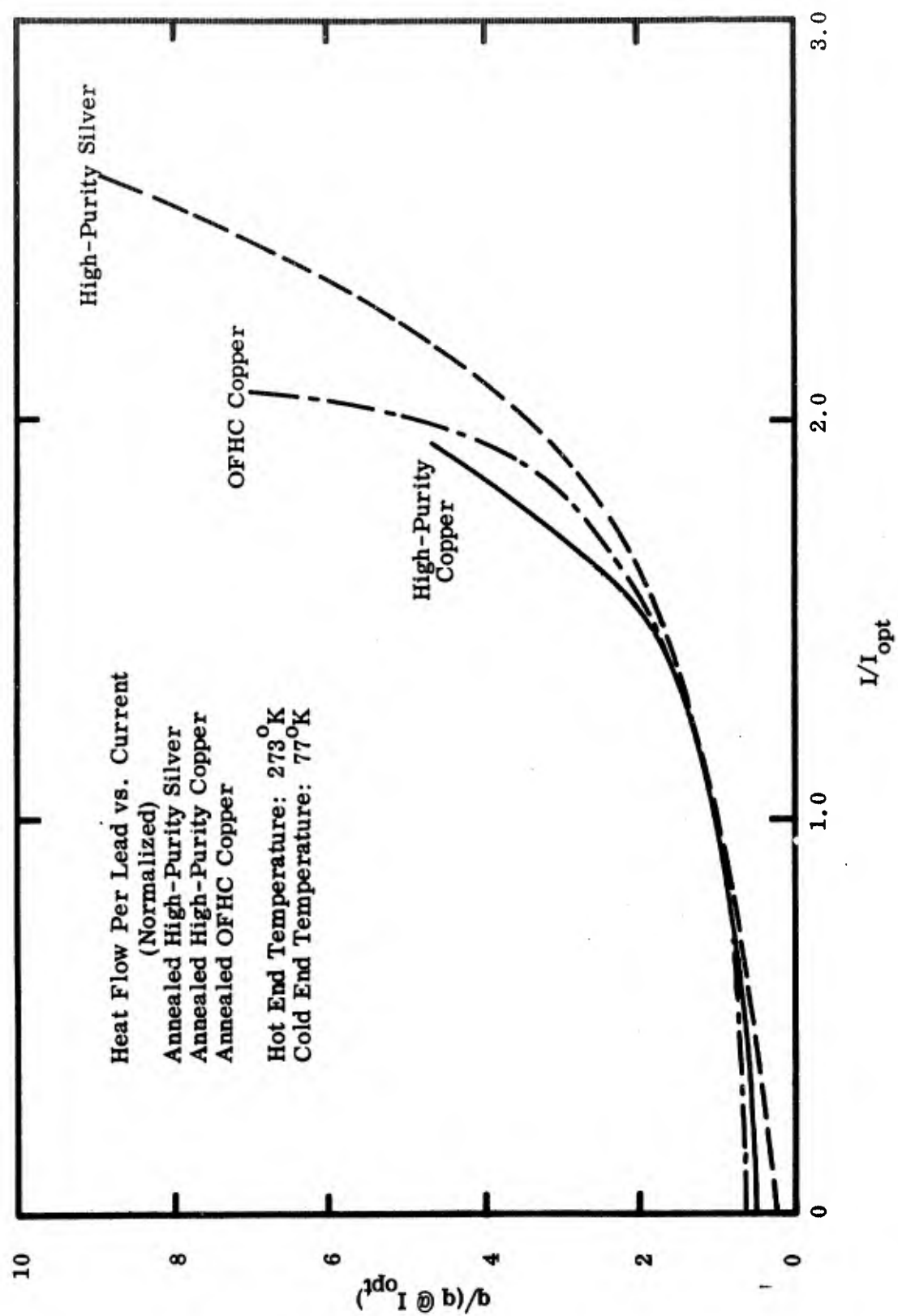


Fig. 16 Upper Stage Heat Flow vs. Current: Ag, Cu, ~F·H·C Cu

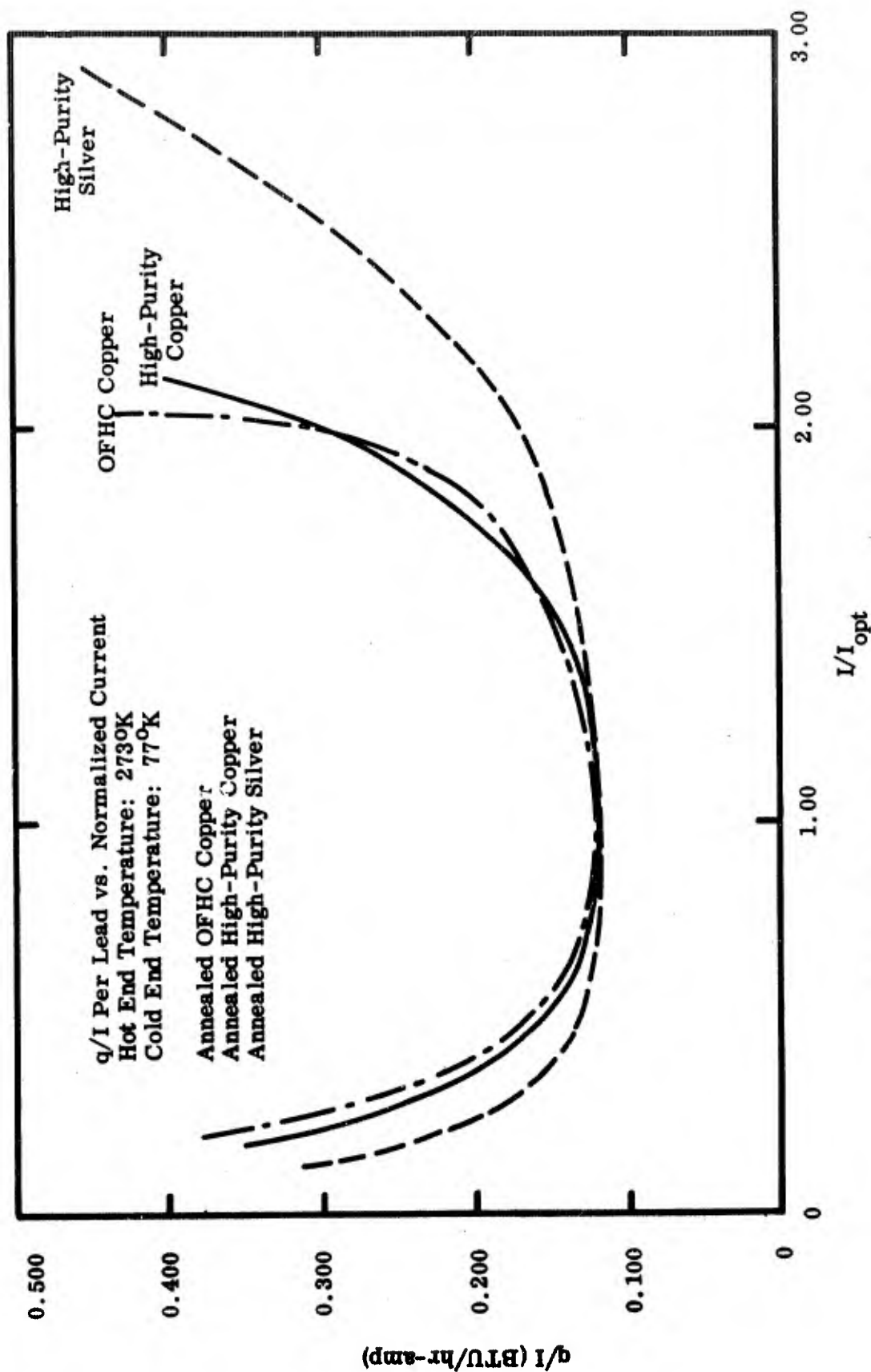


Fig. 17 Upper Stage Lead Electrothermal Characteristics: Ag, Cu, O.F.H.C Cu

### 3.2.2 Field and Armature Lead Heat Exchangers

Operation of the leads in the manner described in the previous section requires maintaining specific points on the leads at certain temperatures. This requires heat exchangers at those points to remove the heat flowing down the leads. In the case of the field leads and the upper-stage armature leads, these are better described as heat sinks, since they conduct heat into other members which are cooled. Each of the lower-stage armature leads, however, has a small copper plate-fin heat exchanger in the coolant gas stream. The helium gas passes through these four heat exchangers in series. They are placed in the incoming stream, where the gas is coldest.

The upper-stage armature lead heat sinks are ceramic sleeves in one of the liquid-nitrogen-cooled flanges. These conduct heat away from the leads and prevent electrical breakdown to the flange.

The intermediate and low-temperature field lead heat sinks use a plastic sleeve to provide electrical isolation from the shaft. As stated in the previous section, the intermediate-temperature heat load from the internal field lead is 5.1 Btu/hr; the low-temperature heat load is between 1.1 and 2.2 Btu/hr. Criteria for satisfactory operation of the field-lead heat sinks is necessarily somewhat arbitrary without a detailed knowledge of how the critical current of the field will be affected by temperature. In general, we would like the temperature difference between the heat sink and the coolant stream outside the shaft to be as small as possible. We have defined satisfactory maximum temperature differentials of 2° K for the low temperature heat exchanger and 6° K for the intermediate heat exchanger. Preliminary test data from one of our present heat sinks is given in Figure 18.

Figure 18 shows plots of the temperature differential from the coolant to the center of the heat sink versus heat power being removed (input power to a small heater soldered to the heat sink, in this test). The curves indicate that this design of field lead heat sink operates within the given limits at coolant temperatures of 77.4° K (liquid nitrogen) and 4.2° K (liquid helium). The curves also indicate that the thermopiles used to measure temperature had some zero offset, as evidenced by the zero-power temperature differentials being greater than zero. This offset represents a very small voltage error (about 5 microvolts), which is of the same order as the accuracy of the measuring instrument. The true curve can be obtained by shifting the given curves to the left so that they pass through the origin. This will result in a smaller temperature differential for any given power input.

### 3.2.3 Windage

Windage power dissipation in the low-temperature (10° K) region is a source of a significant portion of the total heat load. Windage was investigated analytically and experimentally in the two previous Air Force contracts on this project (Ref. 1 and 2), with good correlation between experiment and theory. Calculated windage for this machine is 104 Btu/hr at test operating conditions (10° K, 15 psia). With a refrigerator supplying 10° K cooling at 10 psia, the windage would drop to 74 Btu/hr, because of the lower gas density at the decreased pressure.

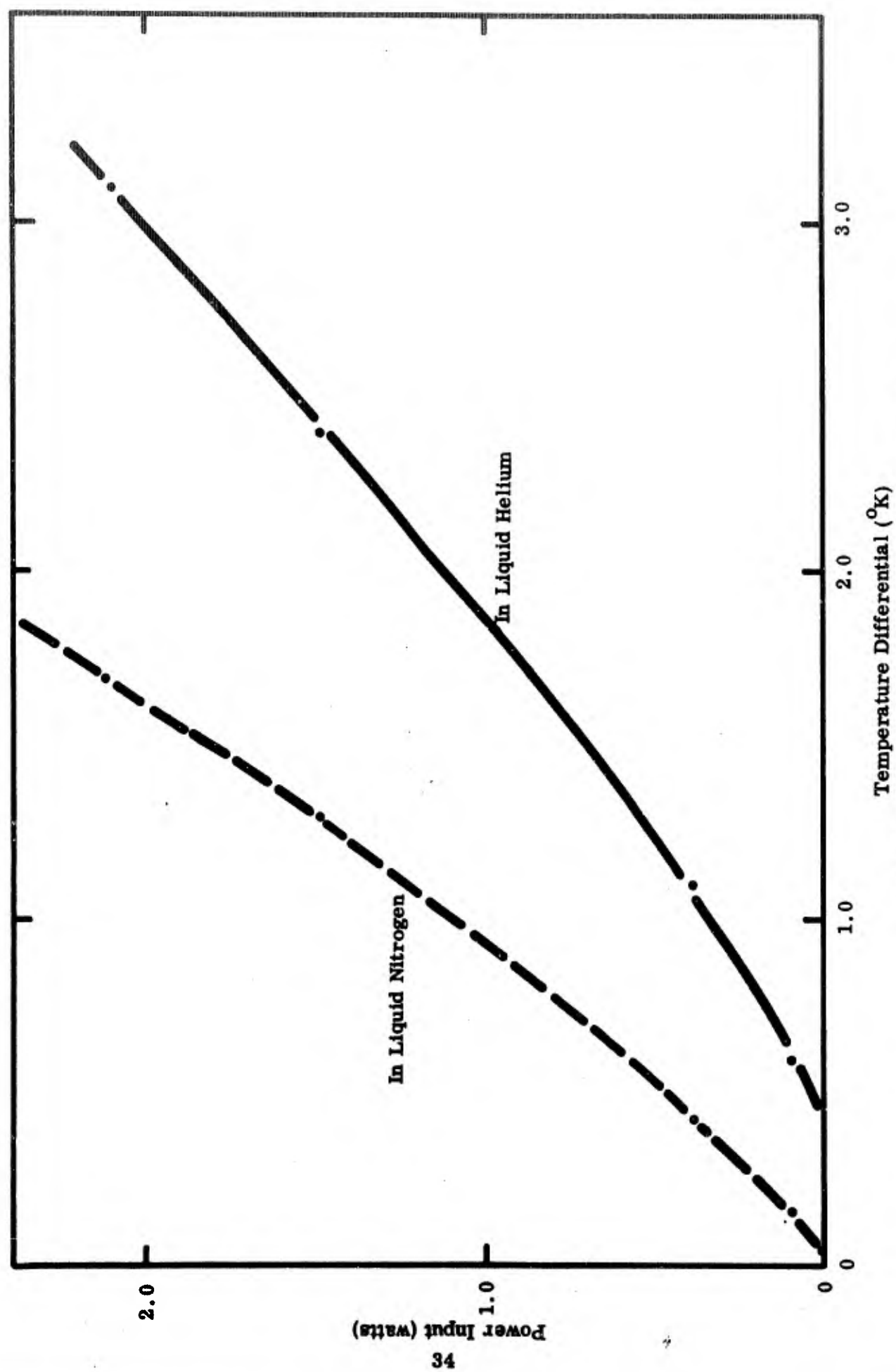


Fig. 18 Field-Lead Heat Exchanger Temperature Differential vs. Power Input

#### 3.2.4 Investigation of Candidate Armature Frame Materials

As shown in the analysis in the next section, the thermal conductivity of the armature frame material has a pronounced effect on the operating temperature of armature conductors. This was realized at the start of the program, and a literature survey was undertaken to determine what insulating materials were available having the desired properties. These were:

1. Excellent electrical insulating characteristics at 10° K
2. High thermal conductivity at 10° K
3. Thermal coefficient of expansion compatible with other adjacent materials (reinforced plastics and stainless steel)
4. Easy and economical fabrication (by machining or casting) into the complex shape required.
5. Ability to withstand a 950° C curing process required for some forms of Nb<sub>3</sub>Sn
6. Adequate mechanical strength and impact resistance

Initial investigations produced several candidates: two ceramics (alumina and boron nitride) and two composites (alumina or aluminum particles in an epoxy resin matrix). Thermal conductivity data at about 10° K was found only for alumina. This data had a wide spread in thermal conductivity at 10° K, depending strongly on the purity and crystallinity of the samples. Therefore, it was obvious that the required data could only be obtained from actual tests of commercially-available forms of the candidate materials. The ceramic samples were ordered from vendors; the filled-plastic samples were prepared at Dynatex Corporation.

Tests were conducted in a modification of the apparatus used to determine the thermal characteristics of the electrical leads. Net heat flux down the specimen was obtained by measuring the boiloff with the specimen removed. Thermocouples installed along the length of the specimen gave temperature differentials which allowed calculation of the thermal conductivity, given the measured heat flux down the specimen. This method of measurement does not give highly accurate results, but they are close enough for engineering purposes.

In all, six samples were tested for evaluation as possible armature frame materials: two alumina (different grades), one boron nitride, one alumina-filled epoxy (different particle sizes of aluminum). The test results for the filled-plastic specimens were very disappointing in that the thermal conductivities at 10° K were all estimated to be below 0.1 Btu/hr. ft° K. Therefore, these materials were judged unacceptable. Test results for the alumina and boron nitride samples are shown in Figure 19. Both grades of alumina are superior to the boron nitride. However, the total spread is less than an order of magnitude. Also, the thermal conductivity of the boron nitride sample was measured parallel to the pressing direction. In the armature frame, the important direction is that perpendicular to the pressing direction, and test results by others at higher temperatures show that the thermal conductivity in the perpendicular direction is the higher by a factor of two.

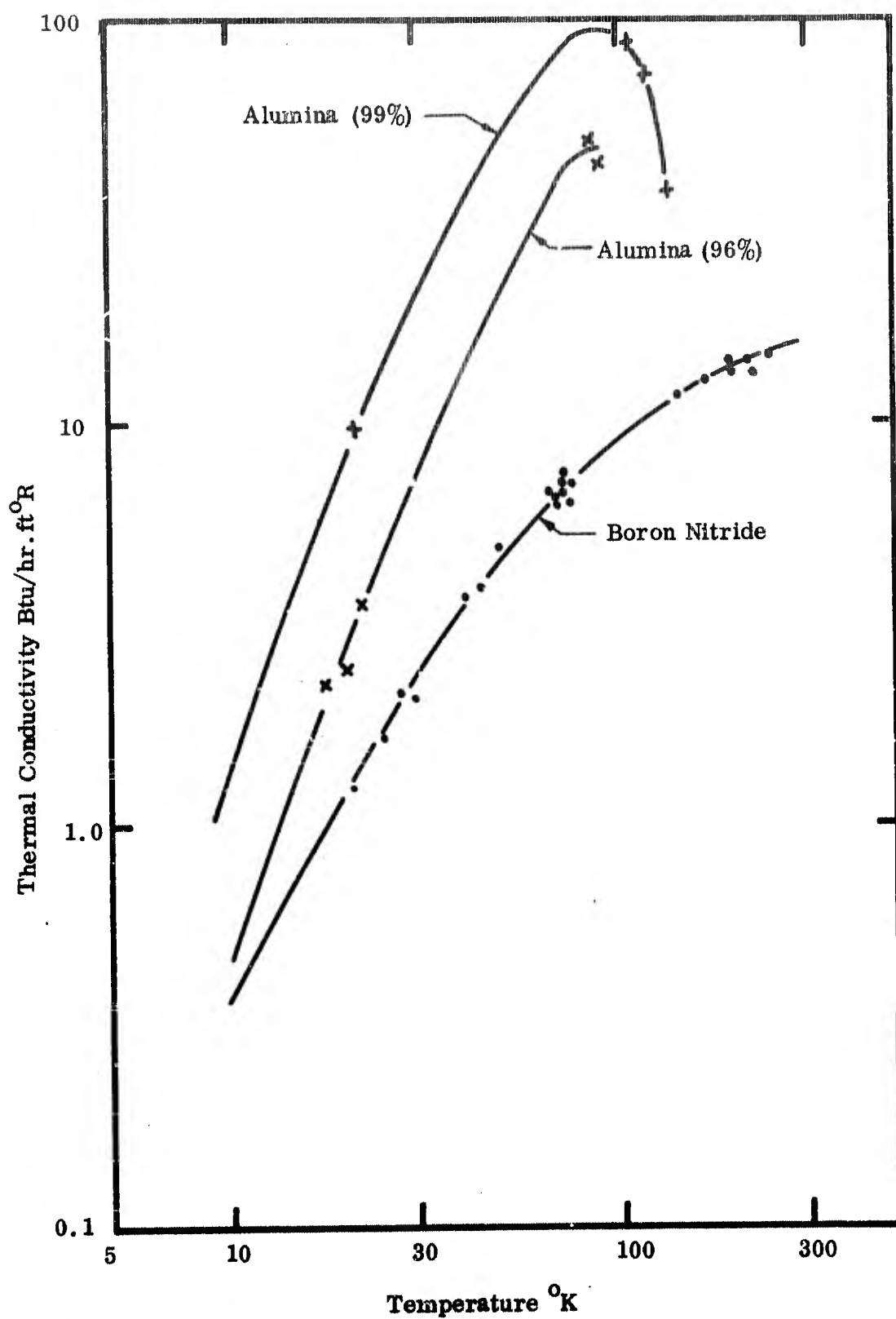


Fig. 19 Thermal Conductivity of Ceramics vs. Temperature



At the time these results became available, the shape of the armature frame was well defined, so various vendors were approached to determine the practicality of producing such a shape in high-purity alumina. Opinions received ranged from unfeasible to barely feasible but very expensive. Therefore, it was judged that the use of alumina for the armature frame carried a high degree of risk and high expense. For these reasons, boron nitride was selected for this use.

Boron nitride is a glossy white material which feels like chalk, but is somewhat stronger. Like most ceramics, it is an excellent electrical insulator with good breakdown strength. Boron nitride machines very easily and cleanly, facilitating fabrication. To date, no problems have arisen from the use as the armature frame material.

### 3.2.5 Investigation of Heat Transfer in the Generator Armature

#### 3.2.5.1 Purpose

An analytical study and tests were carried out to investigate the heat transfer into the coolant (gaseous helium at around 10° K) from the shaft and the armature. The purpose of this study was two fold. First, to determine whether the heat transfer coefficients between the cooled surfaces and the coolant were high enough to prevent large temperature differentials. Second, to determine how the thermal conductivities of the armature frame material and conductor potting material affect the temperature of the superconducting armature windings.

#### 3.2.5.2 Summary

The initial part of this study involved an extensive literature survey to find experimental values of film coefficients for the geometric configuration of concentric cylinders with the inner one rotating. The search revealed that for the higher rotational speeds of interest here, the Taylor Number is the controlling parameter. The heat transfer correlation of Tachibana (Ref. 6) was assumed to adequately predict the heat transfer film coefficient

$$Nu = .42 [Ta Pr]^{.25}$$

in the shaft-armature gap. For the present design geometry and speed, the calculated film coefficient is 118 Btu/hr-ft<sup>2</sup>-° F.

Utilizing this value of film coefficient, a heat balance on the armature and cryogenic helium flow was completed. A simplified model was assumed, based on convective transfer of the heat generated in the armature windings to the helium gas stream from the armature surface.

This model resulted in a set of differential equations relating helium flow rate, helium inlet and exit temperatures, windage losses in the helium, and armature winding heat loss, temperature and geometry, to the configuration and thermal conductivity of the armature frame. The results showed that for the present geometry and a total heat load of 185 Btu/hr, a thermal conductivity of the armature frame material of 1.0 Btu/hr-ft-° R is sufficient to keep the windings at an average temperature of 18° R (10° K) with a helium flow rate of 29 lbm/hr, and an inlet temperature of 14° R (7.8° K).

The film coefficients on the sides and over the outer diameter of the armature were reviewed. These should be closely predicted by the ordinary fully developed turbulent flow correlation (Ref. 7).

$$\text{Nu}_D = .023 \text{Re}_D^{.80} \text{Pr}^{.40}$$

The only problem area here would appear to be around the corners of the cylinder, where a poor flow passage design could result in a hot spot in the windings due to a local lowering of the film coefficient (Ref. 8). This is strongly dependent on both flow passage design and Reynolds Number.

The initial armature heat balance was based on the assumption that the conductors were in intimate contact with the armature frame (i.e., that there was no thermal resistance along the plane of contact). This analysis was later refined to examine the effect of using a potting compound to secure the conductors in the armature frame material. This is the method used in the prototype generator.

Finally, tests were performed at generator operating temperature on a simulated armature section with potted-in conductors and on a room temperature model of the complete armature with the flow ducting later installed on the prototype generator. These tests verified that heat transfer in the active (field-swept) and inactive regions of the armature was satisfactorily predicted by the analyses and that the coolant ducting was adequate as designed.

The results of these analyses and tests are presented below in detail.

### 3.2.5.3 Nomenclature and Geometry

A schematic of the armature and shaft assembly geometry is shown in Figure 20. The nomenclature is shown in the following table.

$n$	number of windings	
$l$	armature length	[ ft ]
$t$	winding thickness	[ ft ]
$\delta$	winding height	[ ft ]
$W$	width $W = \pi r_i / n$	[ ft ]
$r_i$	inside radius = $r_1 + b$	[ ft ]
$r_o$	= $r_1 + \delta$	[ ft ]
$b$	gap height	[ ft ]
$r_1$	shaft radius	[ ft ]

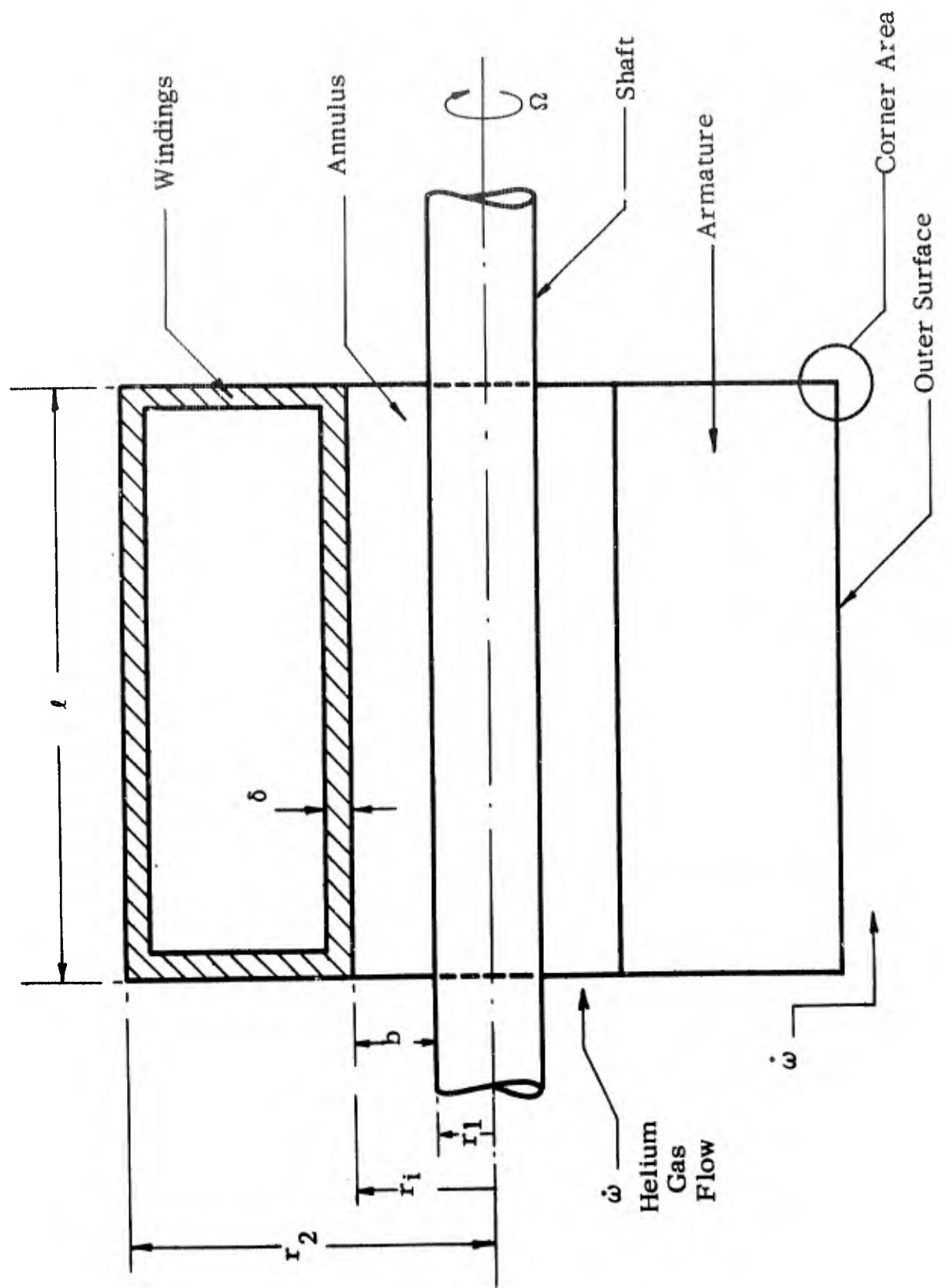


Fig. 20. Schematic of Armature and Shaft Assembly.

$r_m$	$= (r_1 + r_i)/2$	[ ft ]
$\Omega$	rotational speed	[ rpm ]
$V$	axial gas velocity	[ ft/sec ]
$r_2$	outer diameter-armature	[ ft ]
$\xi$	fin efficiency	
$\dot{\omega}$	flow rate	[ lbm/hr ]
$T_\infty$	gas temperature	[ ° R ]
$T_1$	winding temperature	[ ° R ]
$h$	film coefficient	[ Btu/hr-ft <sup>2</sup> -° R ]
$T_m$	mean winding temperature	[ ° R ]
$\dot{Q}_1$	total electromagnetic heat generation in the winding	[ Btu/hr ]
$\dot{q}_1$	specific heat generation per winding	[ Btu/hr-ft <sup>3</sup> ]
$\dot{Q}_\infty$	total windage heat generation	[ Btu/hr ]
$\mu$	viscosity	[ lbm/hr-ft ]
$\rho$	density	[ lbm/ft <sup>3</sup> ]
$k$	thermal conductivity	[ Btu/hr-ft-° R ]
$C_p$	specific heat	[ Btu/lbm-° R ]
$\nu$	kinematic viscosity	[ ft <sup>2</sup> /hr ]
$Ta \equiv \frac{r_m \Omega^2 b^3}{\nu^2}$	Taylor Number	
$Re \equiv \frac{2 V b}{\nu}$	Reynolds Number	
$Pr \equiv \frac{C_p \mu}{k}$	Prandtl Number	
$Nu \equiv \frac{2 h b}{k}$	Nusselt Number	

$$Re_D \equiv \frac{\rho V D_h}{\mu} \quad \text{Hydraulic diameter Reynolds Number}$$

$$Nu_D \equiv \frac{h D_h}{k} \quad \text{Hydraulic diameter Nusselt Number}$$

$$D_h = \frac{4 \text{ Cross Sectional Area}}{\text{Wetted Perimeter}}$$

#### 3.2.5.4 Heat Transfer Correlation Between Two Concentric Cylinders With the Inner Rotating

Despite the wide use of rotating machinery, relatively little work was published on the heat transfer between the rotor and stator prior to a paper by Kaye and Elgar (Ref. 9). In this paper, the authors extended the classic work of Taylor to propose a four region map of possible flow situations for the fluid flowing in the annular gap between rotating concentric cylinders. This resulted in a Taylor number,

$$Ta = \frac{r_m \Omega^2 b^3}{\nu^2}$$

versus Reynolds Number,

$$Re = \frac{2 v b}{\nu}$$

flow map. This is schematically represented as follows:

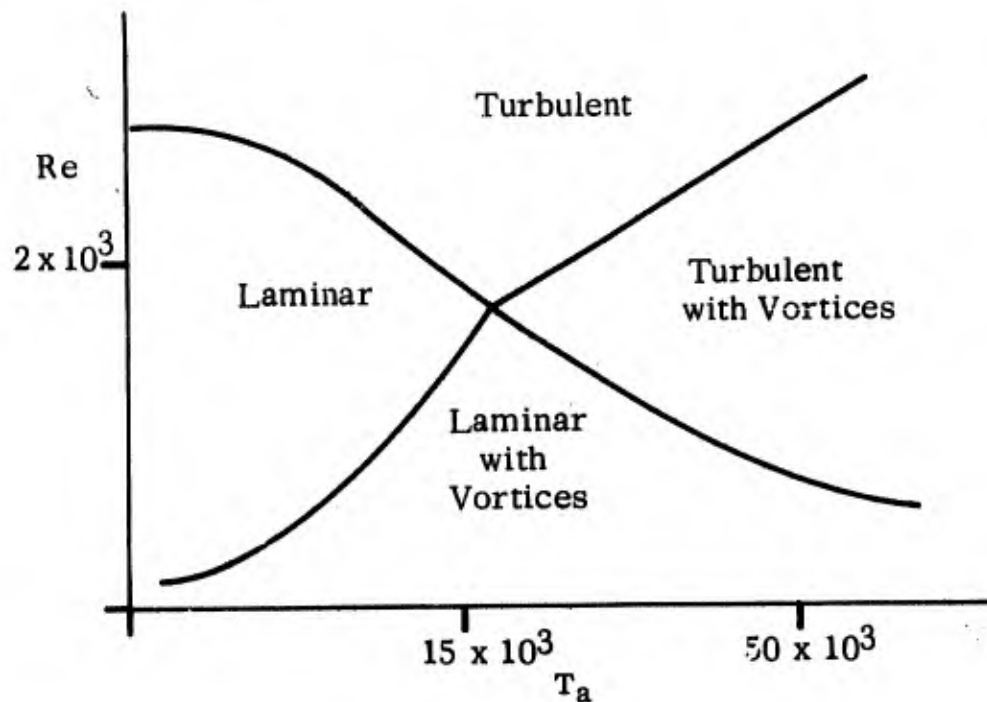


Figure 21. Schematic Representation of Different Regions Of Flow in an Annulus

The limits indicated above are only approximate since a large amount of discussion on the exact shape and value of the transition values exist amongst various investigators (Ref. 6). However, it is well established (Refs. 6, 10, and 11) that the vortices do occur above  $Ta \geq 1600$ .

The Taylor Number is the parameter that represents the onset and establishment of a secondary flow phenomenon within the gap known as Taylor vortices. In a higher Taylor number, low Reynolds number situation, these cells of fluid rotating in a fixed axial position, as presented below, completely dominate the momentum and heat transfer to the fluid.

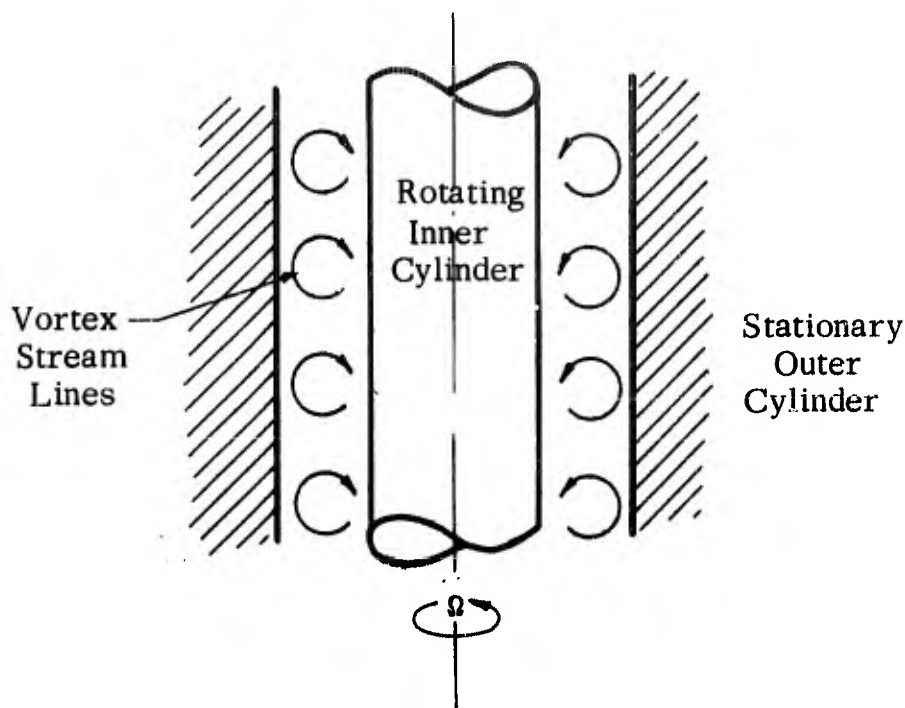


Figure 22. Vortex Pattern in a Rotating Annulus

Continuing the heat transfer work of (Ref. 9), papers by Bjorklund and Kays (Ref. 12), Tachibana and Fukui (Ref. 6), and Becker and Kaye (Ref. 11), established a Nusselt number versus Reynolds and Taylor numbers correlation for a heated rotating inner cylinder and axial flowing gas stream.

For no axial flow ( $Re = 0$ ), Bjorklund (Ref. 12) and Tachibana (Ref. 6) correlated the data in the range ( $1600 \leq Ta \leq 10^{10}$ ) within 15% of each other. Becker (Ref. 11) independently not only repeated Tachibana's (Ref. 6) data for  $Re = 0$  within 5%, but showed that for a constant Reynolds number, the data tends asymptotically to the zero Reynolds number correlation, for sufficiently high Taylor numbers.

For the present case under analysis, the Taylor number is approximately  $10^{10}$ , while the axial flow Reynolds number is approximately  $10^4$ . Thus, based on the information presented above, it was confidently assumed that the Taylor number does control and that the gap Nusselt number defined as:

$$Nu = \frac{2 h b}{k}$$

where

$h$  = the film coefficient of the inner and outer cylinder can be represented by (Ref. 7)

$$Nu = .42 [Ta \cdot Pr]^{1/4}$$

using this correlation, and the properties of gaseous helium at 18° F with the following geometry a film coefficient in the gap of 118 Btu/hr-ft<sup>2</sup>-° R was calculated.

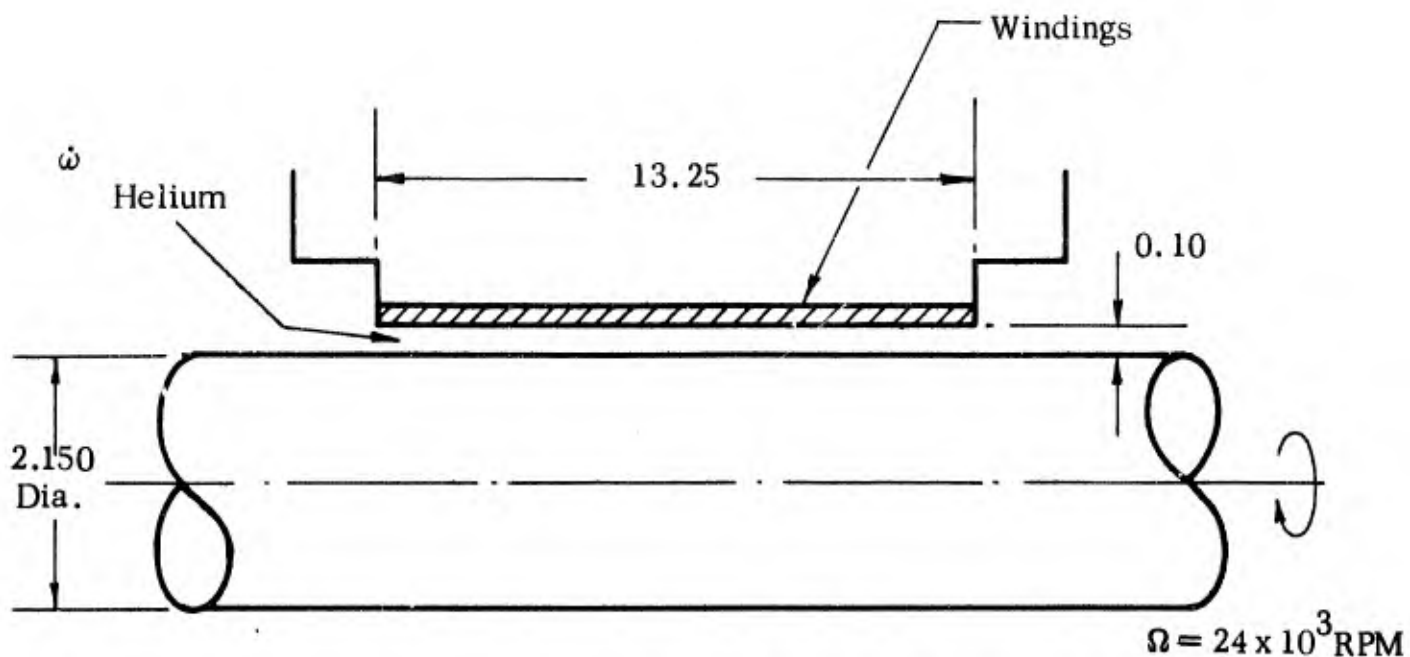


Figure 23. Geometry Used for Calculating Gap Film Coefficients

### 3.2.5.5 Heat Transfer Analysis of the Armature Windings

Physically, the heat transfer can be broken down into the following parts: heat generation in the superconducting armature windings due to time varying current and magnetic fields; the transfer of part of this heat to the gas flow by convection; the transfer of the remainder to the surrounding armature frame by conduction; convective heat transfer between the frame and the fluid; and, finally, the heat generation in the gas due to frictional heat generation (windage). A simplification of the many and complex heat paths can be achieved by assuming that the armature windings are set in the armature frame material as shown in Figure 24.

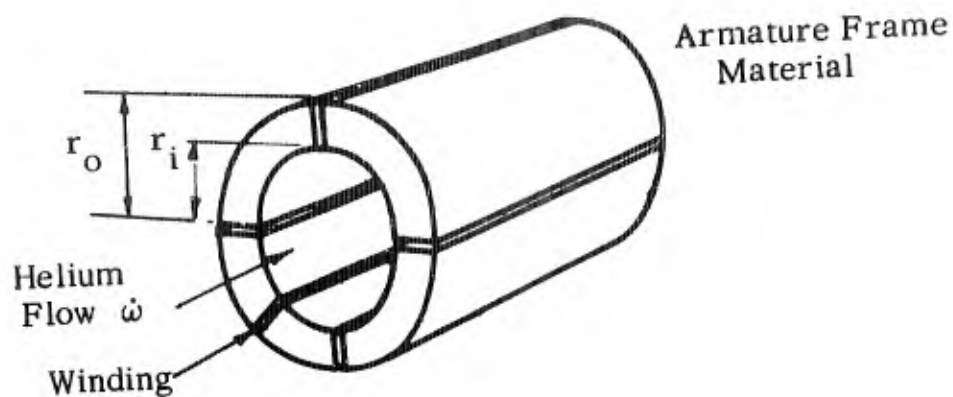


Figure 24. Armature Model

Consider one winding with the dimensions shown in Figure 25.

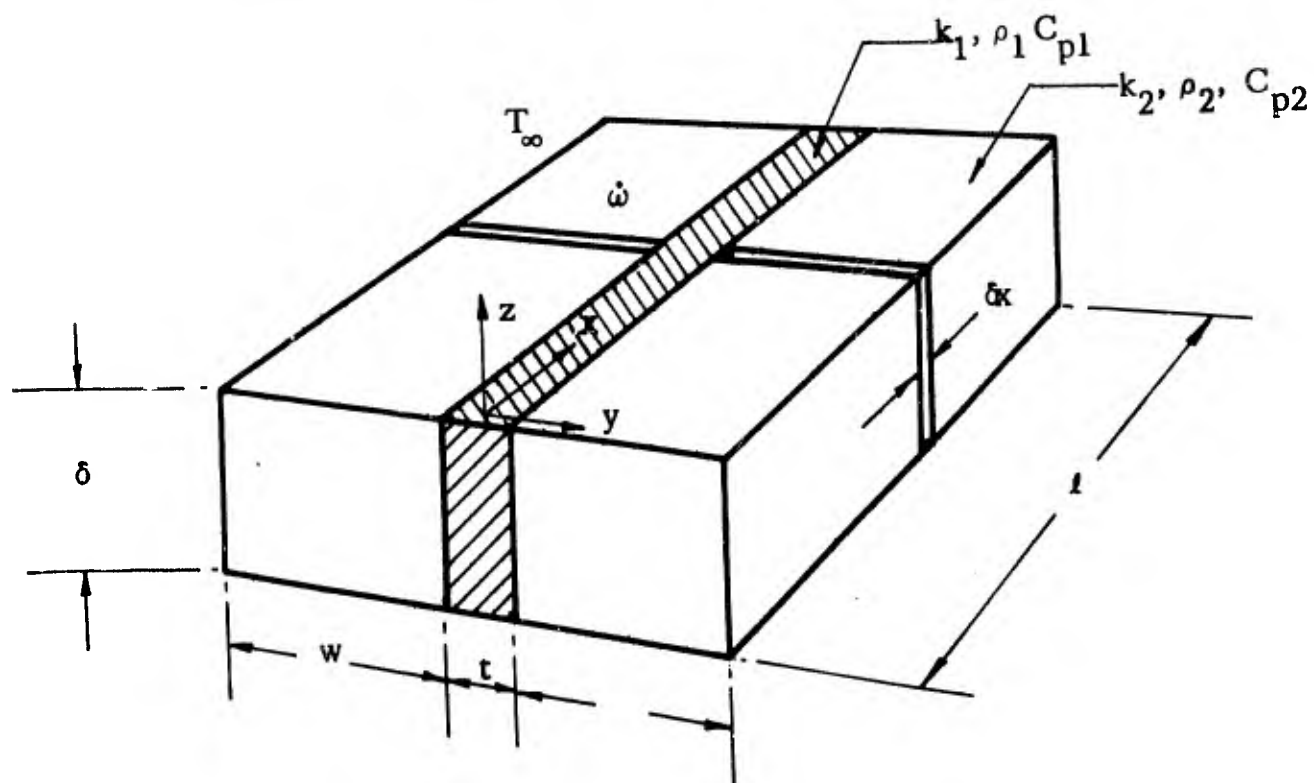


Figure 25. One Winding Model

Thus,  $2\pi r_o \cong n(2W)$  for  $t \ll W$ , where  $n$  is the number of windings. Based on this typical element, it was assumed that the heat uniformly generated per unit length in the winding is convected from its surface and conducted in the  $y$  direction to the armature frame material. The armature frame is assumed to be made of a series of layers  $\delta x$



thick which are insulated in the x direction from each other, thus having negligible axial heat flow. The material 2W wide is assumed to act like a fin attached to the winding through a zero contact resistance bond. The heat from the winding is then lost to the fluid flowing over the surface of the winding and armature frame at the rate  $\dot{Q}$ , as set forth in the previous section. Based on this model which incorporates the following assumptions:

In the winding:

- a. no z temperature dependence
- b. insulated surface at  $z = 0$
- c. constant properties

In the armature frame material:

- a. no z temperature dependence
- b. no axial (x) heat conduction  $\partial T / \partial x = 0$
- c. insulated surface at  $z = 0$
- d. constant properties
- e. temperature symmetric with y; at  $y = W$ ;  $\partial T / \partial y = 0$

In the fluid:

- a. constant velocity
- b. constant properties at 18° R (7)
- c. no axial conduction
- d. perfect gas

the following set of differential equations were derived:

For the winding and the armature frame material

$$\frac{\partial^2 T_1}{\partial x^2} - N_1^2 \left(1 + \frac{2W\xi}{t}\right) (T_1 - T_\infty) + \frac{q_1}{k_1} = 0 \quad (1a)$$

where

$$N_1^2 \equiv \left[ \frac{h}{k_1 \delta} \right]$$

Fin efficiency (Ref. 13)

$$\xi = \frac{\tanh N_2 W}{N_2 W} \quad (1b)$$

where

$$N_2^2 \equiv \left[ \frac{h}{k_2 \delta} \right]$$

The fluid

$$\frac{\partial T_\infty}{\partial x} = \frac{2Wh\xi}{\omega C_p} (T_1 - T_\infty) + \left( \frac{Q_\infty}{n l} \right) \frac{1}{\omega C_p} \quad (2)$$

An estimation of the conduction in the winding shows that it is of the order of less than 1% of the total heat loss. By assuming that

$$\frac{\partial^2 T_1}{\partial x^2} \cong 0$$

the following sets of equations are obtained

$$\left( \frac{h}{\delta} \right) \left[ 1 + \frac{2W\xi}{t} \right] (T_1 - T_\infty) = q_1 \quad (3)$$

$$\frac{\partial T_\infty}{\partial x} = \frac{2Wh\xi}{\omega C_p} (T_1 - T_\infty) + \frac{Q_\infty}{n l \omega C_p} \quad (4)$$

with boundary conditions that

$$\begin{aligned} @ x = 0 \quad T_1 &= T_o \\ T_\infty &= T_\infty(o) \end{aligned}$$

$$\begin{aligned} @ x = l \quad T_1 &= T_l \\ T_\infty &= T_\infty(l) \end{aligned}$$

The solution for the winding temperature, Equation (3), can be easily carried out, with the result

$$T_1 - T_\infty = \frac{q_1}{h} \frac{\delta}{\left( 1 + \frac{2W\xi}{t} \right)} \quad (5)$$

which is independent of  $x$ . Substituting for  $q_1$ :

$$q_1 = \frac{Q_1}{n t \delta \ell} \quad (6)$$

and noting that

$$\frac{2W}{t} \gg 1.0$$

The solution reduces to

$$\Delta T_1 \equiv (T_1 - T_\infty) = + \frac{Q_1}{2h(\ell W) \xi n} \quad (7)$$

Thus,  $(T_1 - T_\infty)$  is a constant for any  $x$ , and the heat lost per unit area of surface is also constant.

Returning to the equation for the fluid, and substituting for  $(T - T_\infty)$ ,

$$\frac{\partial T_\infty}{\partial x} = \frac{\xi Q_1}{n \ell \xi \omega C_p} + \frac{Q_\infty}{n \ell} \quad (8)$$

Integrating between 0 and  $\ell$

$$\Delta T_\infty \equiv [T_\infty(\ell) - T_\infty(0)] = [Q_1 + Q_\infty] \frac{1}{n \omega C_p} \quad (9)$$

The total heat transfer to the fluid is

$$Q_{\text{Total}} = n \omega C_p [T_\infty(\ell) - T_\infty(0)] = Q_1 + Q_\infty \quad (10)$$

Equation (7) can be averaged to give a length average winding temperature

$$T_m = \frac{1}{\ell} \int_0^\ell T(x) dx = T_\infty(0) + \Delta T_1 + \frac{\Delta T_\infty}{2} \quad (11)$$

Equations (1b), (9), (10) and (11) will be used to generate a relationship between  $T_\infty(0)$ ,  $T_m$ ,  $\omega$ , and  $k_1$ ;  $k_1$  is left as a variable since at the time of the study a specific armature frame material has not been chosen.

### 3.2.5.6 Heat Transfer Away From the Sides and Outer Diameter of the Armature

The film coefficient along the sides and outer diameter of the armature can be predicted by the correlation for fully developed turbulent flow in a duct (Ref. 7).

$$Nu_D = .023 Re_D^{0.80} Pr^{.40}$$

The only problem area in the cooling of the outside of the armature could arise in the corner areas. Local hot spots could arise due to a local lowering of the film coefficient, dependent on flow passage design and the Reynolds number of the flow. An experimental study by Ede (Ref. 8) presents a study of these two effects on the local Nusselt number in the bend. He showed that at the point of the bend, an increase in Nusselt number always takes place for laminar to turbulent Reynolds numbers, the increase being greater the sharper the bend. Since, for a constant wall heat flux, Nusselt number is inversely proportional to wall temperature, this indicates a local lowering of wall temperature. However, shortly downstream of the bend a local decrease in Nusselt number occurs, in the flow separation portion, causing a local increase in wall temperature. This occurs at a location nearer the bend for larger Reynolds numbers and smoother bends. The magnitude of this decrease increases as the bend becomes smoother and the Reynolds number lower. This effect is approximately schematically represented:

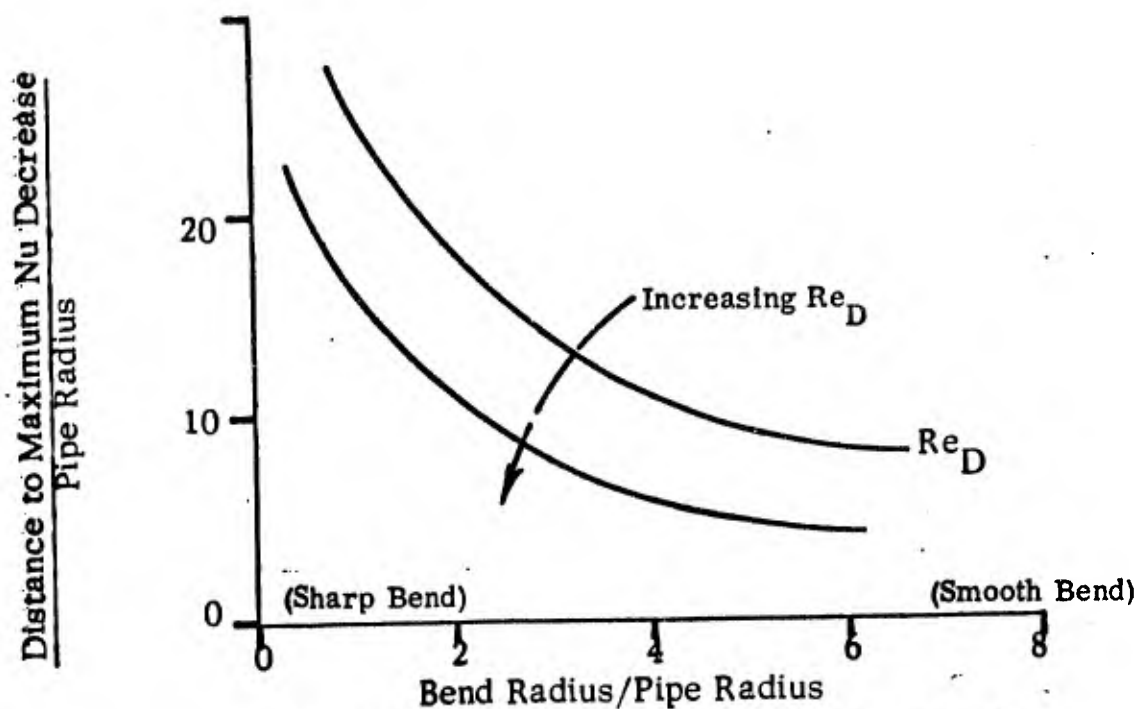


Fig. 26. Local Nusselt Number in a Bend.

The magnitude of the increase in  $Nu$  at the bend can be as high as 200% at laminar Reynolds numbers, while the maximum decrease is about 30%. The exact value is strongly dependent of the exact conditions.

As applied to the armature cooling, this means to reduce the chances of a hot spot, the cooling flow should be highly turbulent and the passage sharp.

### 3.2.5.7 Numerical Evaluation

The present design case involves the following values:

$\delta$	=	.090"	$T_m$	=	18° R
$t$	=	.003"	$\dot{Q}_1 n$	=	100 Btu/h
$w$	=	.033"	$Q_\infty$	=	85 Btu/hr
$c$	=	13.25"	$C_p$	=	1.30 Btu/lbm-° R
$r_o$	=	1.375"	$k_1$	=	variable
$n$	=	132	$h$	=	118 Btu/hr-ft <sup>2</sup> -° R

The results of the evaluation appear in Figures 27 and 28. Basically, the asymptotic value of  $T_\infty$  versus  $k_1$  is due to the fact that the frame material fin is "short" and "fat", thus efficient for any value of  $k_1$  greater than 1.0 (Ref. 13). Therefore, for  $k_1 = 1.0$  and  $\omega = 25$  lbm/hr, a helium inlet temperature of 14° R with a  $\Delta T_\infty$  of 5.8° R is sufficient to remove 185 Btu/hr total heat load.

By assuming  $k_1$  is high enough so that  $\xi = 1.0$ , the equations can be solved to relate  $Q_{Total}$ ,  $\omega$ ,  $T_\infty(0)$  and  $T_\infty(\ell)$ . This result is shown in Figure 29. The solution assumes that the windage load is constant but that the heat load in the windings can vary. With the same geometry, Figure 29 gives an indication of what a variation in  $T_\infty$  will do to the heat removal rate.

From a practical viewpoint, Figures 27 and 28 show that very little benefit derives from having an armature frame material with a thermal conductivity higher than 1.0 Btu/hr-ft-° R. Indeed, a conductivity of 0.1 Btu/hr-ft-° R only results in a small penalty. This is fortunate for we did not find any practical armature frame materials with conductivities much in excess of 1.0 Btu/hr-ft-° R at 10° K.

### 3.2.5.8 Extension of Analysis to Investigate the Effect of Potting Adhesive Between the Conductors and the Armature Frame

The previous analysis was extended to investigate the effect of potting the conductors into the armature frame with a thin layer of adhesive of variable thermal conductivity. A schematic of the new geometry is shown in Figure 30. Nomenclature is as before, with the addition of ( $k_o$ ) as the thermal conductivity of the adhesive and ( $a$ ) as the thickness of the adhesive layer, with dimensions of [Btu/hr-ft-° R] and [ft], respectively.

The only difference from the preceding analysis is the addition of a series thermal resistance between the conductor and the armature frame material. This thermal resistance will simply be  $1/k_o (a/\delta)$ . The governing equations are given below and correspond to Equations (5), (9), and (11) of the previous analysis:

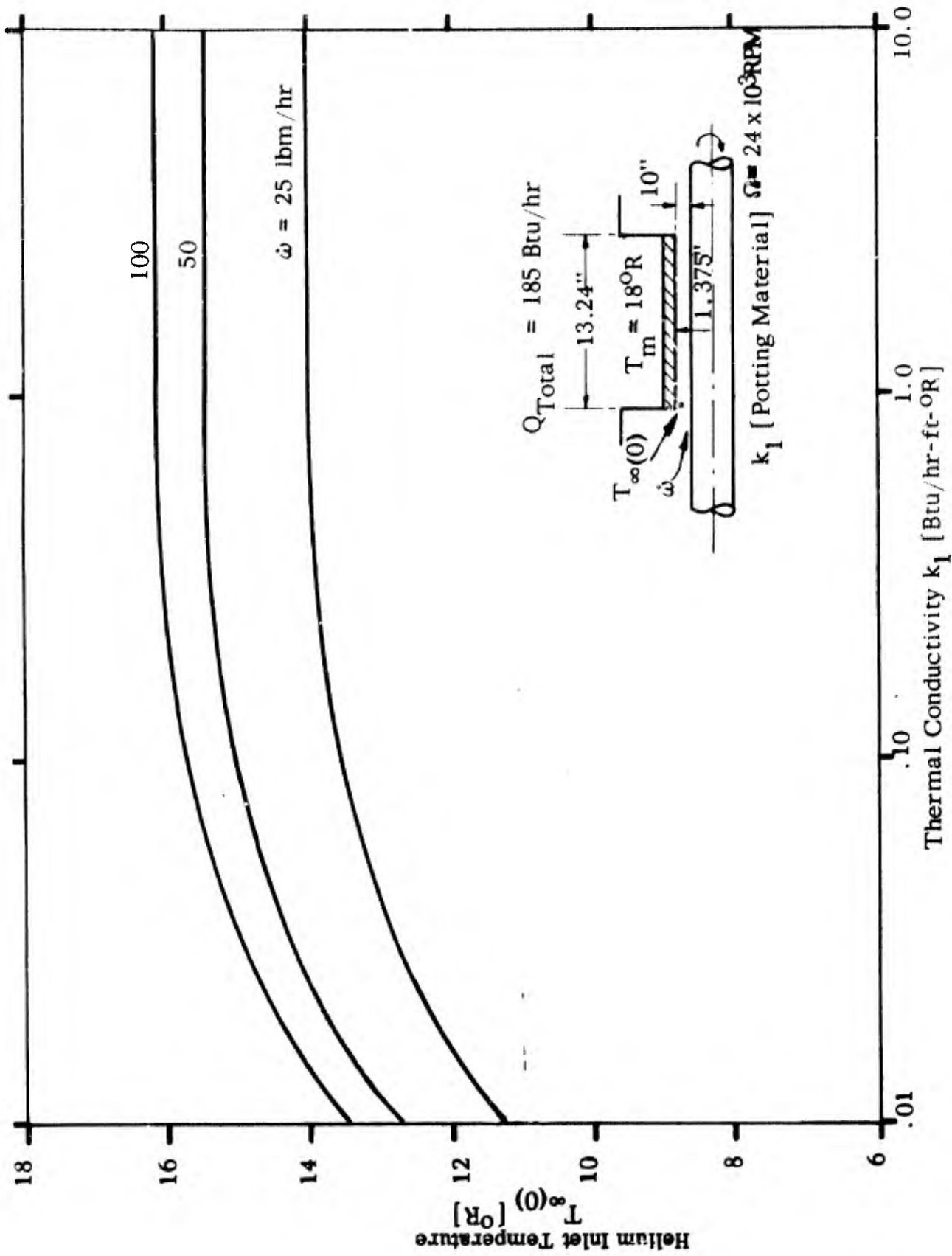


Fig. 27. Helium Inlet Temperature vs. Thermal Conductivity of Armature Frame Material

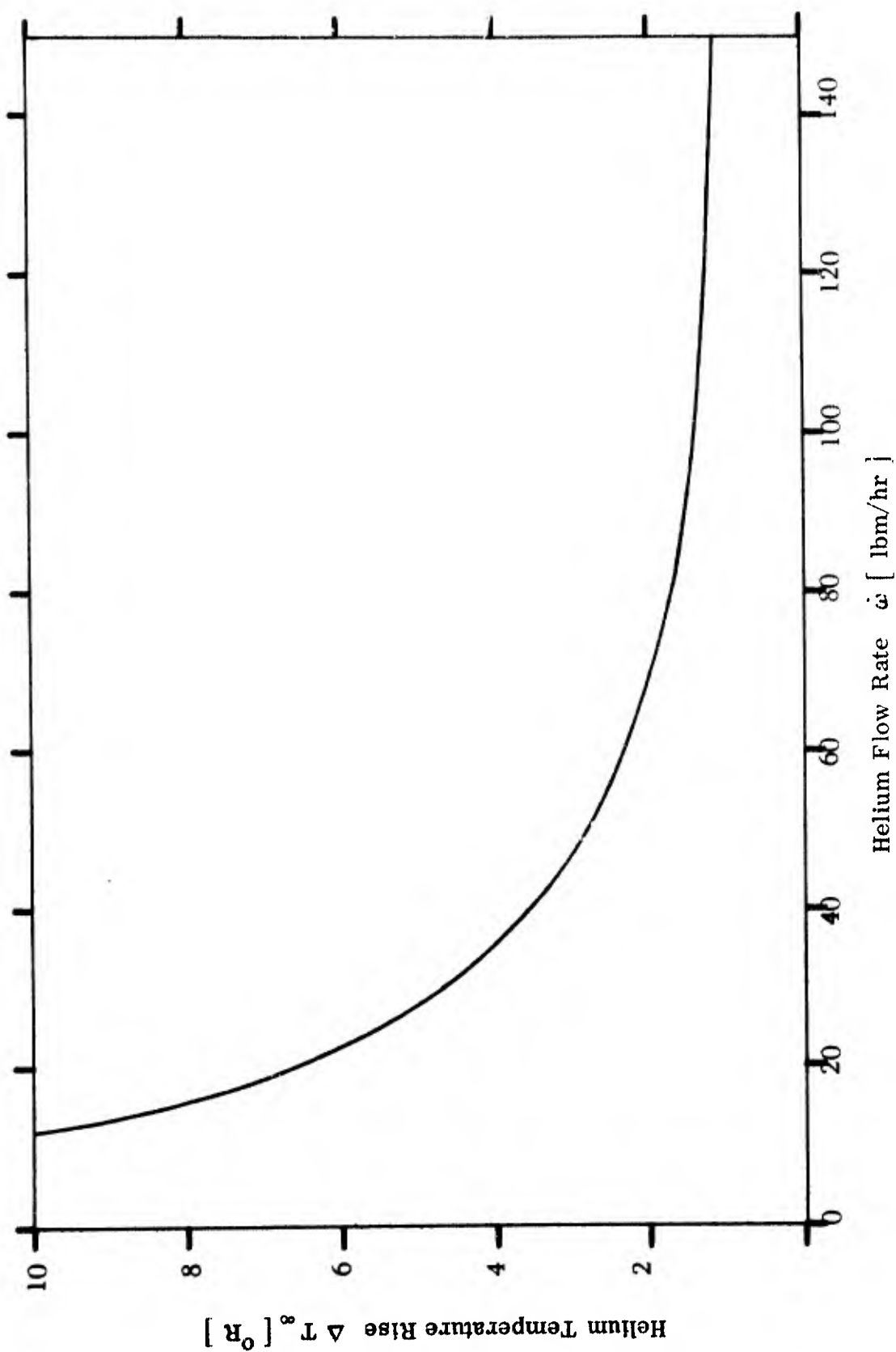


Fig. 28. Helium Temperature Rise vs. Helium Flow Rate

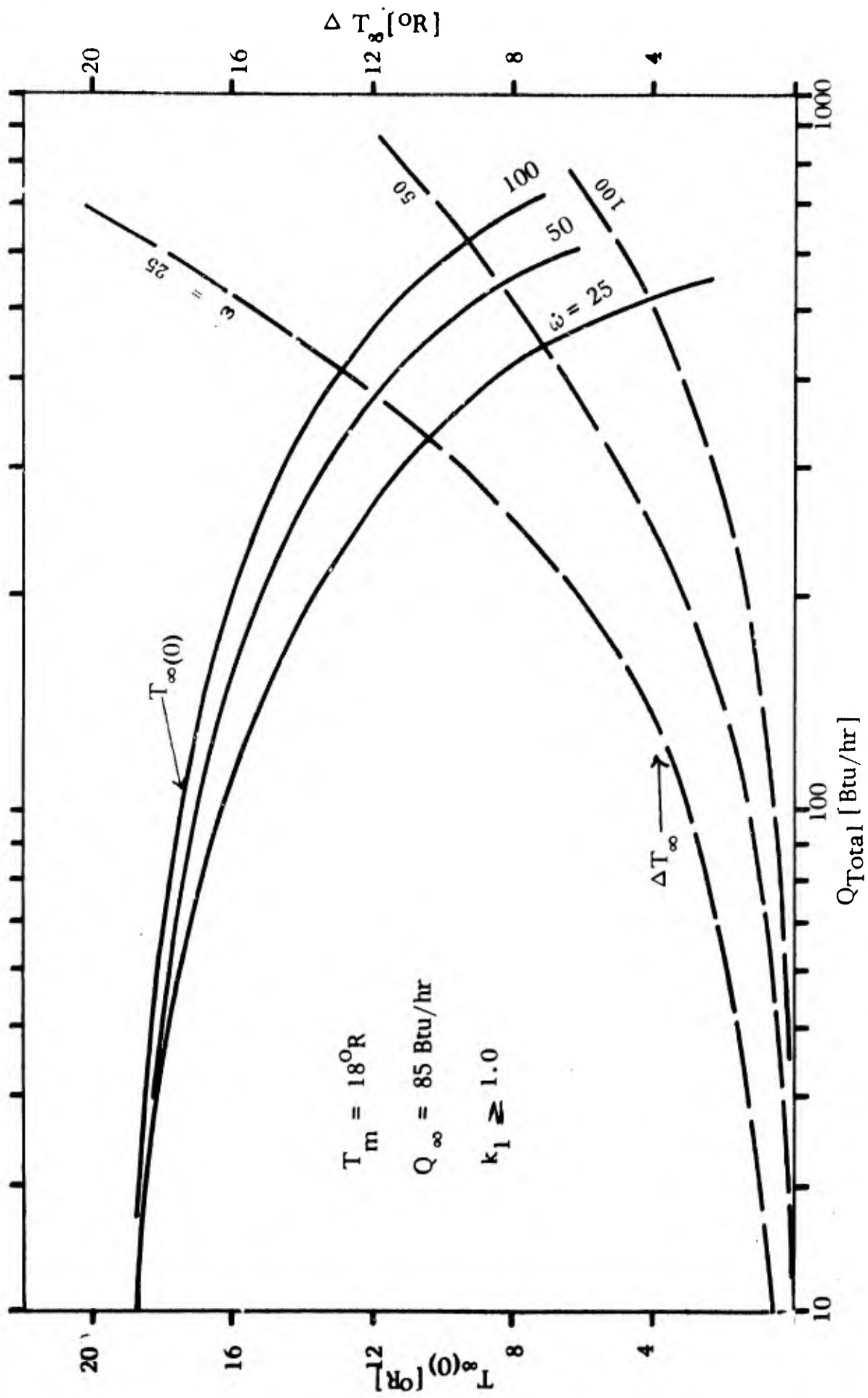


Fig. 29. Helium Inlet Temperature vs. Total Heat Load



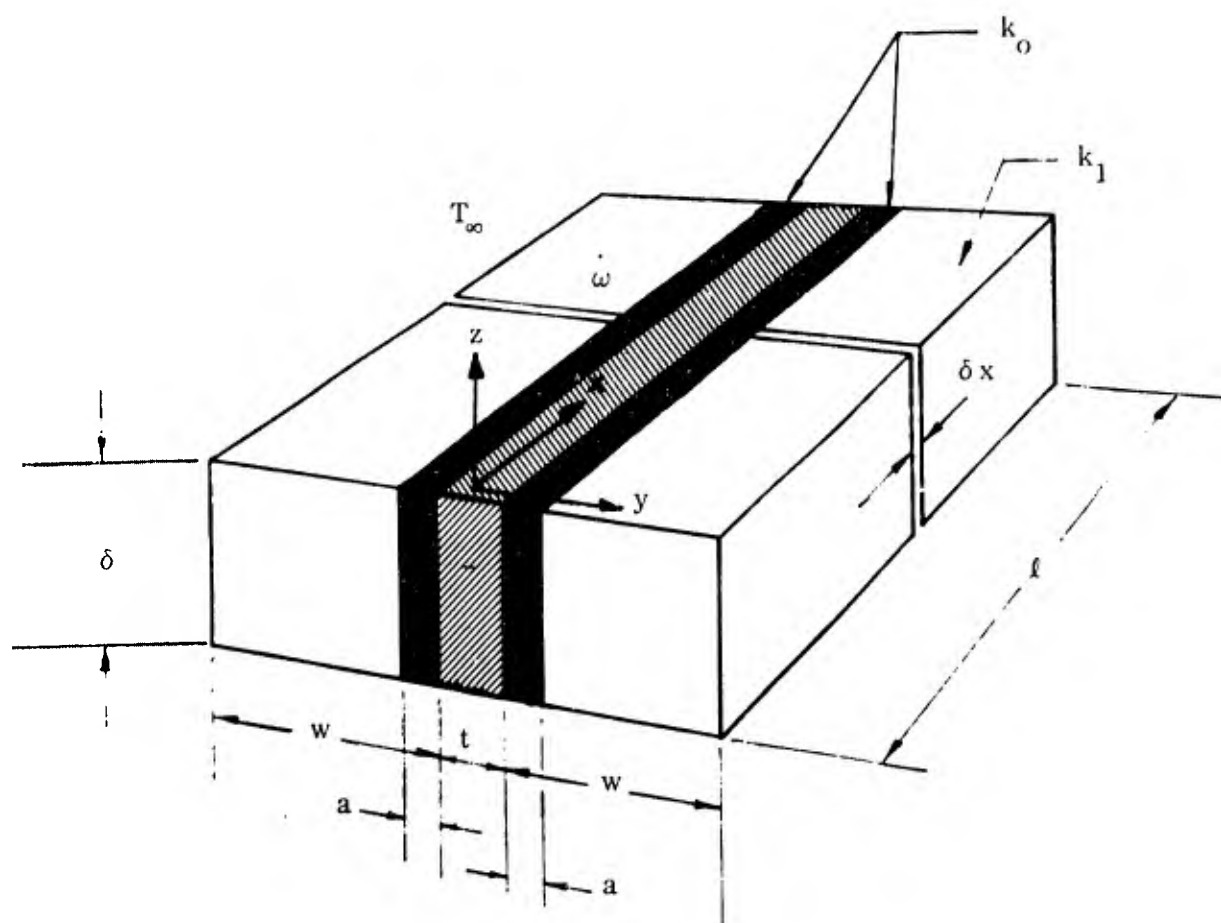


Fig. 30. One Winding Model

$$\dot{w} C_p [T_{\infty}(\ell) - T_{\infty}(0)] = (Q_0 + Q_{\infty}) \quad (1)$$

$$(T_1 - T_{\infty}) = \left( \frac{Q_0}{2\pi r_0 \ell} \right) \frac{1}{h} \quad (2)$$

$$T_m = T_{\infty}(0) + \Delta T_1 + \frac{\Delta T_{\infty}}{2} \quad (3)$$

where

$$\frac{h_{\infty}}{h} = \frac{1}{\xi} + \left( \frac{a}{\delta} \right) \frac{Wh_{\infty}}{k_0} \quad (4)$$

(Nomenclature and geometry are given in the previous section)

If the frame material is assumed to have a thermal conductivity equal to or greater than 1.0 Btu/hr-ft-° R (10° K), then from the previous analysis,  $\xi \approx 1.0$ . Therefore, the evaluation of Equations 1 - 4 may be carried out for a variable  $k_0$  assuming that  $\xi = 1.0$ .

For an armature material thermal conductivity significantly less than 1.0 Btu/hr-ft-° R, it is not permissible to assume  $\xi = 1.0$ . At  $k_0 = 0.10$  Btu/hr-ft-° R,  $\xi = 0.710$ .

The geometry, heats loads, and mean temperature are as in the previous analysis. The results are plotted in Figure 31 for adhesive layer thicknesses of 0.001 inches and 0.010 inches on both sides of the conductor.

Referring to Figure 31, curves A and B show the effect of adhesive thermal conductivity on required helium inlet temperature at two different layer thicknesses. Curve C shows the effect of armature frame thermal conductivity for those cases where the effect of the adhesive layer is insignificant. Curve D shows the effect of varying adhesive thermal conductivity of 0.10 Btu/hr-ft-° R and an adhesive layer thickness (a) of 0.001 inches. Curve E shows the same conditions with an adhesive layer thickness of 0.003 inches.

The curves clearly show that the thickness of the adhesive layer is more significant than the thermal conductivity of either the armature frame material or the adhesive. A drop in frame material conductivity to 0.10 Btu/hr-ft-° R only lowers the maximum permissible coolant inlet temperature by about 0.5° R. For  $a = 0.001$  inches, the adhesive has virtually no effect on inlet temperature as long as its thermal conductivity is above 0.01 Btu/hr-ft-° R.

From test results reported in Section 3.2.4 the thermal conductivity of the boron nitride armature frame is between 0.20 and 0.40 Btu/hr-ft-° R at 18° R (10° K). This value was measured parallel to the pressing direction. Test data by other investigators at higher temperatures indicate that the thermal conductivity perpendicular to

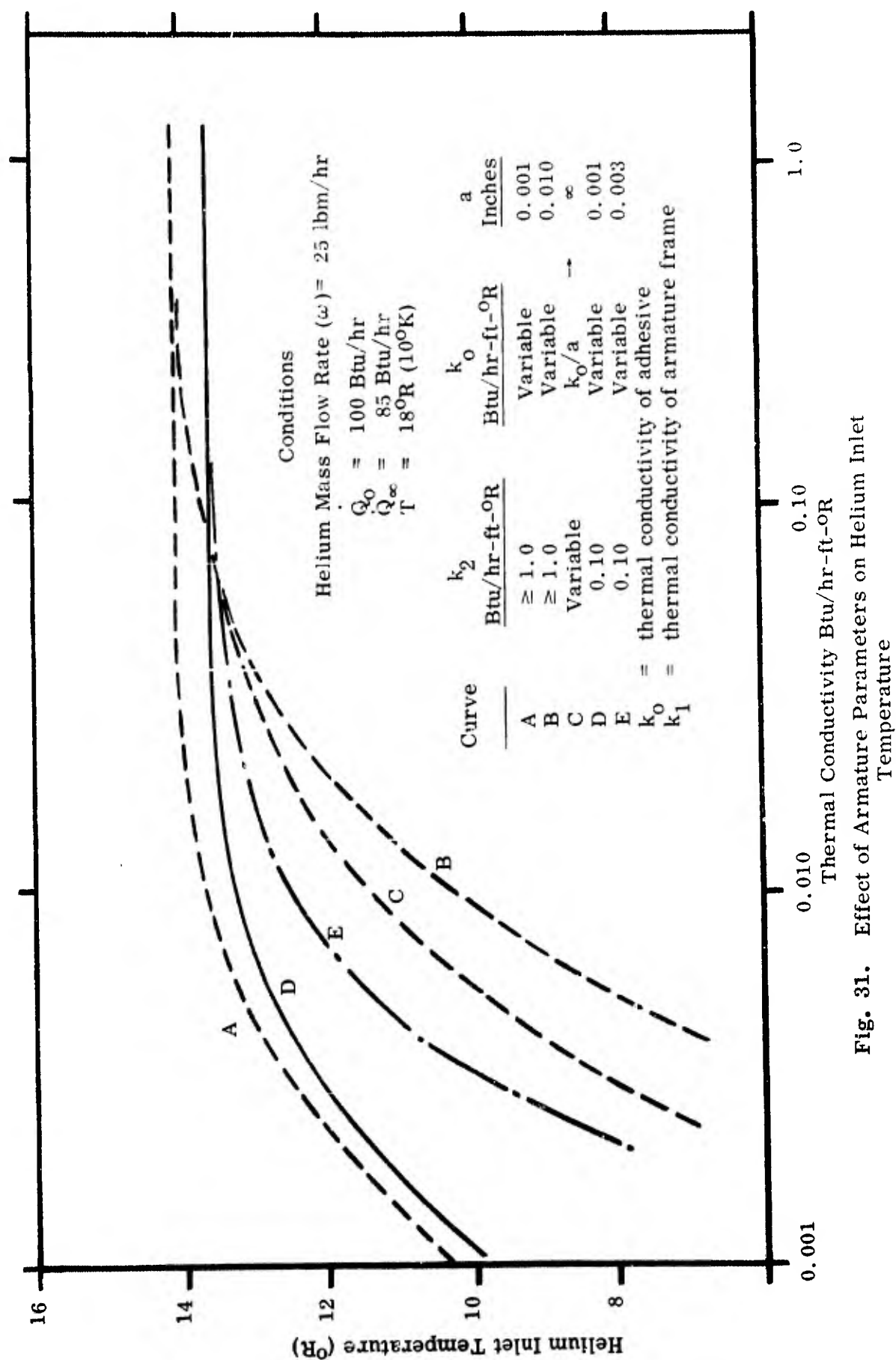


Fig. 31. Effect of Armature Parameters on Helium Inlet Temperature

the pressing direction is higher by a factor of two. Therefore, the total possible range of thermal conductivity at 18° R is from 0.20 to 0.80 Btu/hr-ft-° R. The slots in the armature frame are cut with a five-thousandths inch thick slitting saw. The total width of the slots varies between six and eight thousandths of an inch. Since the conductor is about three thousandths thick, the adhesive layer on each side will average one-and-a-half to two-and-a-half thousandths of an inch in thickness. The thermal conductivity of the adhesive has not been measured, but is expected to be about 0.01 Btu/hr-ft-° R at 18° R. Therefore, Figure 31 suggests that the coolant inlet temperature will have to be kept below about 13° R to maintain an average conductor temperature of 18° R at the given thermal loading and coolant flow. In general, for these conditions, the armature will operate somewhere in the region bounded by curves A and E.

#### 3.2.5.9 Armature Conductor Cooling Test

The purpose of this test was to obtain an order-of-magnitude verification of the results of the foregoing analysis. The materials and geometry were maintained as close to those of the generator as was practically feasible. The only departure was the use of Nichrome heater wire instead of superconducting ribbon.

The test apparatus (Fig. 32) consisted of a piece of boron nitride with slots cut in it having the same spacing as that in the generator armature frame. Nichrome heater ribbon was potted into these slots to act as a source of heat. This test piece was mounted in a vacuum-jacketed test apparatus with a flow of cold helium gas over the surface to simulate the coolant stream. Instrumentation consisted of a helium gas thermometer to measure the mean temperature of the boron nitride and a multiple-junction differential thermocouple to measure the temperature difference between the conductor and the surface of the test piece. The thermocouple materials were gold + 2.1 atomic % cobalt vs. copper.

The results of the test are shown in Figure 33 in terms of temperature differential vs. power loss density (watts/sq. inch of conductor surface area). Present calculations indicate that the full-load power loss density of the model (50 kva) generator in the active region of the armature is 0.3 watts/sq. inch. Figure 33 indicates that this will produce a temperature differential of 0.8° K between the surface of the armature frame and the bottom of the conductor. This is considered a perfectly acceptable value.

#### 3.2.5.10 Armature Cooling Test

The heat transfer coefficient along the ends and the outer diameter of the armature can be predicted as a function of the Reynolds number and Prandtl number. An experimental study by Ede has indicated that local hot-spots can develop on the lee side of a bend in the flow passage. This hot spot occurs as a result of a lowering of the film heat transfer coefficient where the flow tends to separate from the surface following the bend. The situation is more pronounced at lower Reynolds numbers and for larger bend radii. The local heat transfer coefficient can be reduced by as much as 30% under the worst conditions.

A test was conducted to determine the adequacy of the armature ducting to direct the coolant flow over the ends and outer diameter of the armature and prevent the occurrence of hot-spots. The test was performed using a model of the armature

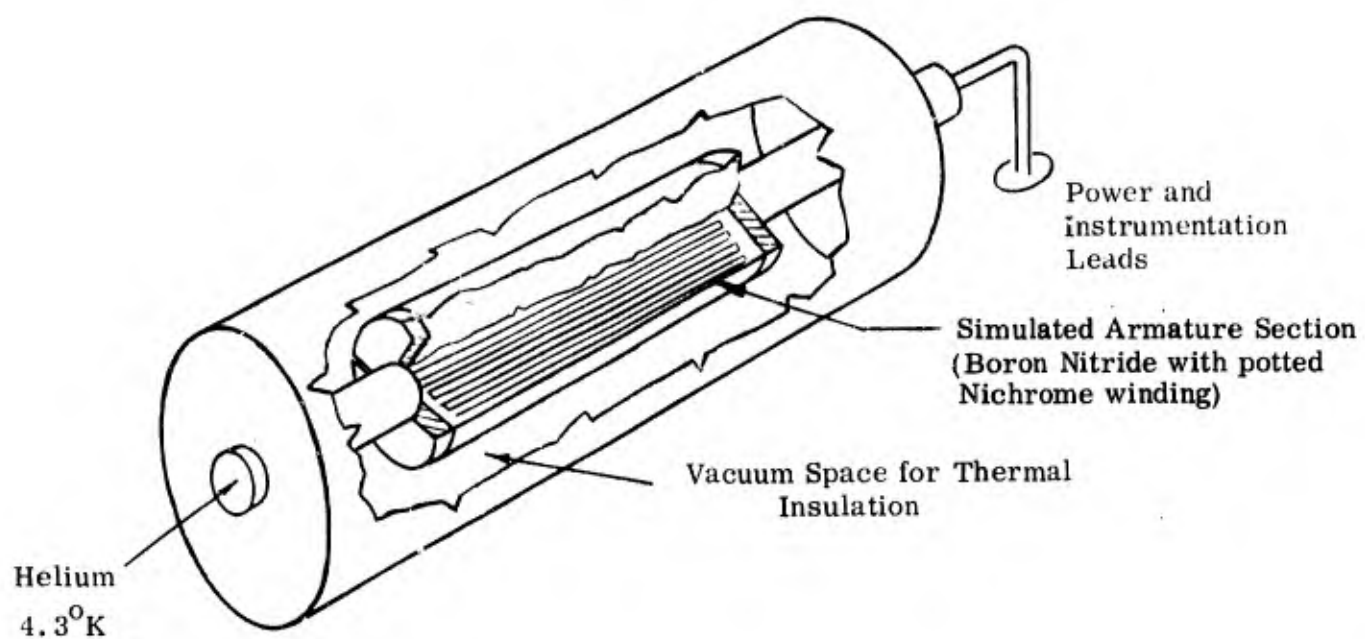


Fig. 32. Armature Conductor Cooling Test Apparatus

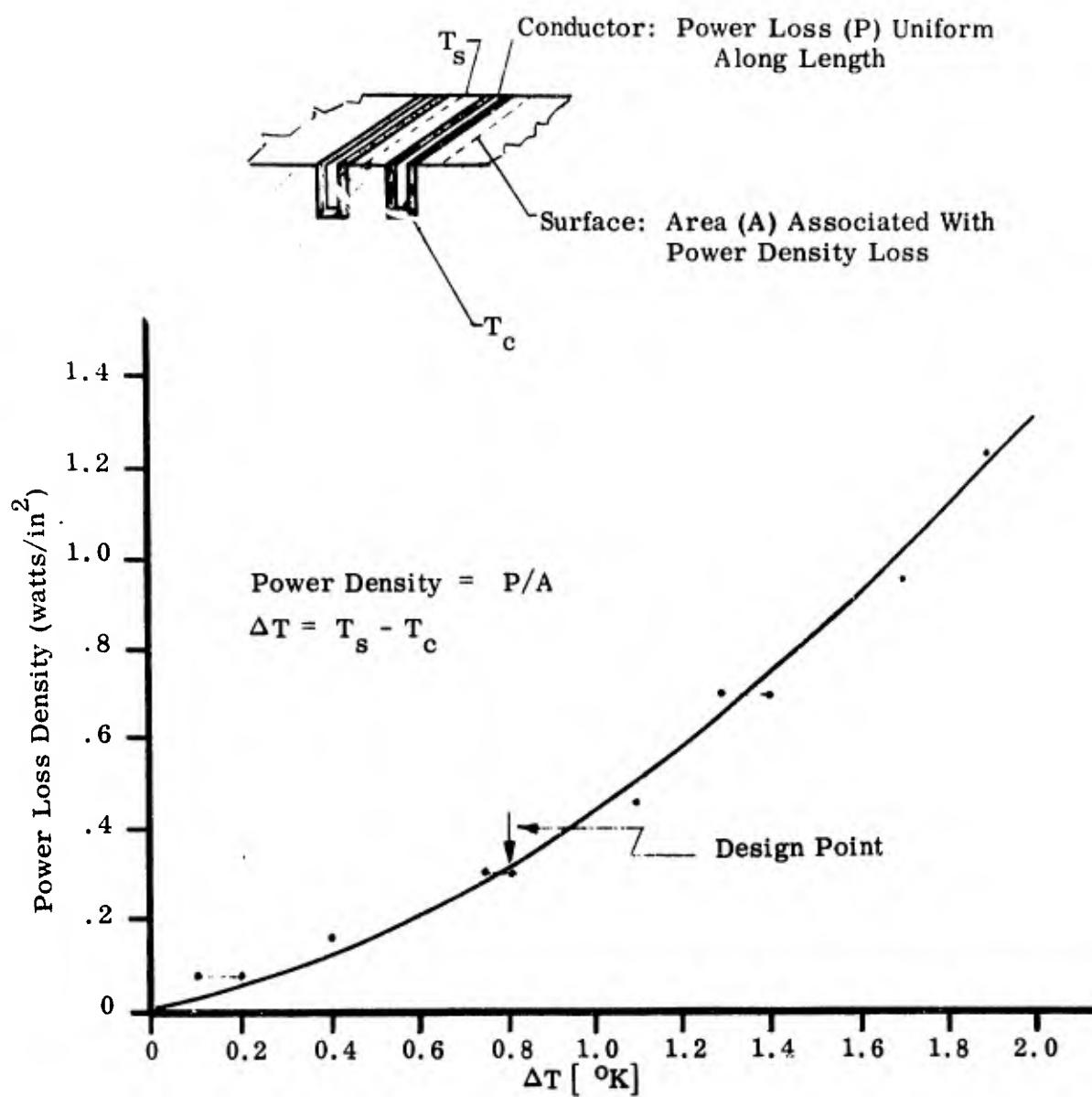


Fig. 33.  $\Delta T$  vs. Power Loss Density

model. Air was blown through the ducting to provide the cooling. The air flow rate was adjusted to match the Reynolds number of the test flow to the actual helium flow.

The ducting arrangement is shown schematically in Figure 34. The location of the thermocouples is also shown. The areas of interest are at the inlet, following the corners on the end of the armature, and at the outlet where the flow makes a sharp turn toward the exhaust. The thermocouples are all located directly under a heat wire and electrically insulated from the heater.

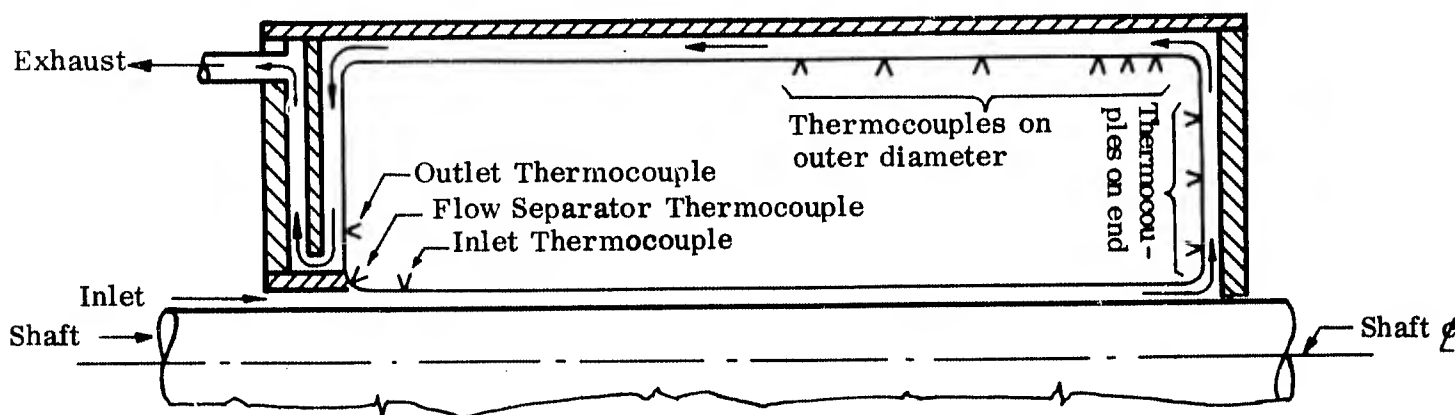


Figure 34. Ducting Schematic

The results of the test are shown in Figure 35. The two curves indicate the readings taken on two different sets of thermocouples located  $180^\circ$  apart on the armature model. Even accepting the reading error, the variation in temperature along the ends and outer diameter is within  $1.5^\circ \text{K}$  and this was with a heat generation in this area of 30 watts or approximately 1-1/2 times the heat generation in actual machine in this same area.

### 3.2.6 Other Sources of Heat Transfer Into the Intermediate Stage Structure

#### 3.2.6.1 Radiation From the Outer Casing

The outer casing is at approximately  $300^\circ \text{K}$ . The intermediate structure (radiation shield and liquid-nitrogen-cooled flanges) have a mean radiation temperature from a radiation standpoint of about  $90^\circ \text{K}$ . Thermal radiation transfers about 50 Btu/hr from the outer casing into the intermediate structure.

#### 3.2.6.2 Convection from Outer Chamber

If we assume that the main component of the residual gas in the vacuum space is helium, then convection will transfer  $53 p \text{ Btu/hr}$  from the outer chamber to the intermediate structure, where  $p$  is the pressure in microns of mercury. During operation, pressure in the vacuum space of the prototype generator is usually  $10^{-4} \text{ Torr} = 0.1 \text{ micron}$ . Therefore, heat transferred into the intermediate structure by convection would be about 5.3 Btu/hr.

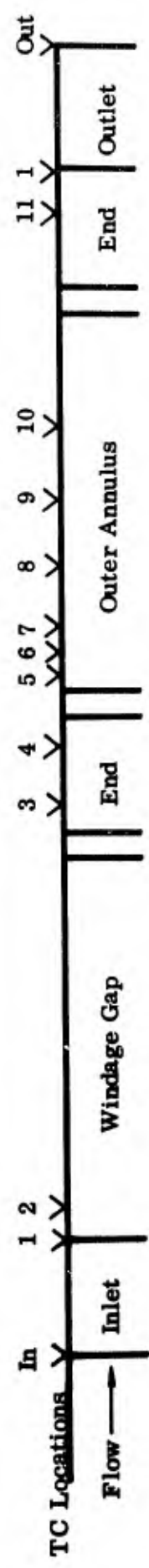
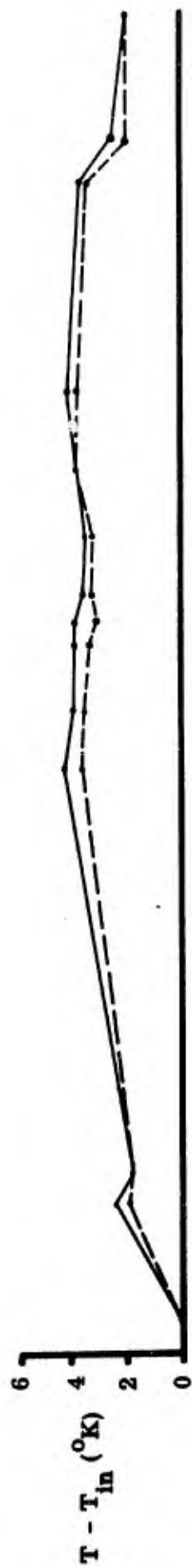


Fig. 35 Armature Cooling Test Results



### 3.2.6.3 Conduction From Connecting Tubes and Convection From Shaft

Heat is conducted down the connecting tubes into the intermediate structure (the liquid-nitrogen-cooled flanges). In addition, heat is removed from the shaft at this point by convection across the "air" gap between the shaft and the interior of the connecting tubes. The total heat input to the intermediate structure from these causes is calculated to be 120 Btu/hr (both ends).

### 3.2.6.4 Boiling Heat Transfer Between Liquid Nitrogen and Iron Return Path

The iron return path has eddy and hysteresis losses of 85 Btu/hr (25 watts). This is removed by direct contact with liquid nitrogen inside the return path container.

### 3.2.7 Other Sources of Heat Transfer Into the 10° K Region

#### 3.2.7.1 Radiation From Intermediate Temperature Structure

With the intermediate structure at a mean radiation temperature of 90° K, radiating to the inner chamber at 10° K, about 0.7 Btu/hr will be transferred into the 10° K region.

#### 3.2.7.2 Convection From Intermediate Temperature Structure

With the same assumptions as in Section 3.2.6.2, convective heat transfer will be 54 (p) Btu/hr, where (p) is pressure in the vacuum space in microns of mercury. Therefore, at an operating pressure of 0.1 micron ( $10^{-4}$  Torr), 5.4 Btu/hr of heat will pass into the 10° K region by convection.

#### 3.2.7.3 Conduction Along Shaft and Connecting Tubes (Shaft Closures)

Conduction along the shaft (from both ends) will transfer a total of 15.0 Btu/hr into the 10° K region. The connecting tubes contribute a total of 7.6 Btu/hr.

#### 3.2.7.4 Conduction and Radiation From Iron Return Path Enclosure

The heat in flux from the return path enclosure into the 10° K region is difficult to estimate. This item was fabricated by an outside vendor, and some details of its construction are not known. A conservative estimate places the heat transfer from this component into the 10° K region at a total of 3.4 Btu/hr, most of which is due to conduction through supports.

### 3.3 Mechanical Design

The design of the prototype superconducting generator is shown in somewhat simplified form in Figure 36. The major subassemblies are the environmental chamber, the drive shaft assembly, and the drive.

#### 3.3.1 Environmental Chamber

The requirement to provide a 10 - 12° K region for the superconductors with a minimum of heat leak requires that a vacuum chamber be provided operating

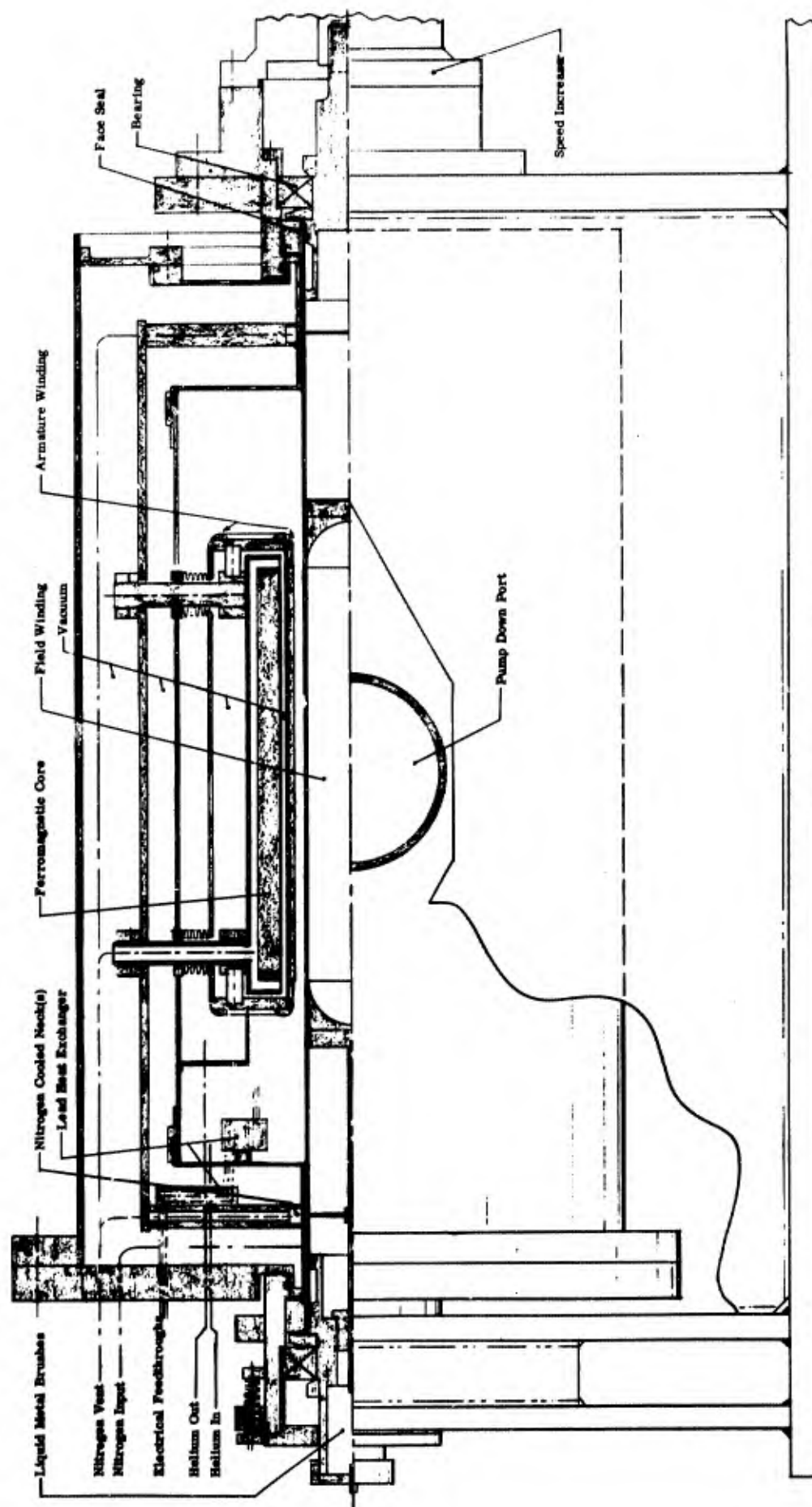


Fig. 35. General Assembly of 50 kva Laboratory Model Superconducting Generator

at  $10^{-5}$  to  $10^{-6}$  torr. The two horizontal necks through which the shaft penetrates are provided with liquid nitrogen cooling to minimize the heat leak to the  $10^{\circ}$  K region. A nitrogen-cooled baffle is also provided to remove the radiational heat leak from ambient.

Electrical and windage loss calculations were made for a number of design configurations using recommended superconductor design ratings. These studies led to the conclusion that a ferromagnetic flux return path would minimize total losses. The flux return core structure is maintained at  $80^{\circ}$  K by cooling with nitrogen. In an operational unit this cooling would be provided by the upper stage of a two stage refrigerator. The core chamber shell in contact with the  $10 - 12^{\circ}$  K region is made of a synthetic plastic material developed by Hofman Laboratories. The use of this non-conducting material eliminates eddy current losses in the chamber walls which is an especially important consideration since the core chamber is used as the mounting for the armature.

The core chamber is supported from the nitrogen baffle by six studs. This arrangement provides for concentricity adjustment between the field and armature. Liquid nitrogen is fed to the iron core and vented through two hollow studs. Since the evacuated region of the core chamber is connected to the main chamber through bellows which encircle the support studs, a vacuum joint must be made at the bottom end of the stud and the bottom of the tubed hole with Indium and producing a cold weld when the stud is bottomed in the hole.

The chamber is designed to be disassembled in stages for various contingencies which may be encountered in early prototype testing. The joints on the warm walls are sealed with o-rings. The cold wall disassembled joints are Indium soldered using band heaters. Helium, nitrogen, and electrical feedthroughs are grouped at one end to simplify disassembly operations. Heat is removed from the power leads at  $80^{\circ}$  K and  $10^{\circ}$  K via heat exchangers. In order to achieve proper alignment of the chamber parts, a mandrel is installed to align the two necks when the Indium soldered joints are being made. Chamber heat leaks have been analyzed and are summarized below:

A. Heat leads to  $10^{\circ}$  K region from:

2 Shaft ends (conduction)	15.0 Btu/hr
2 Shaft ends (radiation)	
2 Chamber necks (conduction)	7.6 Btu/hr
Nitrogen baffle (radiation)	0.7 Btu/hr
Core chamber (radiation)	0.1 Btu/hr
Core chamber supports (conduction)	3.3 Btu/hr
Total	26.7 Btu/hr

B. Heat removed by liquid nitrogen from:

2 Shaft ends and 2 chamber necks (conduction)	120 Btu/hr
Iron core (conduction)	140 Btu/hr
Warm wall radiation	50 Btu/hr
Total	310 Btu/hr

Having determined the size and configuration (2 pole) of the field winding (see Section 3.1.1) the mechanical design of the rotor can be undertaken. An important consideration is the rather fragile nature of the superconductor itself. The active region of the superconductor is a thin film made up of a rather brittle intermetallic compound,  $\text{Nb}_3\text{Sn}$ . It is of paramount importance resistance point which would generate heat and "quench" the winding. It was, therefore, decided to install the field in a tube which would serve as the center section of the shaft. The field would be potted in place and the resulting assembly would rely mainly on the tube for structural support.

The length of the shaft between bearing supports was largely determined by the space which was allocated for the armature assembly, outer chamber thermal necks and seals. At the same time, it was necessary to be sure that shaft natural frequencies did not occur near the operating speed of 24,000 rpm.

The first natural frequency was investigated graphically (Ref. 14). Assuming different moments of inertia in two perpendicular planes (in line 10,580 rpm were calculated. Due to the stiffening effect of the potting the lower critical speed did not materialize. The higher one proved to be remarkably accurate as shown by high speed tests employing shaft balancing instrumentation. No reasonable modification in the design enables us to increase the first critical above 24,000 rpm. The second critical can be expected at about 32,000 rpm. We are therefore operating in a good region about midway between the first and second critical speeds.

#### Detailed Design

Having the basic concept of a field mounted inside a hollow shaft and terminated by a solid reduced diameter section on each end, it is now possible to get into the details of the design. A layout of the shaft assembly is shown in Figure 37.

The field is shown mounted in the center of the shaft. Sleeves are provided to center the field winding core in the shaft to prevent gross incorrecable unbalance. The annulus between the winding and the shaft and the region between the winding ends and the heat sinks are vacuum potted to provide mechanical support and to improve thermal contact between the winding and the shaft.

The tubular shaft is .070 inches thick made of stress-relieved 347 stainless steel. This material was selected for its excellent mechanical properties at cryogenic temperatures and because it is not ferromagnetic. A ferromagnetic tube would short-circuit magnetic flux and thus reduce the field seen by the armature.

A stress analysis was made assuming no contributing strength from the field and requiring the tube to withstand the stresses induced by centrifugal loads encountered at 24,000 rpm. The design stress of 28,000 psi compares to a tensile point for 347 at  $-452^\circ\text{F}$  of 236,400 psi. Since materials are relatively brittle at cryogenic temperatures, they are more sensitive to unanalyzable stress concentrations. Thus it is desirable to have a large "factor of safety" as found above.

Another component of stress can be anticipated as the shaft is taken through its critical speed. This stress contribution can only be minimized by carefully balancing the shaft and avoiding sustained operation near the critical speed.

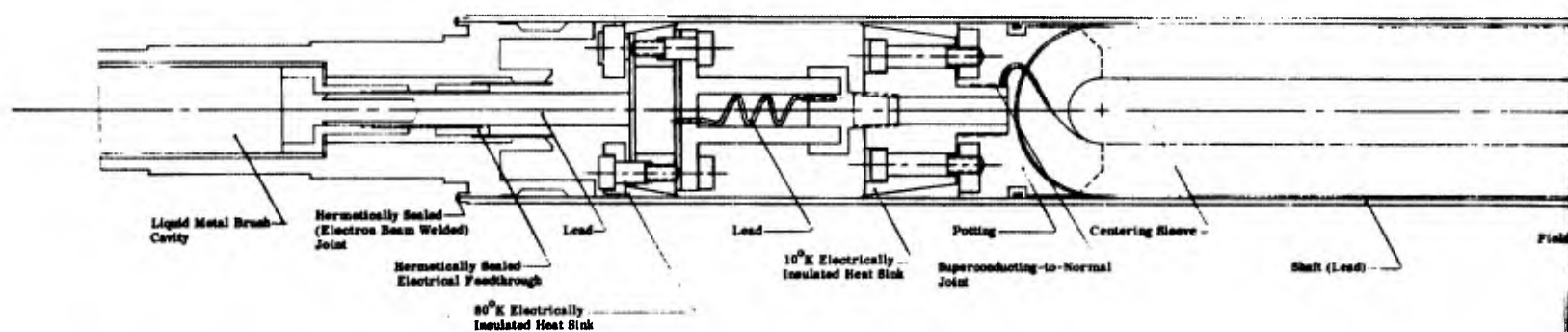


Fig. 37. Rotor Assembly

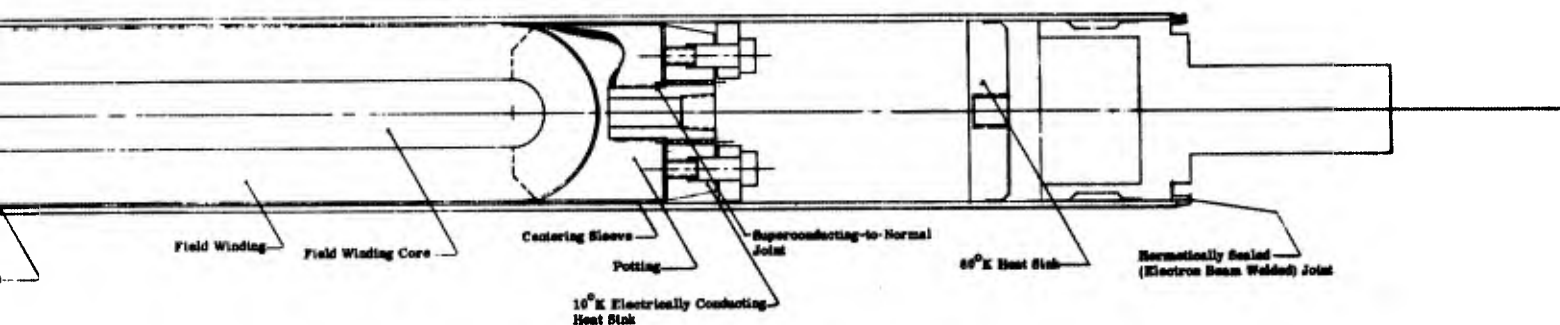


Fig. 37. Rotor Assembly

Returning to Figure 37 the 10° K heat sinks can be found at each end of the field winding. These heat sinks are designed to provide a variety of functions.

#### Drive Shaft Assembly

The drive shaft assembly consists of the rotor, the bearing and seal hubs and the test bed. The test bed is a fabricated steel box open at the top and line-bored to provide close alignment of the bearing hubs. This sub-assembly provides a rigid foundation for the dynamic loads developed in the shaft.

#### Rotor

##### Conceptual Design

The rotor presents a combination of mechanical, thermal, and electrical constraints requiring a fairly sophisticated piece of hardware.

1. The superconductor leads are each soldered to the heat sinks. A long joint is provided so that current can flow in parallel fashion from the superconductor to the copper heat sink thus providing the minimum possible resistance in the vicinity of the superconductor. The small amount of heat generated in these joints can be transferred via the heat sinks to the cooled wall of the shaft with a minimum temperature differential.
2. Heat transfer to the shaft is maximized by insuring a tight fit between the heat sinks and the shaft I.D. This is provided by the wedge type construction which enables sizable preloads to be imposed thus insuring good heat transfer.
3. One of the heat sinks also serves to make an electrical connection with the shaft which serves as one of the field leads (See Section 3.1.1).
4. The heat sinks are also used as balance plains during the first balancing of the shaft. Any sizable imbalance caused by the field winding must be eliminated by adjustments made (holes drilled) as close as possible to the source of the imbalance. The heat sinks serve this purpose.

Again returning to Figure 37, on the right end we have the 80° K heat sink and the shaft end. The shaft end is pressed into the tube and electron beam welded in place. This provides for a hermetically sealed closure inside of the shaft. At the operating temperature trapped gas will freeze out creating a vacuum inside the shaft. The vacuum minimizes heat transfer from the warm shaft ends. The 80° K heat sink is axially located near the liquid-nitrogen-cooled thermal neck in the chamber. The heat sink receives heat by radiation from the shaft end and transfers it to the shaft wall. A major fraction of this heat is transferred through the helium-filled annulus to the nitrogen-cooled thermal neck thus reducing the heat load in the low temperature region. This heat sink is soldered in place to provide good heat transfer.

The left end is again a bit more complicated because we are bringing an electrical lead out on this end. Again an 80° K heat sink is provided. This one, again employing the wedge construction is electrically insulated from the shaft. Heat is absorbed by this heat sink from shaft end radiation and conduction down the electrical lead from the warm end.

Between the 80° K and 10° K heat sinks a silver lead is provided of optimum length and diameter to minimize the heat leak to the low temperature sink. This silver lead is structurally mounted in a phenolic sleeve. At the low end the silver terminates in a copper slug provided with a pipe threaded screw for assembly into the 10° K sink.

The left shaft end is again electron-beam welded to provide hermetic sealing. Also a hermetically-sealed electrical feedthrough is provided to bring the lead out of the evacuated region. The cavity at the left hand end of the shaft is for installation of the liquid metal brush assembly (described in Section 3.1.3).

Following the complete assembly of the shaft including the liquid metal brushes and the shaft bearings, it is necessary to undertake a final balancing operation. Because of the preliminary balancing already accomplished, this balancing is accomplished with a minimum of material removal. Material has been removed from the tubular portion of the shaft by grinding as much as .004 inches from the heavy side of the shaft. The low design stresses in the tube permit this removal of material without creating a hazard.

This discussion has dealt mainly with shaft function. Developing assembly techniques and testing out component performance prior to assembly constituted a major portion of this program. The assembly process is in large measure irreversible and had to be done correctly the first time to avoid expensive time consuming mistakes. This painstaking effort was rewarded by a properly functioning field assembly which performed all functions well on the first attempt at power generation.

#### Bearings and Seals

The rotor shaft bearings and seals shown in Figures 38 and 39 will be lubricated with oil mist lubrication. The bearings used are grade 7 angular contact bearings. To provide the necessary bearing preload for this high speed service and to compensate for the axial thermal contraction of the shaft, the bearing and seal on one end is mounted to allow axial motion and spring loaded as shown in Figure 39. The face seals can, therefore, be set up to operate at a minimum contact pressure over the entire temperature range.

#### Drive System

The input end of the shaft is splined to the output of a 1:6 ratio, double helical gear speed increaser. A 4000 rpm input to this gear box produces the design speed of 24,000 rpm. Testing of the 50 kva generator will employ an internal combustion engine coupled to the speed increaser through a Spicer coupling.



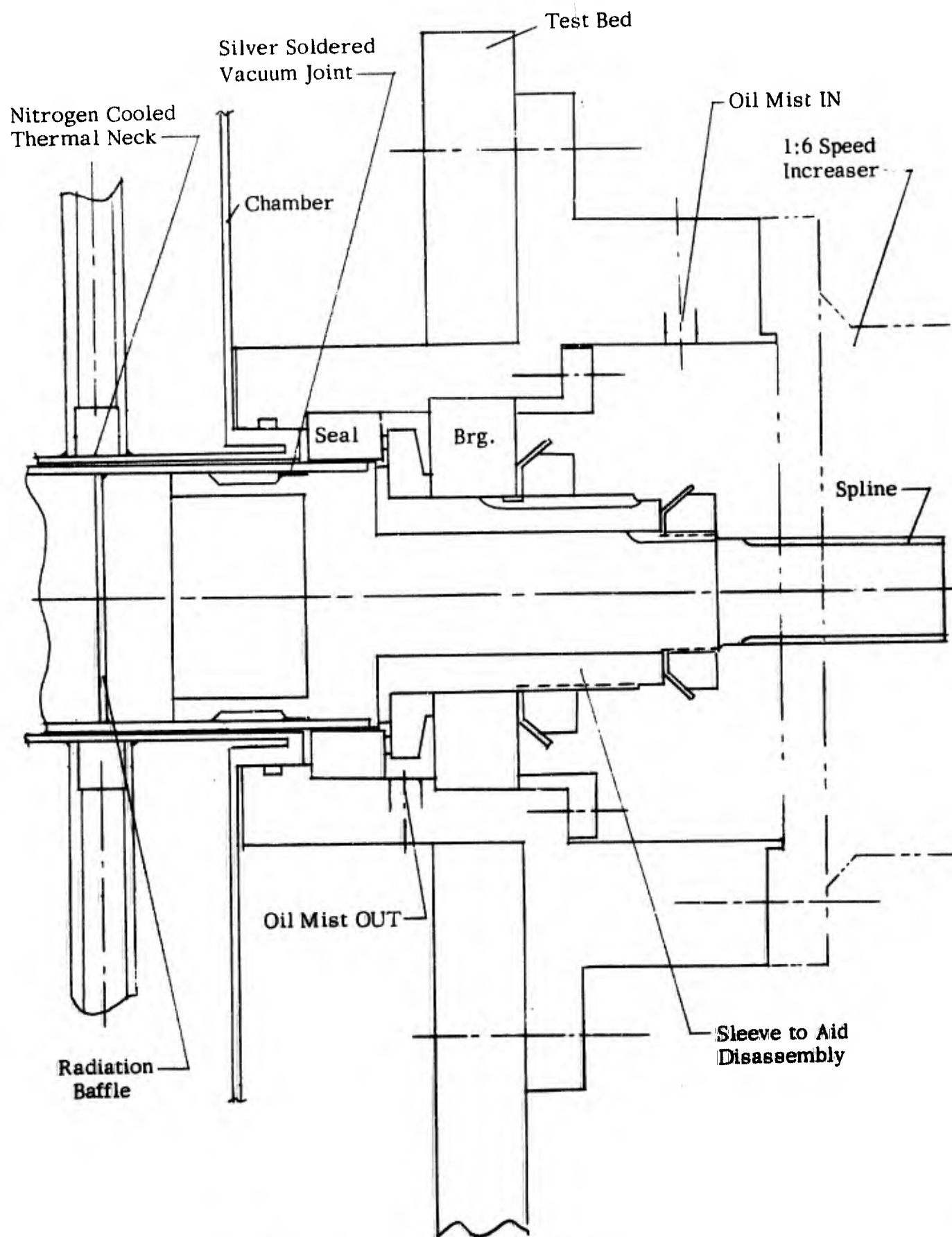


Figure 38. Drive End Shaft Assembly

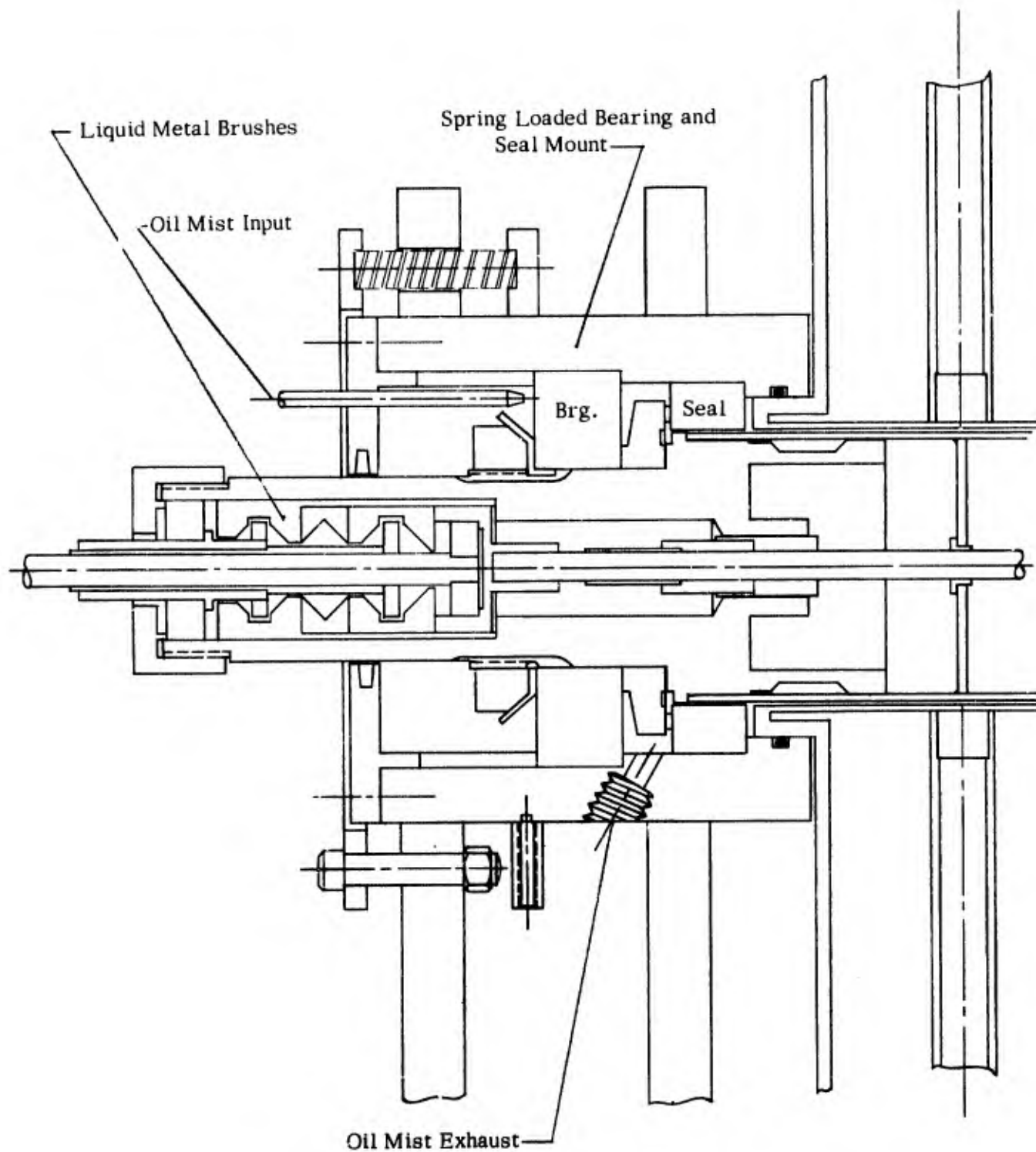


Fig. 39. Liquid Metal Brush End Shaft Assembly

## Section IV

### TESTS AND RESULTS

The objective of the test phase is to experimentally check the laboratory prototype model fabricated from the design developed in Section III. These experiments were to:

1. Demonstrate that the laboratory prototype model generator can be safely cooled down to the desired operating temperature, and maintain its physical integrity while rotating the field.
2. Demonstrate that the superconducting field can be excited and maintained during rotation; and that electric power can be generated in the armature and delivered to a load.

The first result of note was that the entire machine became superconducting after cooling down. The field was slowly energized up to 28 amperes with the current controller and maintained at this value while rotating (up to 10,000 rpm). Power levels of up to six (6) kilowatts were generated during the field excitation data runs.

#### 4.1 Experimental Test Setup

The experimental test setup for the laboratory prototype model superconducting generator is shown in Figure 40. An internal combustion engine was used as the prime mover. Its output speed was increased with a gear system to the required generator speed. A vacuum pumping system was used to maintain the insulating vacuum. The cryogens necessary for each of the two stages are separately supplied. For the intermediate temperature stage, a liquid nitrogen bottle is directly connected to supply liquid nitrogen. For the low-temperature stage, low-temperature helium gas is required. This is obtained by converting the liquid helium from a storage dewar into gas by the use of a converter. The low-temperature gas is then fed into the low-temperature stage of the generator.

##### 4.1.1 Instrumentation

The generator is instrumented primarily to measure electrical and thermal outputs. Generator speed and vacuum are also instrumented.

A schematic diagram of the electrical instrumentation and generator interconnection is shown in Figure 41. The power output leads are connected through fast acting fuses to a resistive load. All electrical instrumentation connected to the generator output leads are connected through potential and current transformers. Because of the high voltage, these transformers serve two purposes: 1) permit isolation of the high voltage from the instrument panel thus providing a margin of personnel safety, 2) permit use of conventional insulation levels on the instruments. The electrical outputs of voltage, current and power are provided. For experimental flexibility, each phase is separately instrumented to promote ease of data recording and reduction.

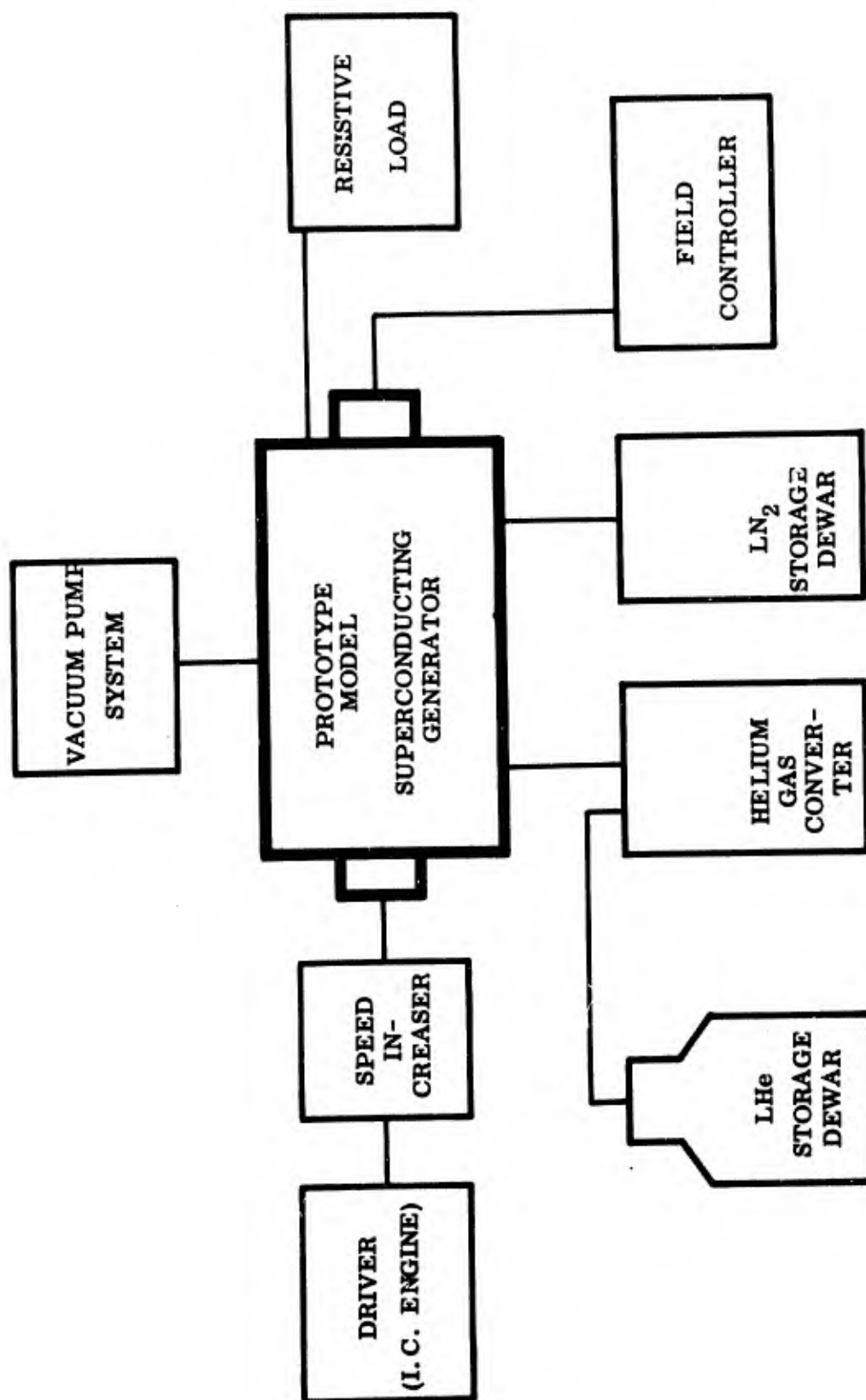


Fig. 40 Experimental Test Setup for Prototype Model Superconducting Generator

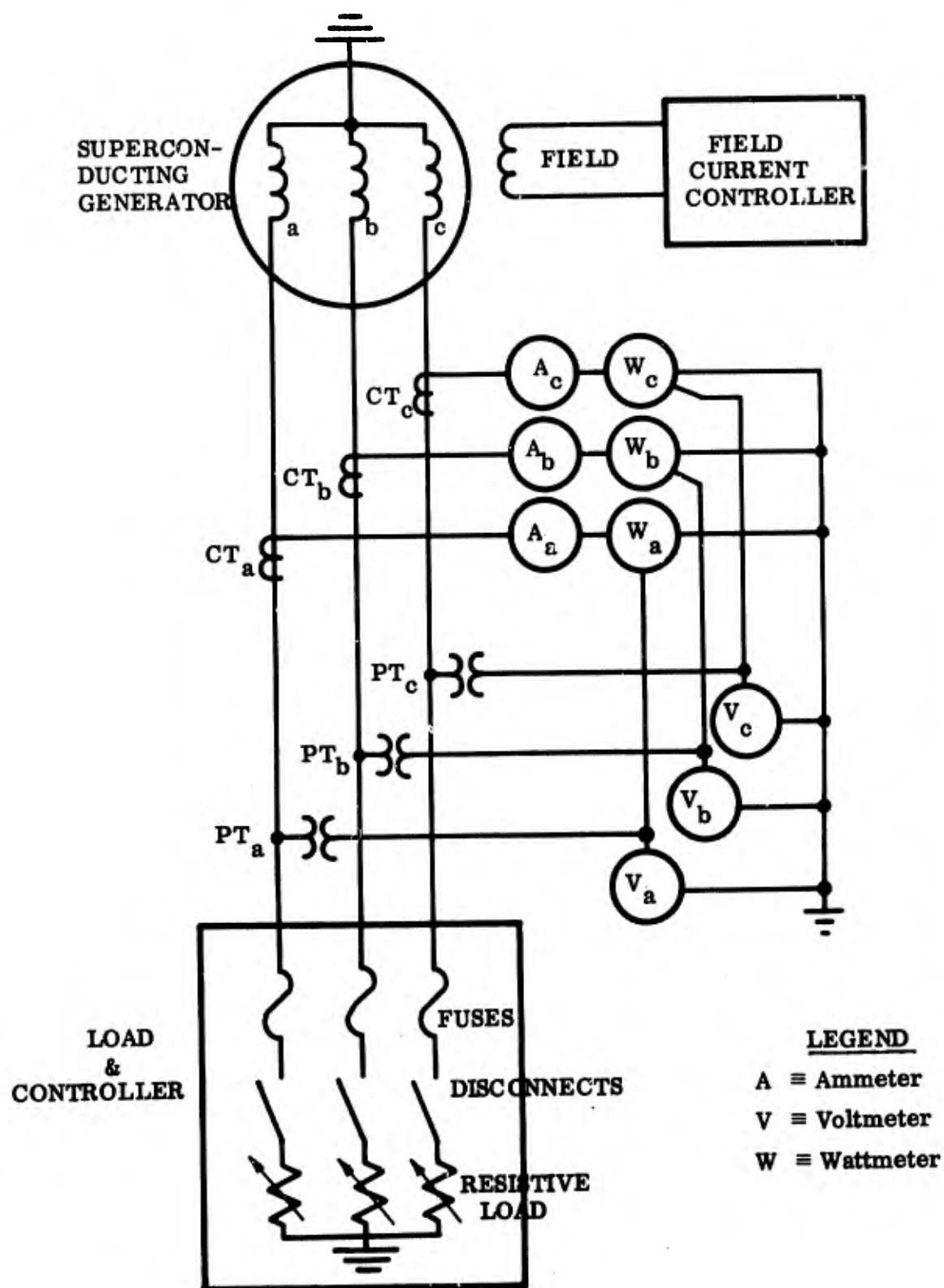


Fig. 41. Electrical Interconnection and Instrumentation Schematic Diagram

A schematic diagram of the thermal instrumentation is shown in Figure 42. Temperatures are measured in various areas of the armature with thermocouples as shown in Figure 43. The inlet and outlet coolant gas temperatures are measured with direct reading gas bulb thermometers. The gas flow rate is measured by a flow meter.

A thermocouple vacuum gage is used to monitor the vacuum system, and a photoelectric tachometer is used to monitor the generator shaft speed.

#### 4.2 Experimental Tests

Three exploratory tests were conducted with the prototype model superconducting generator:

1. A preliminary cooldown test to investigate the structural integrity and vacuum maintenance.
2. An exploratory test to obtain electrical data.
3. An exploratory test to complement the second test and also obtain thermal data.

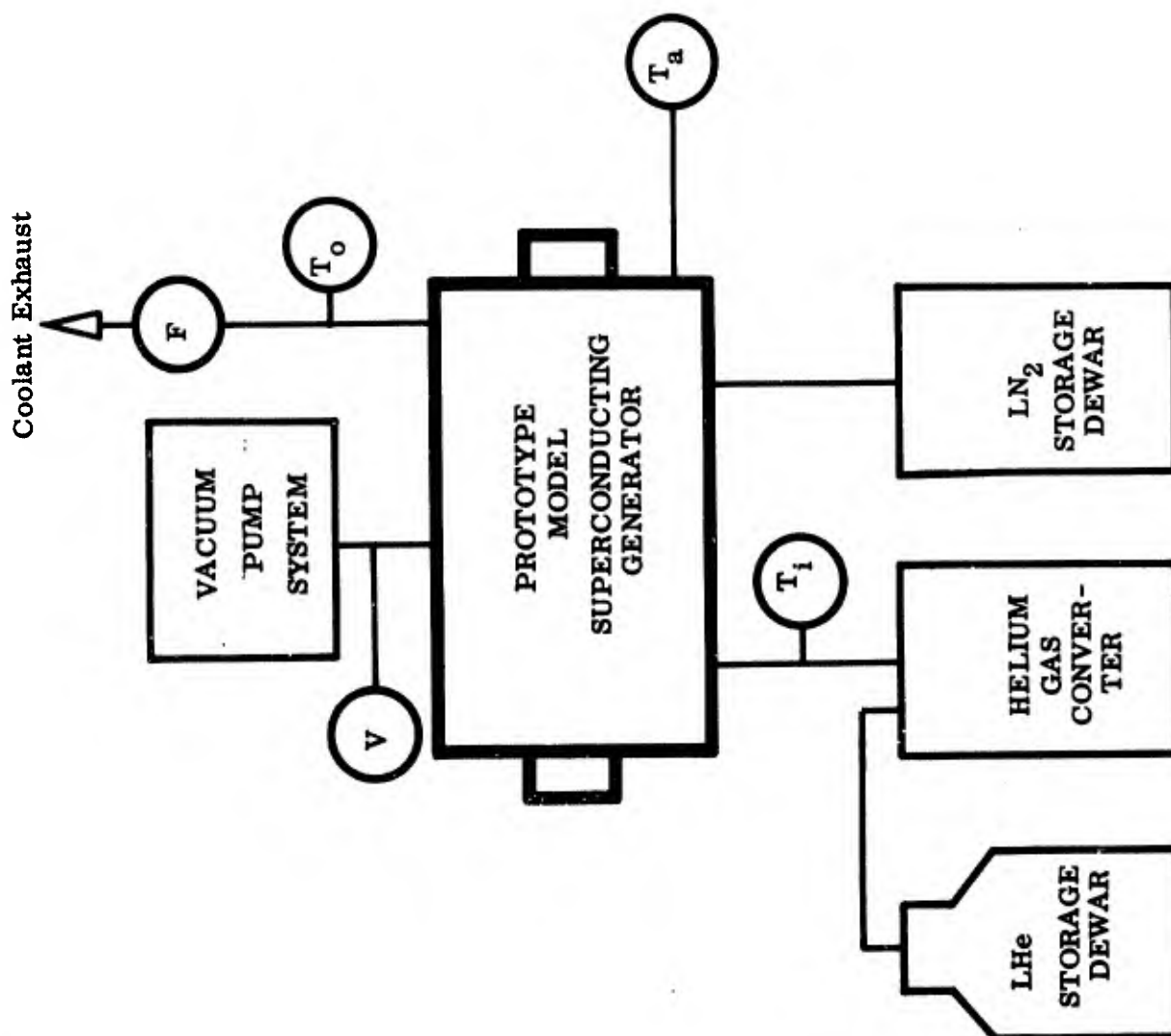
##### 4.2.1 Preliminary Cooldown Test

The objective of the cooldown test was to evaluate the thermal and structural performance of the prototype generator while the system was undergoing a temperature transition from room temperature to 10°K. The generator was designed and fabricated to withstand the stresses arising from this temperature change. Each component was thermally tested to its operating temperature before assembly into the generator.

The prototype generator was designed to remove heat at two temperature stages, about 10°K and 80°K. The heat load at 80°K is removed by vaporizing liquid nitrogen; the lower stage heat load is removed by gaseous helium. Delivery temperature and flow rate of the gaseous helium are controllable over a large range.

The cooldown procedure involved the following steps:

1. Pump down all vacuum spaces.
2. Purge lines and other unevacuated volumes with warm gaseous helium to prevent condensation and freezing of water vapor of gases.
3. Bleed in liquid nitrogen to the intermediate temperature region until temperature is near 80°K. Meanwhile the shaft is continuously rotated to prevent freezing of the bearings and seals; and the low temperature region is continuously purged with pre-cooled gaseous helium (80°K) in order to maintain a positive pressure and thus prevent any contamination due to leakage of atmospheric air through the shaft seals.



**LEGEND:**

$T_i$   $\equiv$  Inlet Gas Temperature  
 $T_o$   $\equiv$  Outlet Gas Temperature  
 $T_a$   $\equiv$  Armature Temperature  
 $F$   $\equiv$  Gas Flow  
 $V$   $\equiv$  Vacuum

Fig. 42 Thermal Instrumentation Schematic Diagram

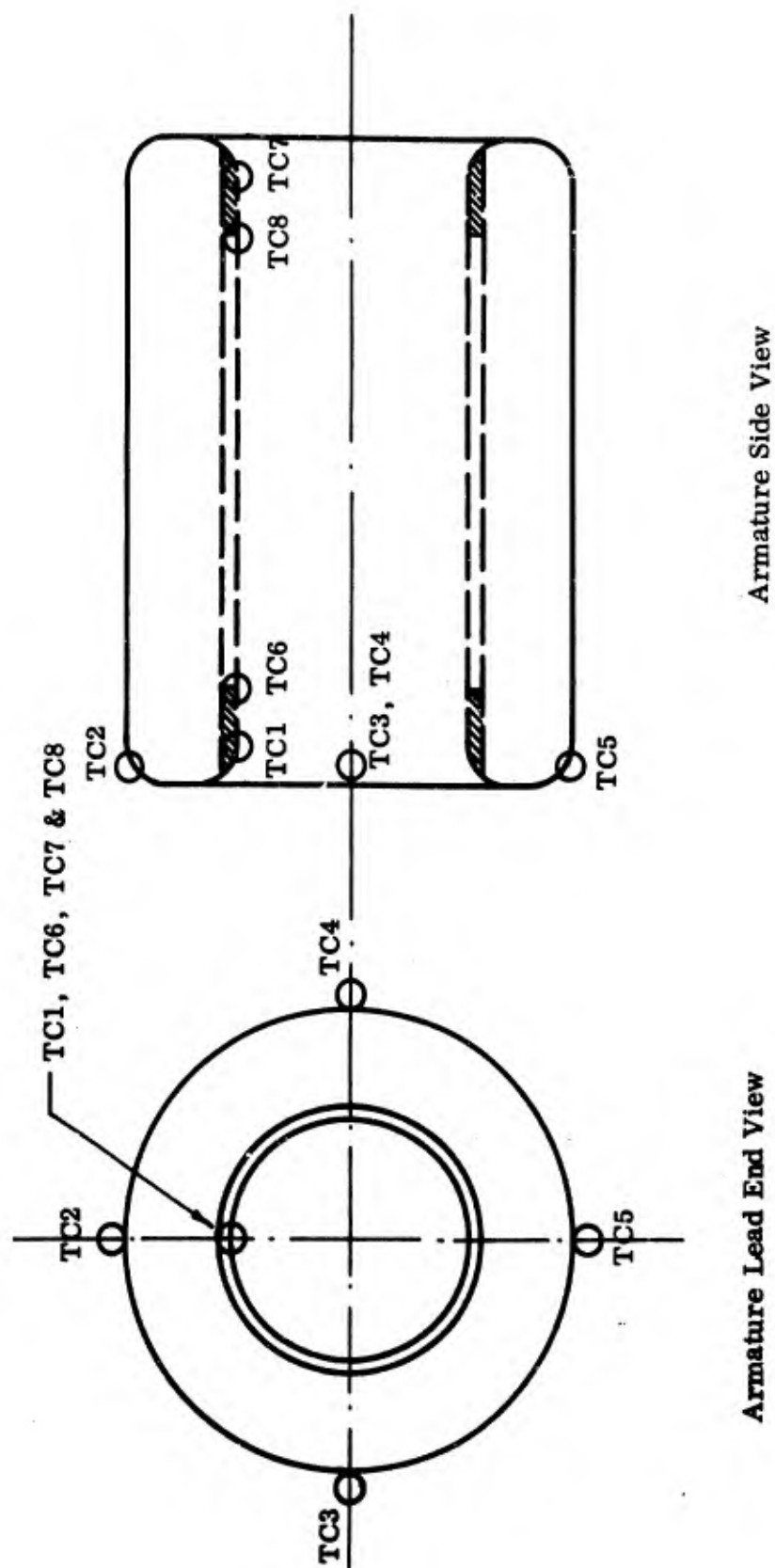


Fig. 43 Thermocouple Location Schematic Diagram



4. Introduce cold gaseous helium slowly to the low temperature region and cool down to an operating temperature near  $10^{\circ}\text{K}$ .

The prototype generator was cooled down slowly over a period of 4 hours by the above procedure. Exposure of the components and piping to the temperature-induced stresses did not result in any major leaks opening up. The pressure in the evacuated volume increased by a factor of two as shown in Figure 44.

The cooldown test proved that:

1. The prototype generator could withstand cooldown to its operating temperature level while retaining structural integrity; and
2. The pressure in the vacuum spaces could be maintained low enough to provide effective insulation against heat input from the ambient (room temperature) environment when the machine was near operating temperature.

Proving the above points was the only purpose of the cooldown test. Therefore, enough liquid helium was ordered to accomplish a cooldown to near operating temperature. By the time the helium supply was exhausted, the generator armature temperature was  $20^{\circ}\text{K}$ . This was very close to the goal of  $10^{\circ}\text{K}$ . Since lowering the temperature to  $10^{\circ}\text{K}$  from  $20^{\circ}\text{K}$  results in almost no additional thermal contraction, the points listed above were considered proven.

The cooldown experience gained during this test was used to develop more efficient cooldown techniques for subsequent tests.

#### 4.2.2 First Exploratory Test

The first exploratory data test of the motor-generator was conducted at shaft speeds of 6000 rpm and occasional 10,000 rpm. The generator was cooled down initially following the cooldown test. All auxiliary systems were operating continuously. The helium gas converter and its connections were checked as expected. The generator maintained a vacuum of  $10^{-4}$  torr at the operating temperature. When the temperature was low enough for the field to attain superconductivity the current controller was energized and a stable current was maintained through the rotating field. No signs of instability were evident.

Most of the data runs were made at the shaft speed of 600 rpm. At this speed a maximum output of 6.1 kilowatts was achieved with a resistive load connected to the generator. The output voltage waveform under load was sinusoidal (see Fig. 45). A number of runs were made at different values of field excitation. Apparent quench effects were noticed in the armature during the higher power runs. The output current of the generator would drop off almost instantaneously and the unloaded drive engine would speed up. The armature recovered rapidly with no noticeable signs of adverse effects.

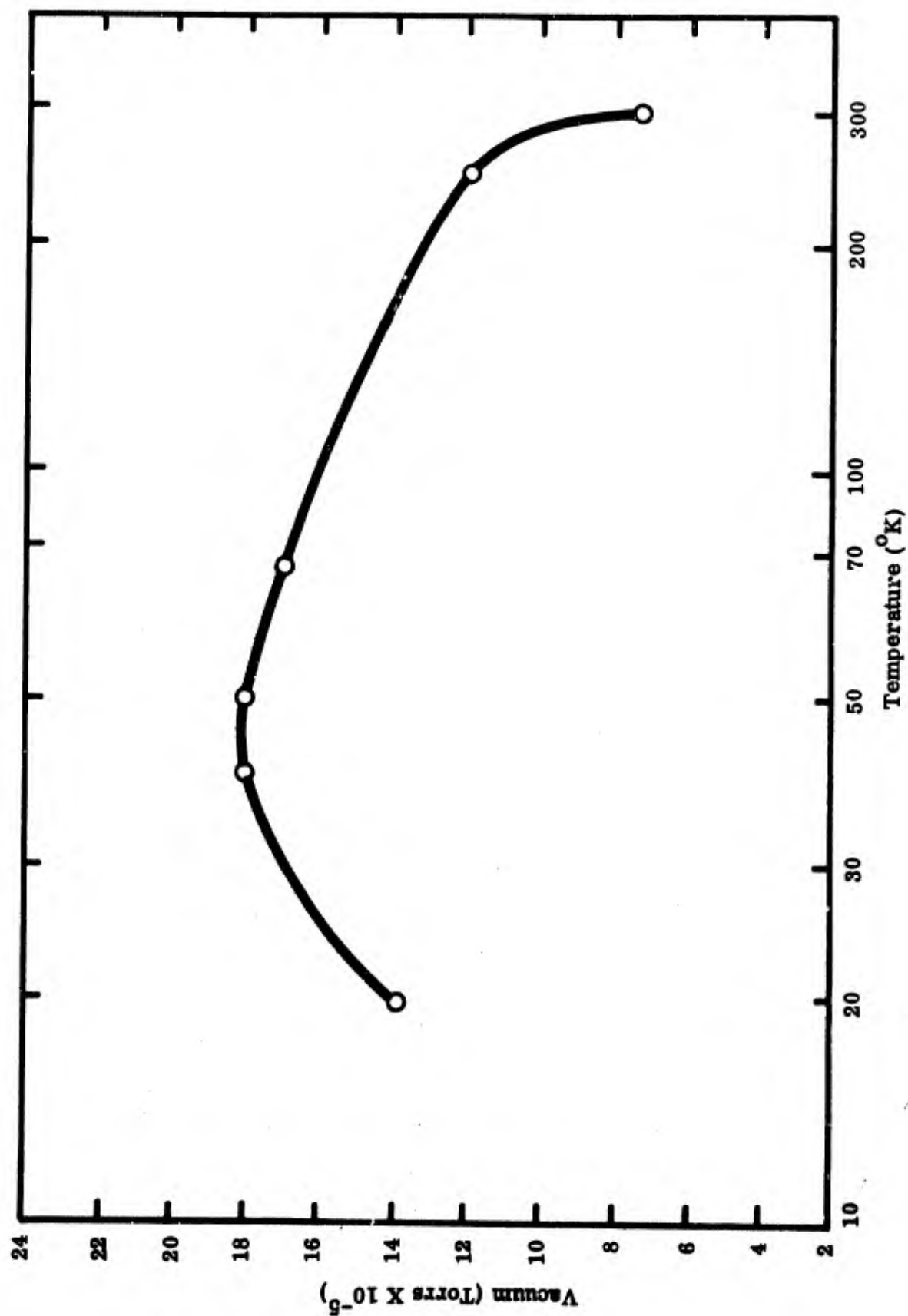
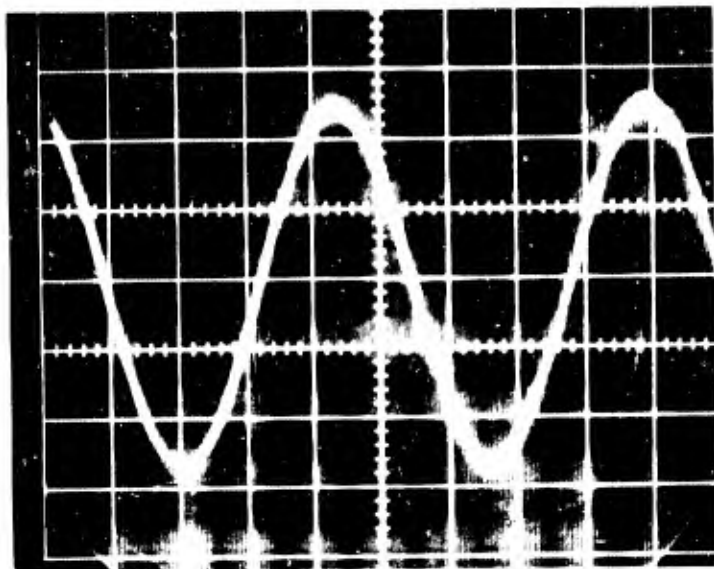
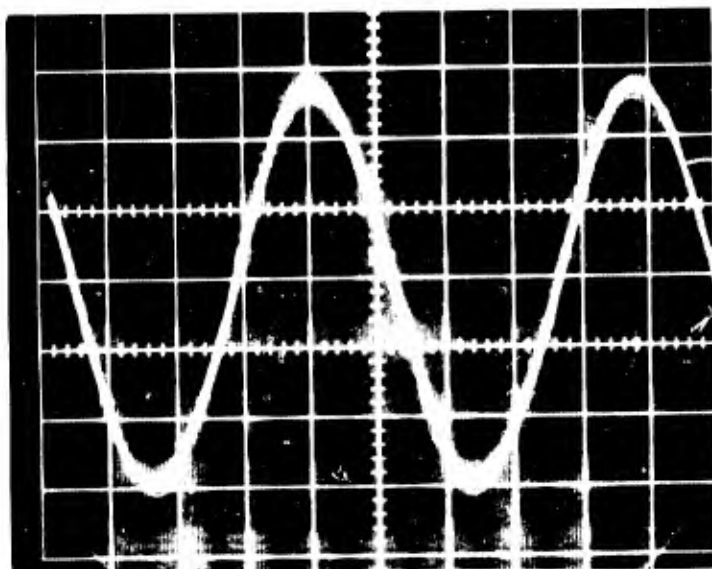


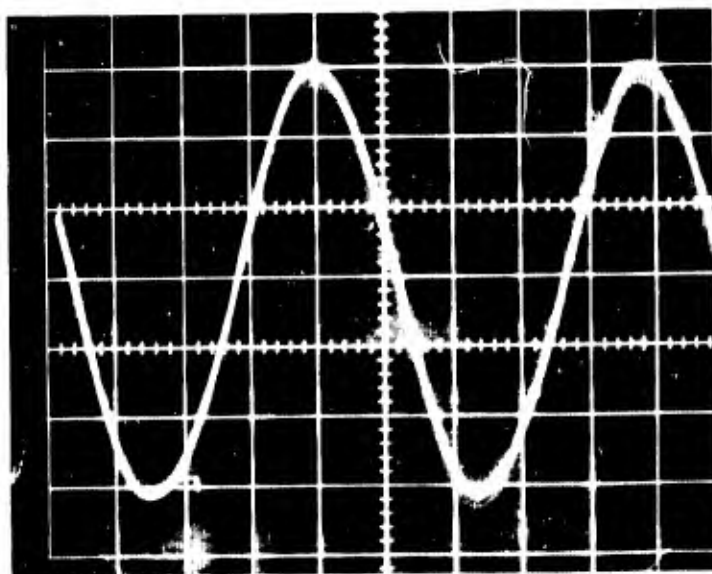
Fig. 44. Vacuum versus Temperature (during preliminary cooldown)



Phase A



Phase B



Phase C

Fig. 45 Sinusoidal Output  
Voltage Waveshapes

The output phase voltage as a function of field excitation is shown in Figure 46. Varying the field current showed that the amplitude of the output terminal phase voltage varied proportionally to the field current. The generated voltage measured was 85% of the calculated design value.

The output power as a function of field excitation is shown in Figure 47. Varying the field excitation showed that the amplitude of the output power varied as the square of the field excitation. The generated power output measured was 72% of the calculated design value. This was due to the value of the generated voltage being slightly lower than the design value.

The first exploratory test showed that:

1. The rotating superconducting field coil would maintain its superconductivity during rotation and against the armature reaction when the generator is loaded.
2. The thermal circuit of the shaft was effective in isolating the field from the external thermal environment.
3. Generation of power in a superconducting armature is possible.
4. The armature exhibited apparent quenching without noticeable adverse effects.
5. The phase voltages and power as a function of field excitation behave in the same manner as a conventional generator.

#### 4.2.3 Second Exploratory Test

The second exploratory test of the superconducting generator was conducted to provide additional low speed electrical and thermal data. The generator was cooled down by following the previous cooldown procedure. An improved cooldown was the result of a more effective use of the first stage cryogen. The cooling effect of the liquid nitrogen on the armature was monitored by following the decrease in resistance of the silver plating of the armature superconductor. Since the resistance of a metal decreases with temperature, this effect can be used as a qualitative indication of temperature. This effect is shown in Figure 48. Gaseous helium was introduced when the cooling effect of the liquid nitrogen was minimized as shown by the decrease in the slope of the resistance curve. The generator maintained a vacuum of  $4 \times 10^{-4}$  torrs at the operating temperature. The liquid metal brushes used in the field excitation system exhibited a high resistance due to an intermittent internal brush connection, and did not permit field excitation. Since the brushes are installed on the generator, repair would be difficult with the generator in the cooled-down state. Nonetheless, an attempt was made with little success by removing the brushes, overhauling and refilling with fresh mercury which resulted in a short-circuited condition between brushes. An attempt at energizing the field with a higher voltage source in order to overcome the short circuit and series resistance was partially successful. Sufficient current was channeled to the field resulting in the generation of 2 kilowatts. This showed that the field was in a superconducting state.

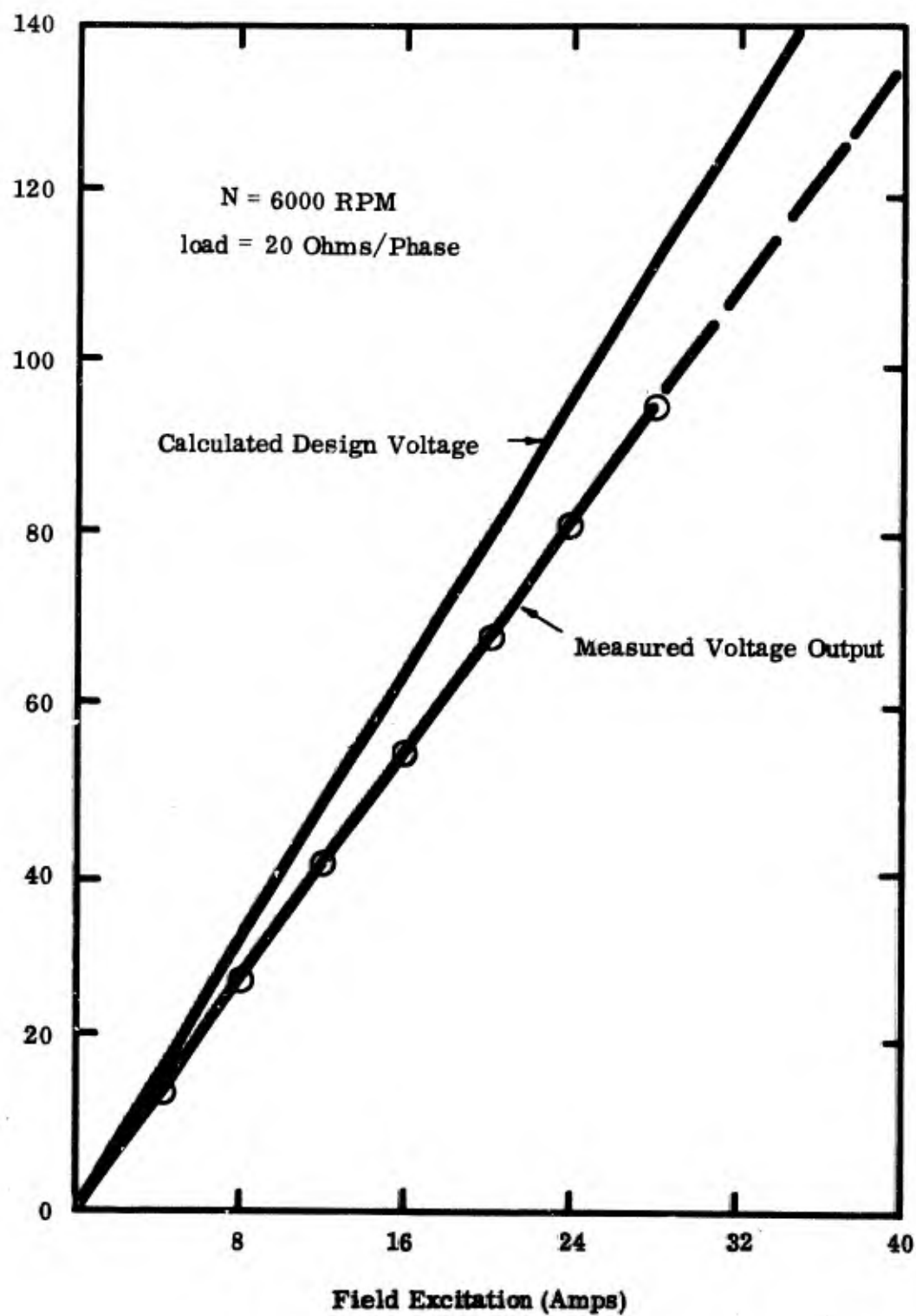


Fig. 46 Phase Voltage vs. Field Excitation

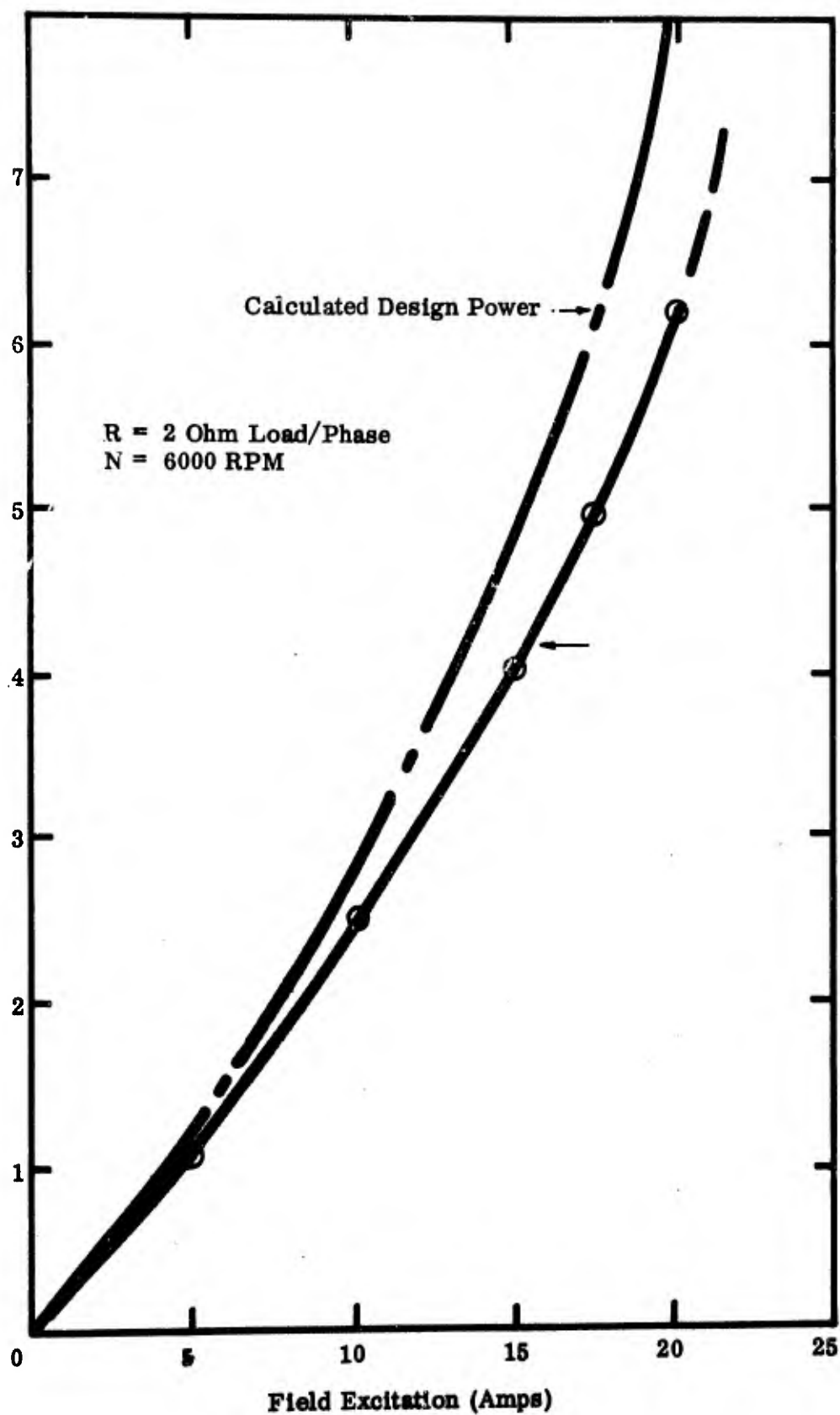


Fig. 47. Power Output versus Field Excitation

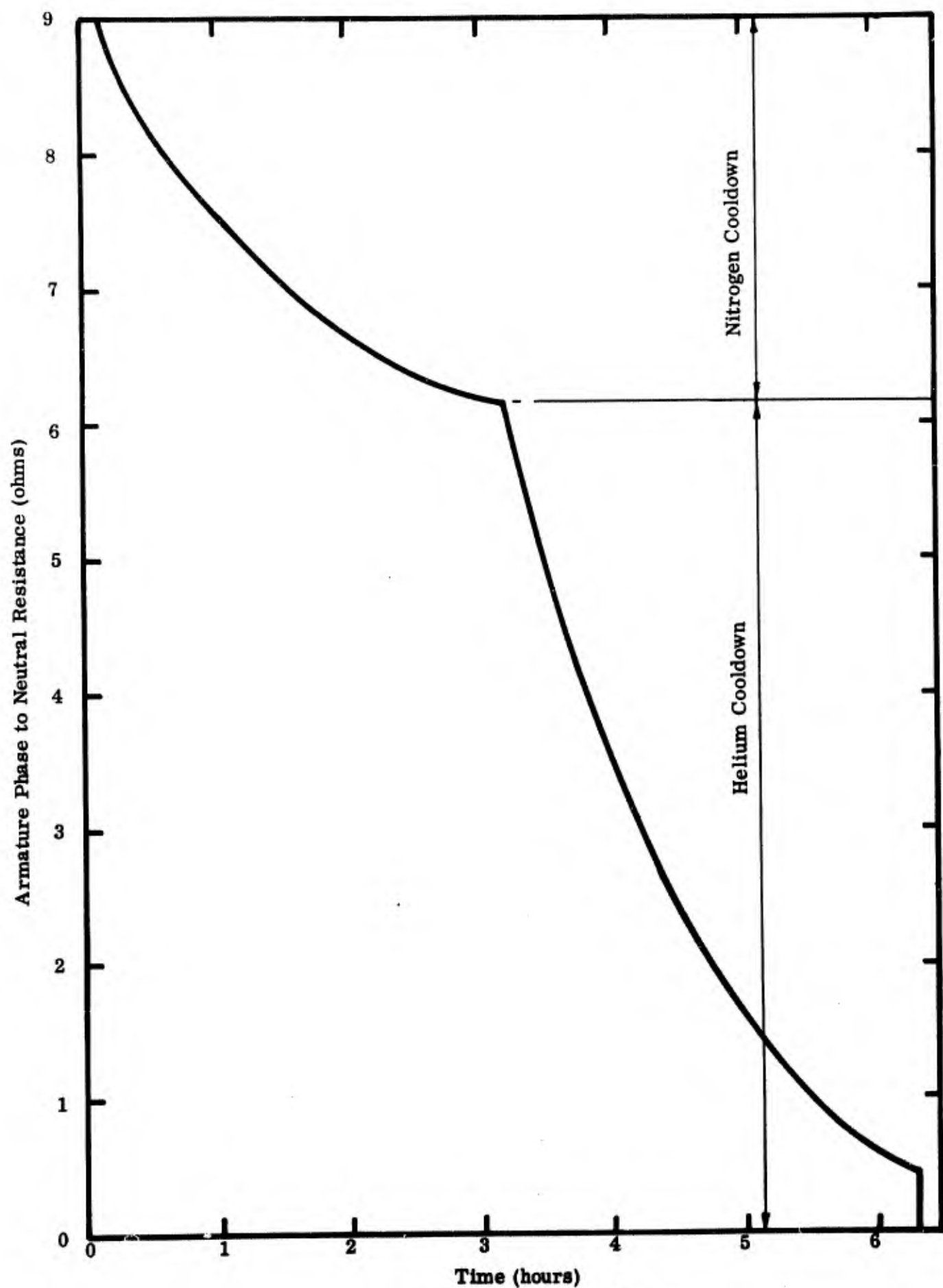


Fig. 48 Cooldown Monitor  
82

Because the field winding could not be energized in a controllable manner, generation suitable for meaningful data was not possible. Therefore, this test for further electrical generation and thermal data was aborted.



## Section V

### 1-MEGAWATT GENERATOR

The starting point for the design of a 1-megawatt superconducting generator is the field. In designing the 50 kw prototype the objective was to provide a field which could also be used in a 1-megawatt machine. The primary difference in the electrical design of the two generators is the addition of additional current carrying capacity to the armature by providing (in parallel) more armature windings. Initial tests on the 50 kw machine indicate that the field design will be adequate for the 1-megawatt design.

Therefore, starting with the 2-inch field diameter, a basis for embarking on a mechanical design is established. The first potential problem which comes to mind is whether or not sufficient armature winding cross section can be provided in the limited circumferential length available for the active windings. An additional problem is that the active superconducting layer must be made thinner to reduce the ac losses. Electrical design suggests a bundle of 56 ribbons. It can be easily determined that each ribbon must be about .0005 inches thick to fit into the available circumference. Discussions with RCA indicate that such a superconductor can be made using state-of-the-art techniques. Winding such an armature would require exercising considerable care but there is no reason why it cannot be done. The toroidal winding configuration would be retained in the 1-megawatt design as well as the iron-core flux-return path.

A conceptual layout of the 1-megawatt machine is shown in Figure 49. Because component designs are not frozen by this preliminary design, we have chosen to show possible innovations which may result in a better machine. Where design options exist, they will be pointed out.

The plastic chamber wall around which the armature will be wound will be very similar to the one in the 50 kw machine. The ducting for directing the helium flow around the armature windings will also be quite similar. The 10°K power lead heat exchangers will be similar in design and arrangement but will be scaled up to handle the additional heat load coming in via the larger power leads.

Inside the plastic chamber, the cooling of the iron-core return path is accomplished by conducting the heat away through the six structural support rods to the outer case which in turn will be maintained at approximately 80°K. In the 50 kw machine it will be recalled that coolant was introduced into an inner chamber thus cooling the core directly. The proposed design modification leads to a simpler, more rugged construction. The elimination of this internal cooling loop will eliminate several joints that are not only difficult to assemble, but are potential points where leaks can develop. A higher temperature can be tolerated in the iron core. At 100°K the radiant heat transfer to the plastic wall would be approximately 1 Btu/ft<sup>2</sup> hr. This is negligible compared to other heat loads encountered during operation of the generator.

Because the generator will be operated in the vacuum of space, the outer wall of the environmental chamber can be eliminated with a significant reduction in weight. The main structural member now becomes the surface which is maintained

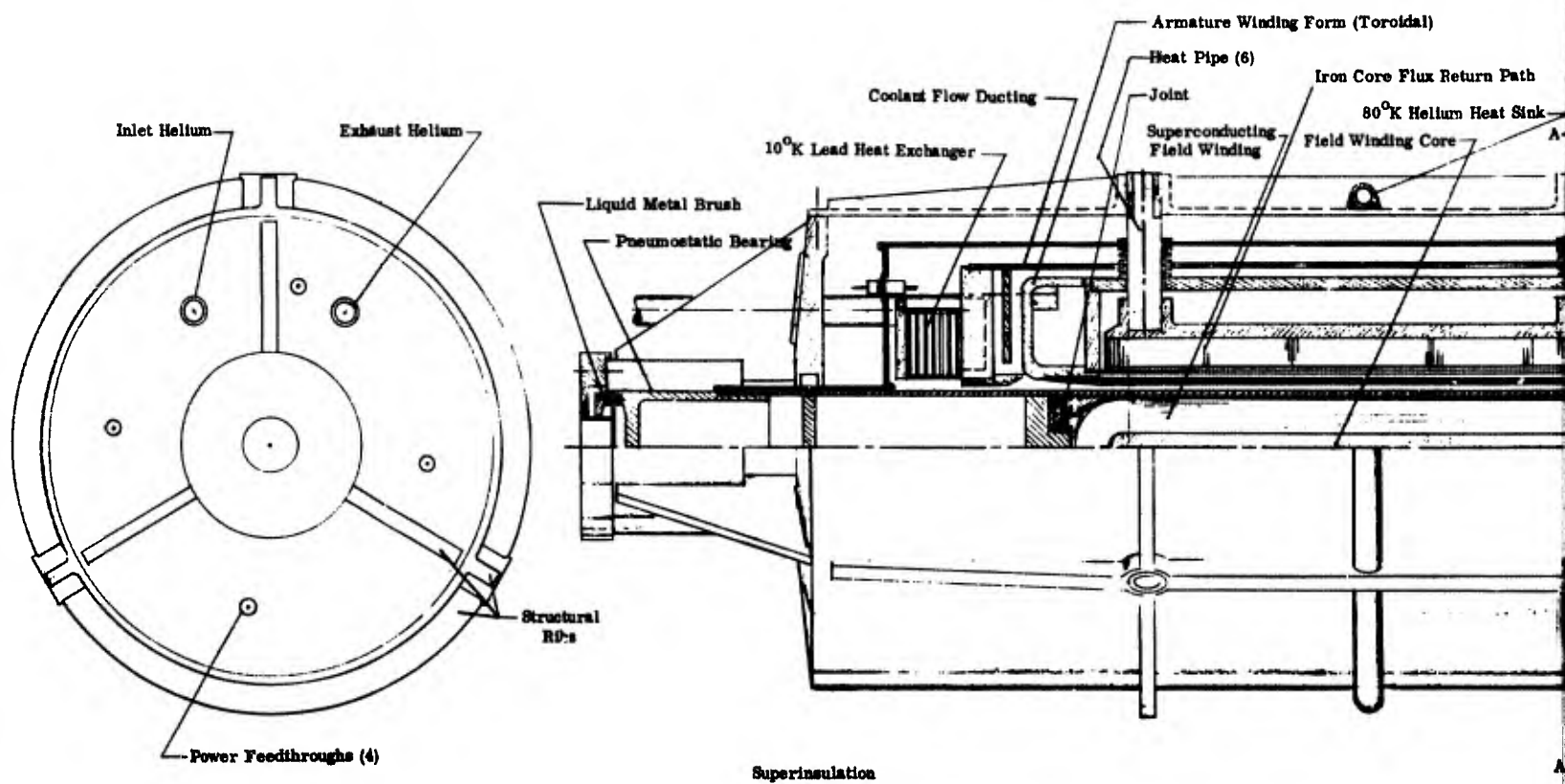
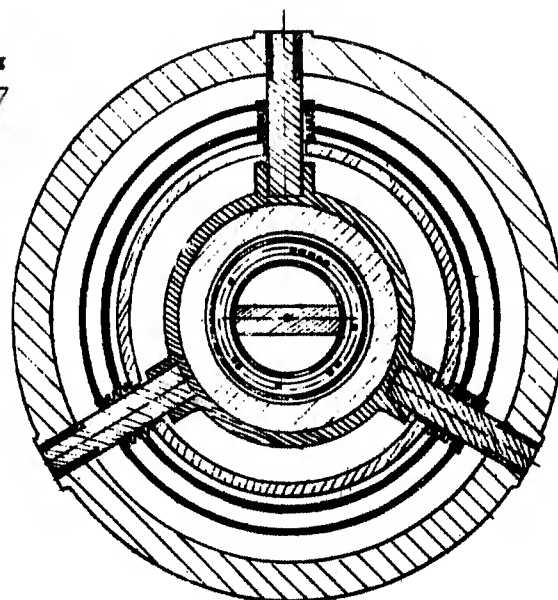
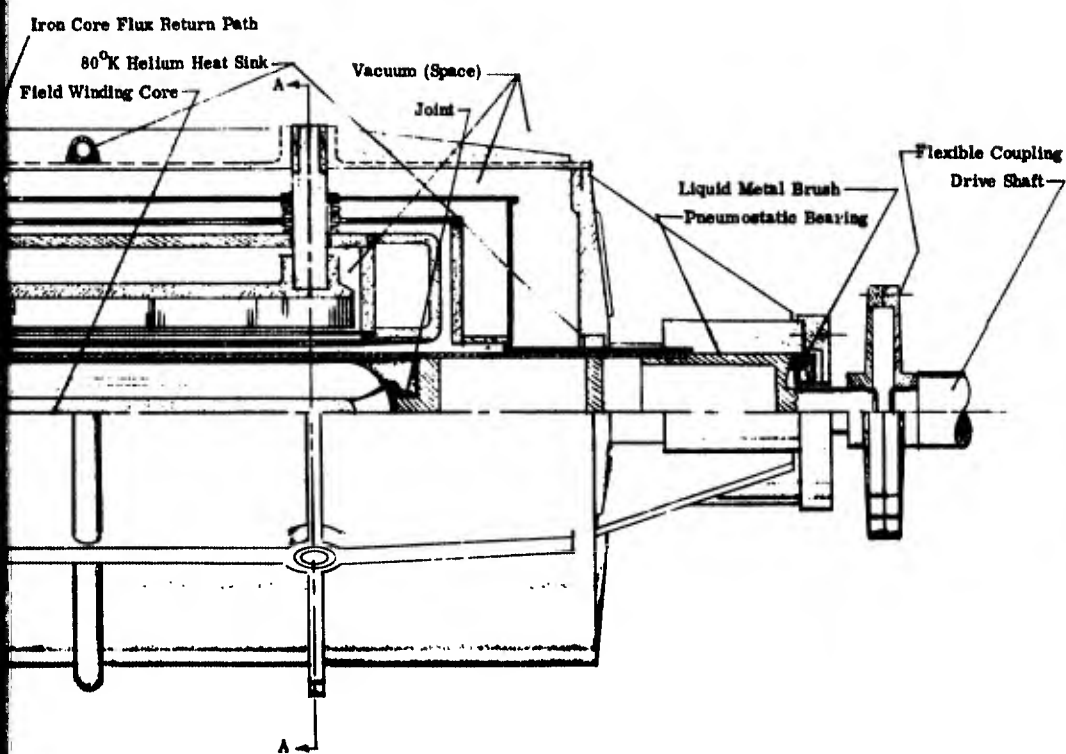


Fig. 49. 1 Megawatt Superconducting Generator

(1/2 scale)

Form (Toroidal)



Section A-A

in the 80°K temperature range. To reduce radiant heating of this surface to a minimum, it is anticipated that superinsulation would be applied to the exterior of the package.

In the space environment it becomes necessary to provide at least one seal between the helium environment and the vacuum of space. Seal technology is currently being developed which may find use in this application. The approach selected for this conceptual design is to utilize one of the liquid metal brushes (which must be provided for field excitation) as a seal as well. Stress calculations indicate that a .875" diameter drive shaft will provide the shaft torque necessary to develop 1 megawatt of electric power at 24000 rpm. It is felt that a liquid metal brush built around this shaft will still be small enough so that heat generation due to hydraulic drag would not be excessive. The brush would be filled with mercury after the rotor has been brought up to speed and make up mercury would be provided to replace boil off to the vacuum.

Now with one brush on the drive end and the second on the opposite end, the internal construction of the field-shaft assembly can be simplified by using both ends of the shaft as electrical leads, thus eliminating the tricky electrical insulating problem associated with two of the four shaft heat sinks. The fact that the shaft "apparently" short circuits the field is no detriment due to the much lower resistance of the superconducting winding. In fact, this "parallel circuitry" may provide a needed energy dissipation path in the event the field quenches. This feature could conceivably eliminate the possibility of doing permanent damage to the winding during a quench.

For bearings we are showing externally pressurized gas bearings employing system helium. The case has previously been made that, by very careful balancing of the shaft, bearing loads of roughly 15 pounds can be attained. Helium bled off the flow entering the third stage of the refrigerator compressor (or 560°R and about 24.5 psia) can be used without further pressurization. Even higher bearing load capabilities can be provided by adding a small auxiliary pump to supply helium at a higher pressure.

It is by no means appropriate to eliminate ball bearings from consideration at this time. Bearings of appropriate size can be run at 24,000 rpm using oil mist lubrication without overheating. Two bearings loaded with 50 pounds radial load would have a better than 95% probability of both running for 10,000 hours without failure providing proper lubrication is maintained. Further detailed study must be made before deciding on the type of bearing to be used.

#### Generator Weight

The weight estimate shown in Table 2 is obtained by weighing some of the parts of the 50 kw machine and calculating the weights of others based on the conceptual design. The specific weight of 0.075 lbs/kw is below the required 0.1 lb/kw.

Table 2

#### Summary of Weights of Generator Components

Armature and Iron Core Subassembly Including Ducting and Heat Exchangers	29.0 lbs
---	----------

Table 2 (continued)

Field-Shaft Assembly	17.5 lbs
Casing Assembly Including Armature Supports	14.5
Coupling	3.0
Bearings-Seals-Liquid Metal Brushes	2.0
Superinsulation	4.0
Misc. (Hardware, Fittings, Flow Lines, etc.)	<u>5.0</u>
	75.0 lbs

## Appendix I

### FIELD WINDING TESTS

The field winding was tested during various stages of construction prior to and after its assembly into the shaft in order to show its superconductivity integrity and operational stabilities.

Tests of the field winding were conducted at the following stages of construction and assembly of the field-shaft assembly:

1. The superconducting winding alone.
2. The superconducting winding with the combustion joint and heat sinks connected to determine the joint resistances.
3. The superconducting winding, lead joints-heat sinks, support rings were assembled into the shaft and encapsulated to form a unit assembly.

All of these tests were successfully conducted and showed that the field winding is performing as designed.

#### Test No. 1

After winding the  $\text{Nb}_3\text{Sn}$  ribbon superconductor over the ferromagnetic core along with the interleaving nylon-copper-mylar and epoxy bonding, a test with liquid helium was conducted to determine its superconducting integrity and performance characteristics of critical current and stability.

#### Test Apparatus

The test apparatus is shown schematically in Figure 50. The superconducting field coil is shown immersed in a liquid helium dewar which is surrounded by a liquid nitrogen heat shield. The current supply leads consisted of #6 stranded copper cables and they were connected to the superconducting field coil by 5"-long indium soldered joints. Since each #6 copper cable was composed of fine strands of copper wire and the superconductor was a flat ribbon, contact area between the fine strands and the ribbon was at a minimum so the joint was built up by the use of indium solder and a 5" long copper sleeve to provide a better mating surface. A pair of potential leads were soldered onto each end of the superconductor leads to monitor any voltage build-up or transients to denote an oncoming quench condition or flux jump instabilities.

Figure 51 shows the test instrumentation and power supply block diagram for the superconducting field winding. The current was supplied from a battery and is controlled with a variable resistor. The current was monitored by the ammeter and any voltage fluctuations were monitored by the oscilloscope. A high power low value resistor was paralleled across the superconducting magnet to act as a protective shunt against the power supply. In the event of a quench, this resistor provided "crow-bar" protection against the driving emf of the battery from being impressed across the

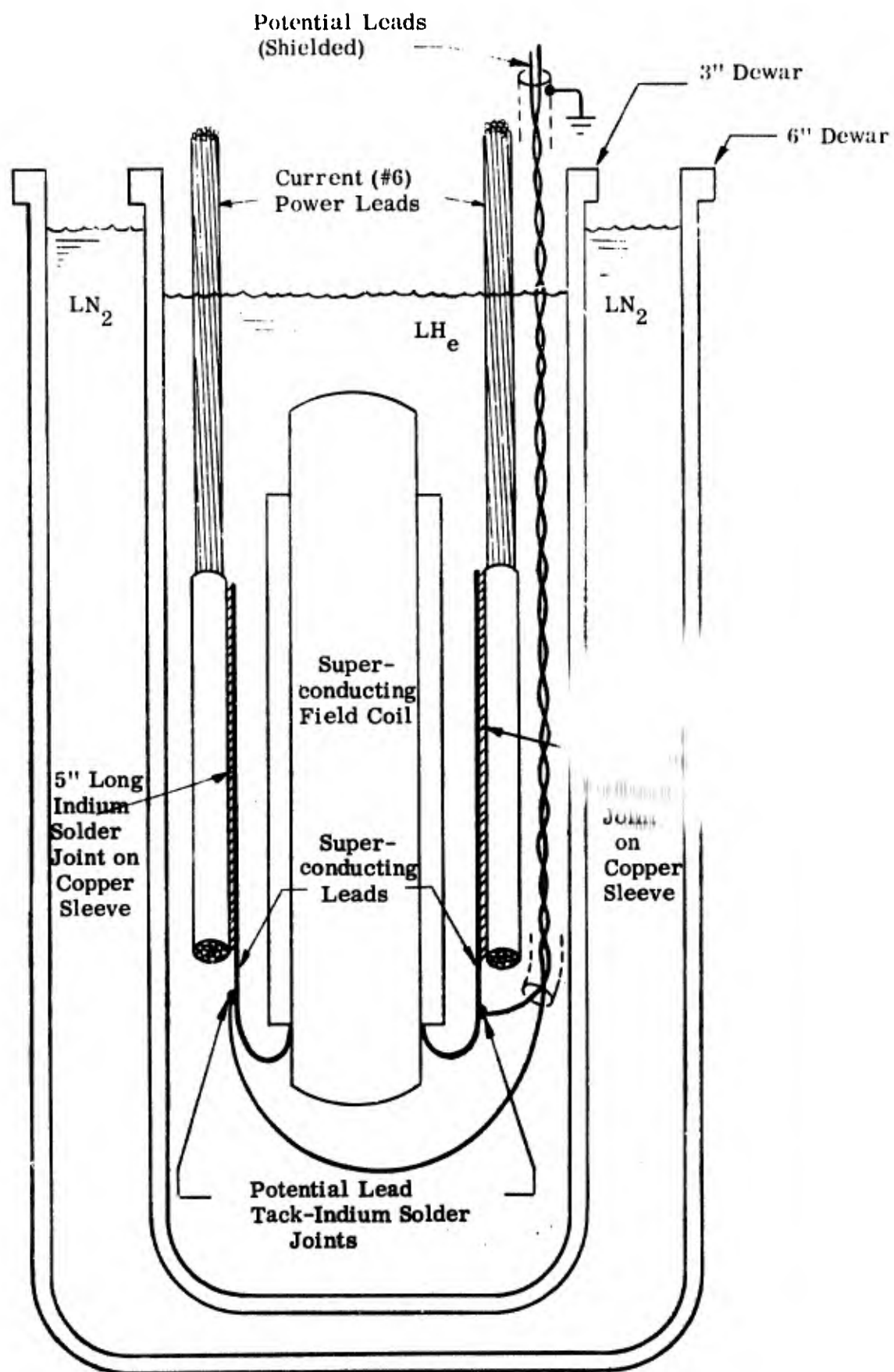
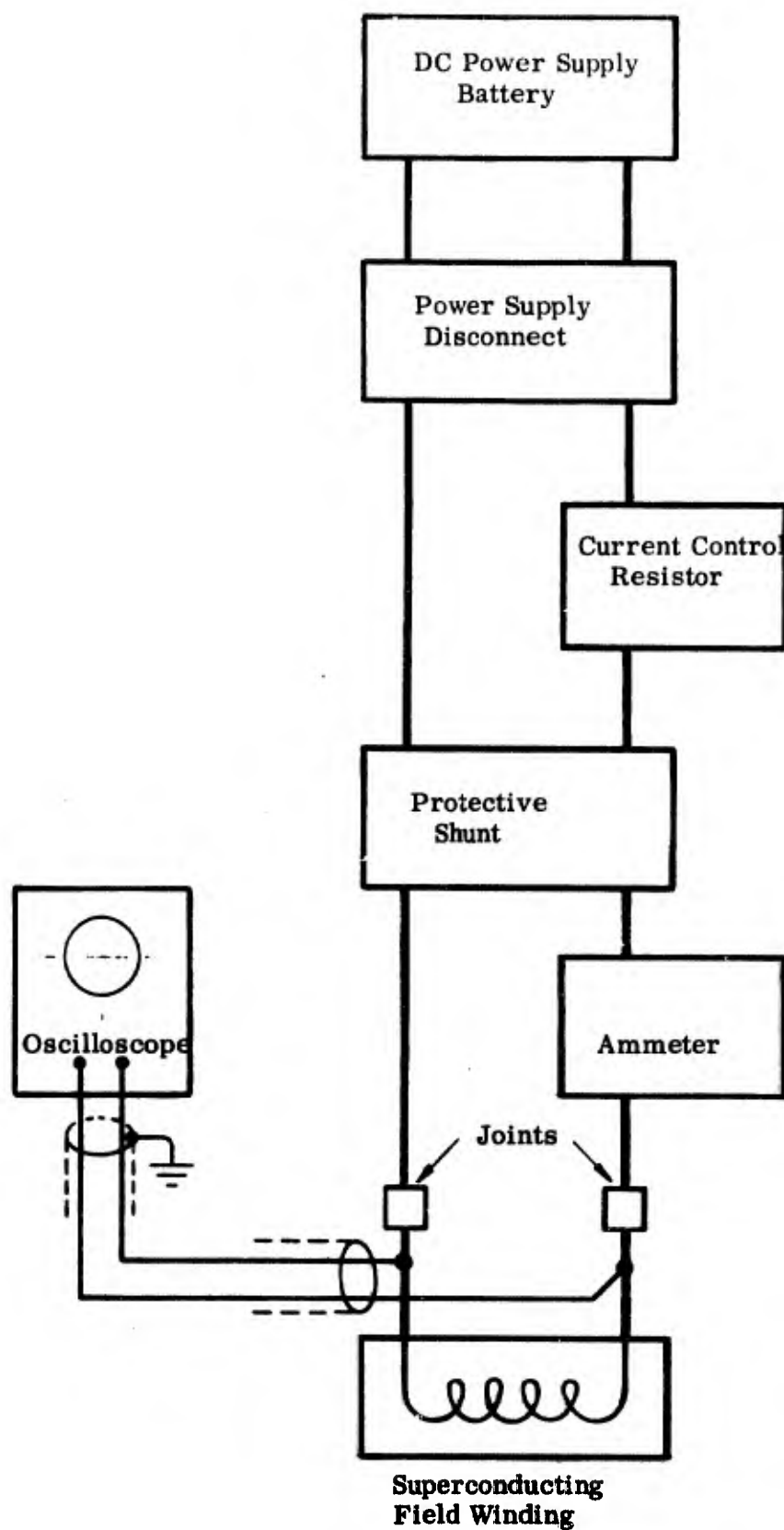


Fig. 50. Test Apparatus



**Fig. 51. Test Instrumentation and Power Supply Block Diagram for Superconducting Field Winding**



superconducting field winding, and to prevent possible damage to the winding from Joule heating.

### Procedure

The superconducting field winding was installed in the helium dewar and precooled by liquid nitrogen to 77°K. Liquid helium was transferred after the liquid nitrogen was purged from the dewar with gaseous helium. Tests were conducted whereby the current was increased until the superconducting field winding quenched, at which point the current was reduced and the excitation circuit was disconnected. These tests determined the critical current value. Also, tests whereby the current was increased to a value just short of the critical current and maintained at this value for periods of five minutes each, determined stability of the field winding.

### Results

The critical current tests showed that the superconducting field winding is capable of carrying 110 amperes at 4.0°K before quenching. This high value of critical current indicates a very good winding for the superconductor used. The stability tests were conducted at a maintained value of 90 amperes for various time periods of five minutes with no signs of instability or quenching.

Observation of the superconducting field winding after the tests showed that it withstood the many thermal cyclings without any visible physical changes. Also, during the critical current test, observations showed that the normal lead to superconducting lead joints were first to generate heat ( $i^2R$ ) and bubble off the liquid helium prior to the field winding quenching. This showed that the joints were a limiting factor and pointed out that a carefully prepared joint with a maximum joint contact area is necessary.

### Test No. 2

This test was conducted to determine the resistance values of the joints used in the generator. These joints were fabricated by indium soldering the superconductor leads to the copper pieces which also served as heat sinks for the normal leads. The test apparatus used was similar to that used in Test No. 1 with the exception of the joints. After cooling down to 4.2°K, the joint resistances were measured by passing a current of 50 amps direct current through the joints and measuring the voltage drop across them. Both joints were very good with resistance values of less than one-third of a micro-ohm. The positive joint had a slightly higher resistance than the negative ground return joint. At the field operating current value, these joints would be 0.30 micro-ohms for the positive joint and 0.22 micro-ohms for the negative joint. The total expected heat dissipation from both joints at the operating current level would be 0.64 milli-watts which is negligible.

### Test No. 3

The third test was performed after the field winding was inserted and encapsulated in the shaft. The field winding, lead joints, support rings, and copper heat sinks were aligned and potted together to form an integral unit before insertion into the shaft. The insertion process required the use of an arbor press so this test was performed to insure the superconducting integrity and performance characteristics of the

## Appendix II

### ARMATURE WAVEFORM TESTS

#### Test Apparatus

The test apparatus with all its components is shown in Figure 52 in an exploded view. In the background the iron flux return path is shown mounted on its stand with the carbon brushes and electric drive motor in place. The foreground shows the copper field magnet and shaft assembly with bearings and slip rings adjacent to it. The brush and slip ring assembly is shown in greater detail in Figure 53. The brushes are mounted in two cylindrical holders and are in contact with the two slip rings mounted on the shaft end coupling.

The instrumentation and power supply schematic diagram is shown in Figure 54. The waveshape was displayed on the cathode ray tube of the Tektronix 502 oscilloscope and recorded photographically. The oscilloscope calibration was checked to assure correct magnitudes of the waveshapes recorded. The power supply used to energize the copper field magnet was a KEPCO regulated dc power supply with very low ripple content to keep the flux generated as free from noise as possible. Additional voltage regulation was obtained by use of a SOLA voltage regulator between the KEPCO dc power supply and the line because the available supply line was subject to large voltage variations. The current to the copper field magnet was monitored by a Simpson 260 ammeter. The speed of the rotor was controlled by a variable voltage dc power supply feeding the dc drive motor and monitored with a Tachlite 830 tachometer. All signal leads were shielded to prevent spurious noise pickup.

#### Tests and Results

##### Copper Field Magnet Field Strength

Tests were conducted on the copper field magnet. A sensor of one turn of copper wire was used to measure the magnitude and map the distribution of the field strength. The field strength as a function of excitation current is shown plotted in Figure 55. As expected, the field strength is a linear function of the excitation current with a slope of 600 gauss per ampere. Since the copper field coil has a resistance of 66 ohms, it was decided not to drive the excitation current beyond 0.5 ampere, otherwise Joule ( $I^2R$ ) heating would damage the coil. The output waveshape of the sensor loop, shown in Figure 56 is not sinusoidal, but possesses a flattened peak. This flattened peak is caused by the use of an iron core with an iron return path. If the air gap would be shorter, then this waveshape would have a wider flat peak and steeper skirts on either side.

##### Distributing the Armature Winding

Since the flux waveshape is not a sinusoid, the output waveshape of one turn (or a bundle of turns) as shown in Figure 57 will not be sinusoidal but will contain the same third harmonic as the flux waveshape. Distributing the winding over a portion of the stator surface should decrease this harmonic content. Figure 58 shows 22 turns

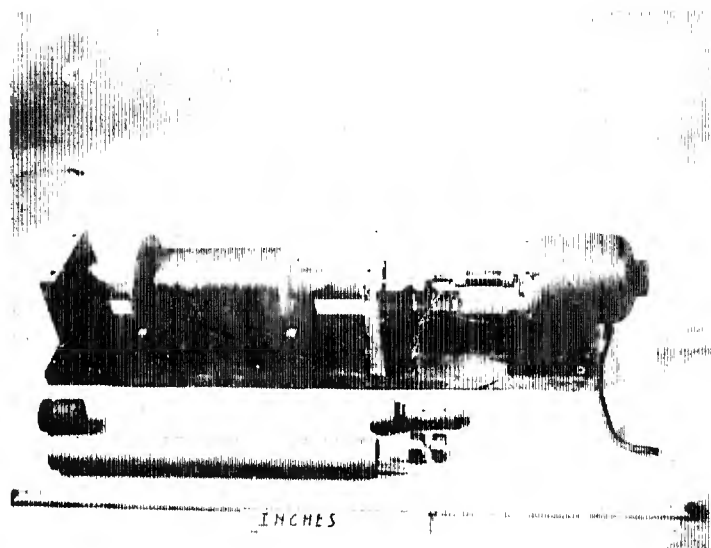


**Fig. 52** Armature Waveshape Test Apparatus. In the background the iron flux return path is shown mounted on its stand with the carbon brushes and drive motor in place. The foreground shows the copper field magnet and shaft assembly with bearings and slip rings adjacent.

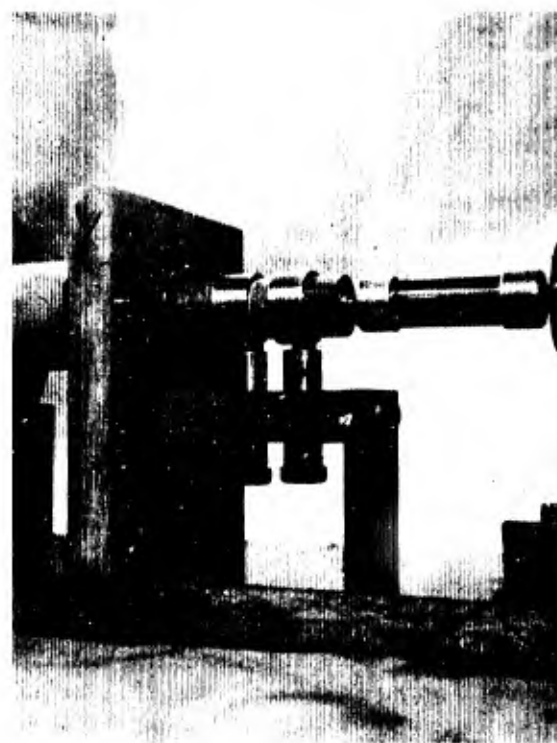


**Fig. 53** Brush and Slip Ring Assembly. The brushes are mounted in the two vertical cylindrical holders. The brushes are in contact with the two slip rings mounted on the shaft and coupling.

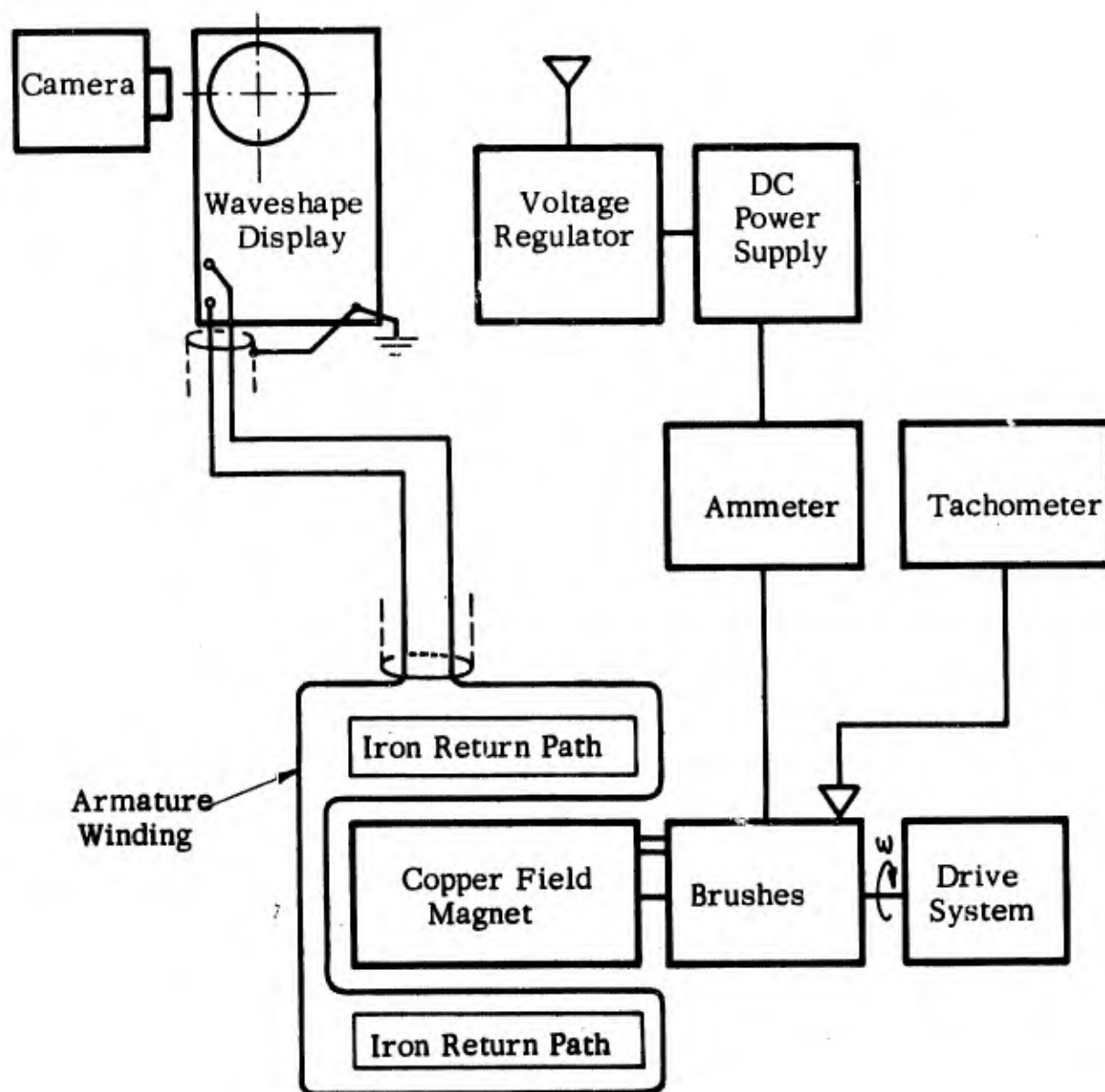


Fig. 54. Instrumentation and Power Supply Schematic Diagram of Armature Waveshape Test Apparatus

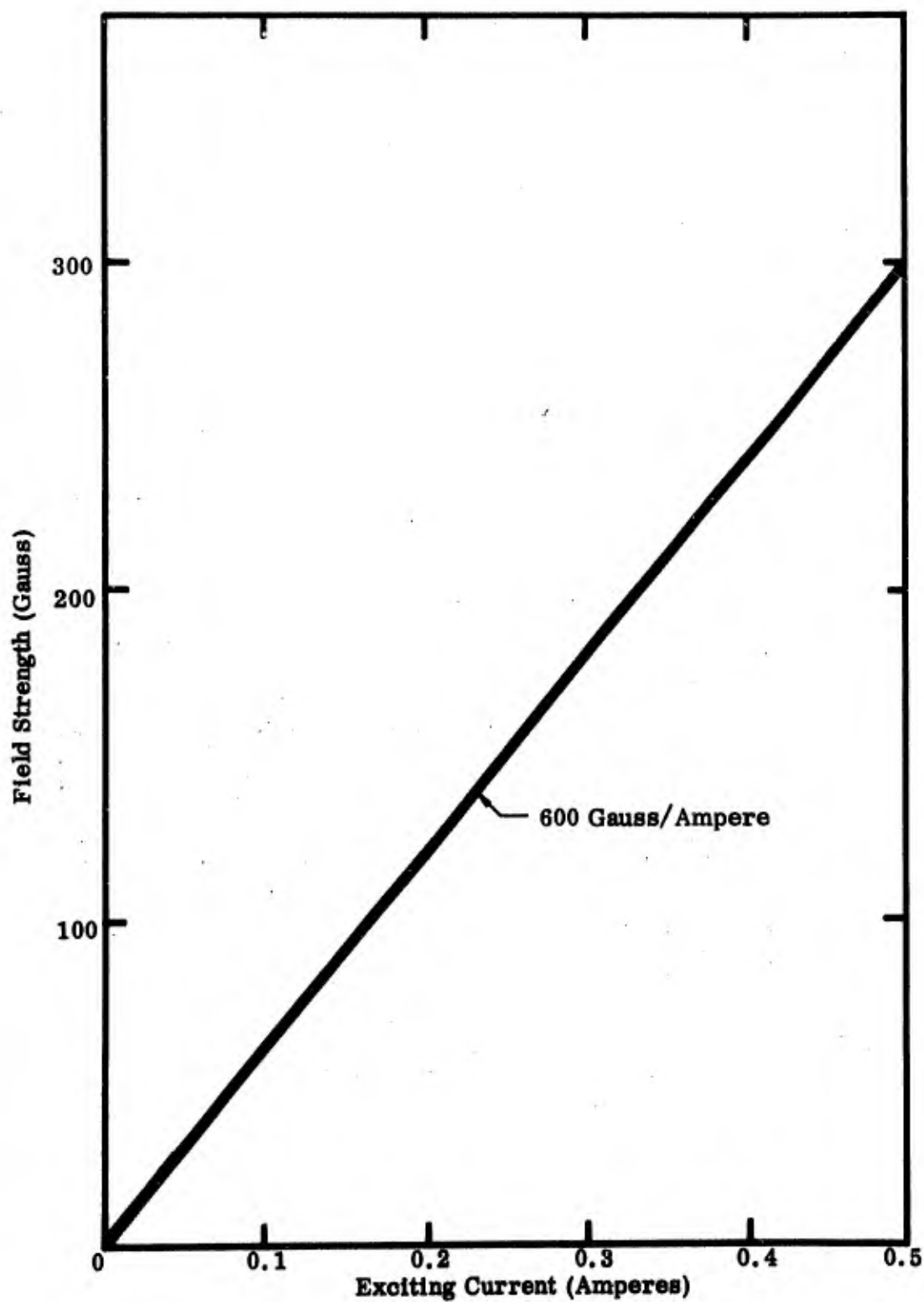
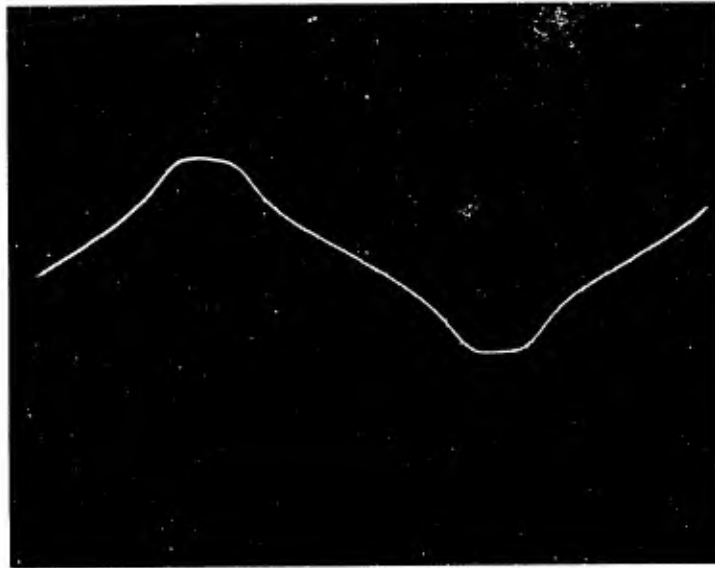


Fig. 55. Field Strength vs. Exciting Current  
of Copper Field Magnet



**Fig. 56** Field Intensity Waveshape of  
Copper Field Magnet

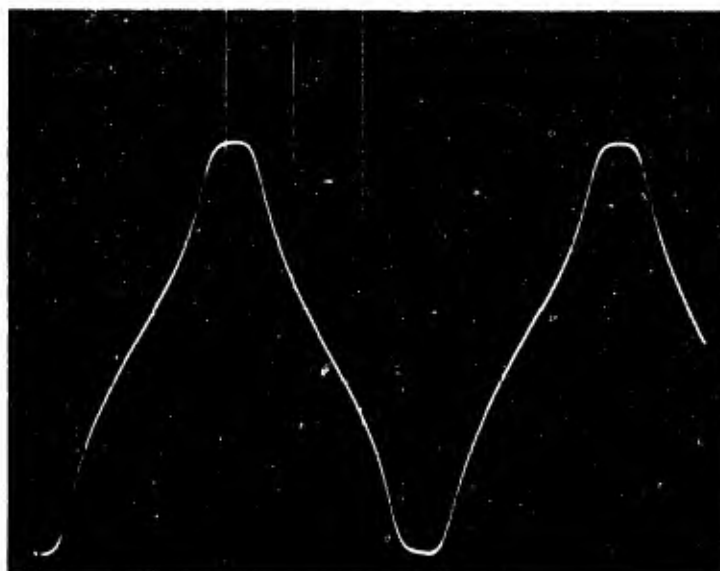


Fig. 57 One turn (or a bundle of turns) with no distribution armature waveshape.



Fig. 58 22 turns distributed over a  $60^\circ$  span armature waveshape.

distributed over a  $60^\circ$  span of the armature. The waveshape is beginning to approach a sinusoid with reduced harmonic content. By further distributing the winding to 44 turns distributed over a  $120^\circ$  span of the armature, the output waveshape is a sinusoid as shown in Figure 59. An enlargement of this waveshape has been compared to a calculated sinusoid with the result that the measured waveshape follows the calculated sine wave extremely closely. The  $120^\circ$  span is also the  $120^\circ$  displacement required between phases of the 3-phase machine in our design so that no design changes are necessary for this armature geometry.

#### Chording (Fractional Pitching) the Armature Winding

The waveshape could also be improved by chording the windings. Figure 60 shows two 22-turn windings distributed over a  $60^\circ$  span with no chording (full pitch or spaced  $180^\circ$  apart). This waveshape is not a sinusoid but is rich in third harmonics. Figure 61 shows the same windings but with a  $30^\circ$  chording ( $5/6$  pitch or spaced  $150^\circ$  apart). This waveshape approaches a sinusoid with almost straight skirts but is slightly peaked thus the harmonic is somewhat reduced by  $30^\circ$  chording. Figure 62 shows the same winding but with  $60^\circ$  chording ( $2/3$  pitch or  $120^\circ$  apart). The third harmonic component has been canceled out and the waveshape is a sinusoid showing all other harmonics are negligible. Chording improves the waveshape immensely if one harmonic predominates since it can be made to cancel out as in this case of the third harmonic. If other harmonics are equally important, then only a compromise can be made on the degree of cancellation of the various harmonics because only one chord angle can be used at one time. This geometry which produced the sinusoid requires that two conductors per slot must be used in winding a three-phase machine and the three phases are intermingled with two different phases in each slot in many of the cases. Thus insulation problems arise as well as fabrication difficulties of winding a double armature (two per slot).

On the basis of isolating the phases electrically and fabrication ease while maintaining a configuration which produces a sinusoidal output waveshape, the 44 turn distributed winding over a  $120^\circ$  span will be used in the laboratory model generator armature as originally designed.



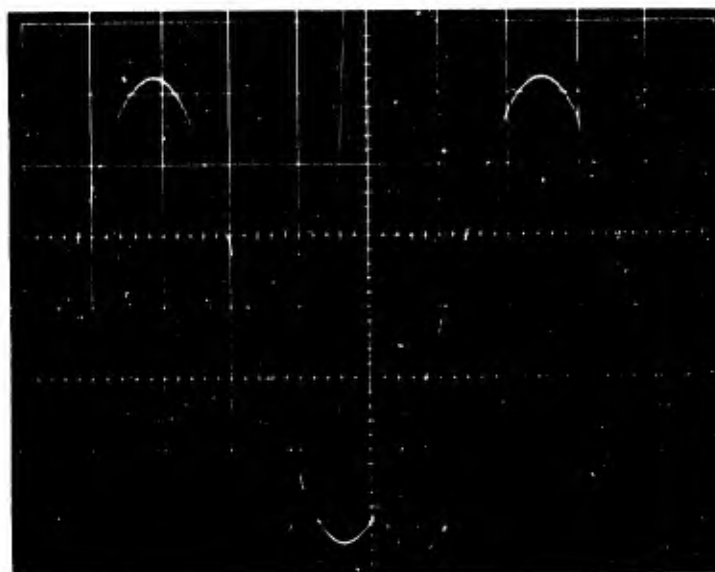


Fig. 59 44 turns distributed over a  $120^\circ$  span armature waveshape. This is our original design armature geometry.

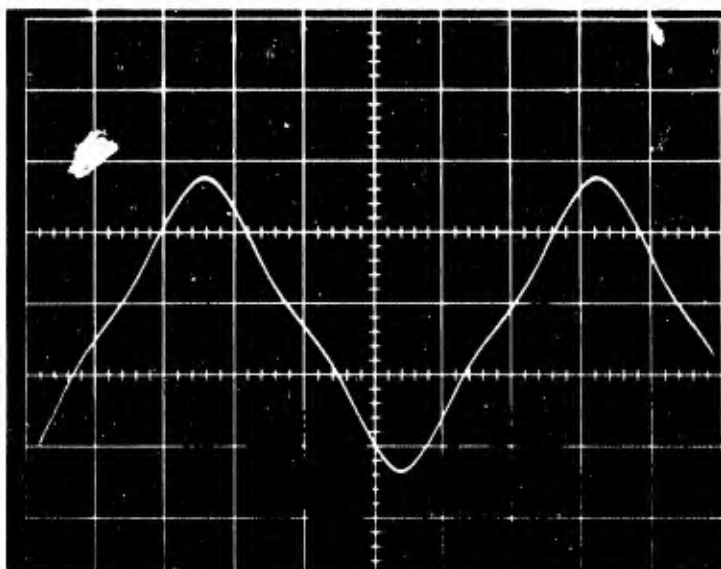


Fig. 60 Two 22-turn winding distributed over a  $60^\circ$  span with no chording (full pitch or spaced  $180^\circ$  apart).

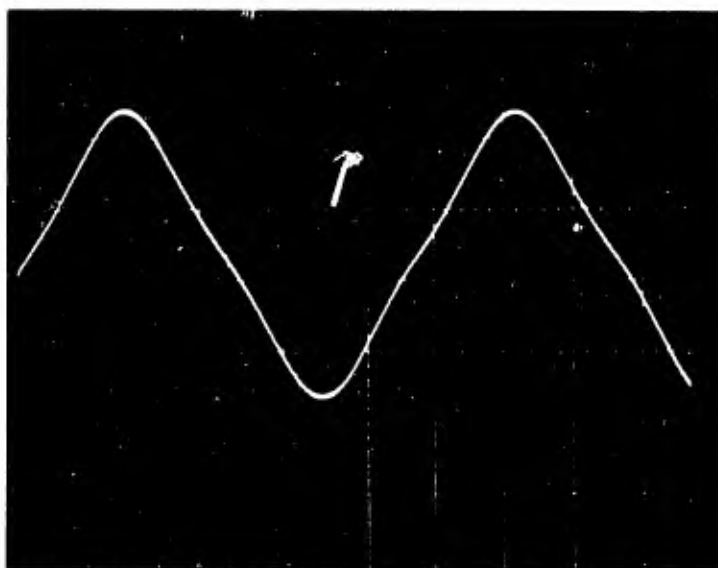


Fig. 61 Two 22-turn winding distributed over a  $60^\circ$  span with  $30^\circ$  chording ( $5/6$  pitch or spaced  $150^\circ$  apart).

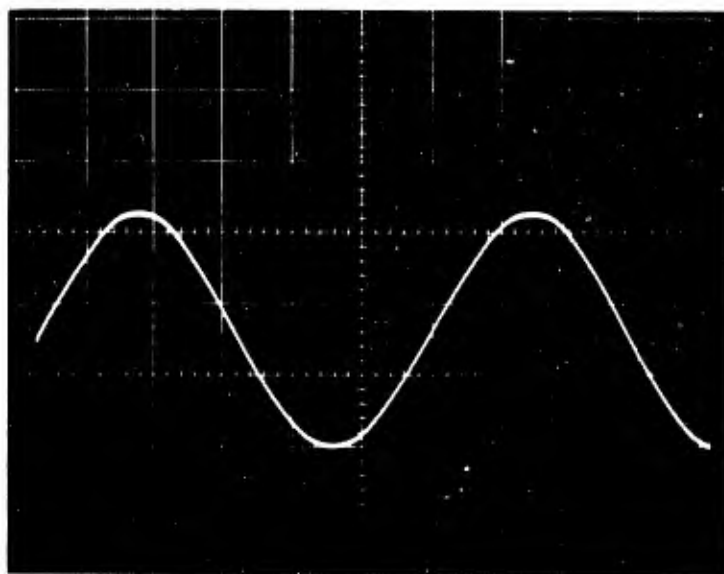


Fig. 62 Two 22-turn winding distributed over a  $60^\circ$  span with  $60^\circ$  chording ( $2/3$  pitch or spaced  $120^\circ$  apart).

## LIST OF REFERENCES

1. Mela, R. L., et al, "Feasibility Study of Application of Superconductor Techniques for Rotating Electrical Generators," APL-TDR-64-71, May, 1964.
2. Mooncai, H. W., et al, "Investigation of Electromagnetic and Thermal Effects in Superconducting Generators," AFAPL TR-65-37, May, 1965.
3. Kim, Y. B., "Superconducting Magnets and Hard Superconductivity," Physics Today, September, 1964.
4. Schrader, E. R. and Kolondra, F., "Analysis of Degradation Effects in Superconductivity Niobium Stannide Solenoids," RCA Review, September, 1964.
5. Fitzgerald, A. E. and Kingsley, C., Jr., "Electric Machinery," McGraw-Hill Book Company, New York, 1952.
6. Tachibana, F. and Fukui, S., "Heat Transfer in an Annulus with an Inner Rotating Cylinder," Bull. of JSME, Vol. 3, No. 9, 1960.
7. Rohsenow, W. M. and Choi, H. Y., Heat, Mass and Momentum Transfer, Prentice-Hall, 1961.
8. Ede, A. J., "The Effect of a Right-Angled Bend on Heat Transfer in a Pipe," International Developments in Heat Transfer, Paper No. 75, 1961 International Heat Transfer Conference, Boulder, Colorado.
9. Kaye, J. and Elgar, E. C., "Modes of Adiabatic and Diabatic Fluid Flow in an Annulus with an Inner Rotating Cylinder," Trans. ASME, Vol. 80, 1958.
10. Astill, K. N., "Studies of the Developing Flow between Concentric Cylinders with Inner Cylinder Rotating," ASME, Journal of Heat Transfer, Vol. 86, August, 1964.
11. Becker, K. M. and Kaye, J., "Measurements of Diabatic Flow in an Annulus with an Inner Rotating Cylinder," Journal of Heat Transfer, Trans. ASME, May, 1962.
12. Bjorklund, I. S. and Kays, W. M., "The Heat Transfer Between Concentric Rotating Cylinders," Journal of Heat Transfer, Trans. ASME, Vol. 81, 1959.
13. Schneider, P. J., Conduction Heat Transfer, Addison-Wesley, Reading, Massachusetts, Second Edition, 1957.
14. Den Hartog, J. P., Mechanical Vibrations, "Method of Stodola," McGraw-Hill, Third Edition, pp. 195 - 196, 1947.

Unclassified  
Security Classification

DOCUMENT CONTROL DATA - R&D		
(Security classification of title, body of abstract and indexing annotation must be entered when the overall report is classified)		
1. ORIGINATING ACTIVITY (Corporate author) Dynatech Corporation 17 Tudor Street Cambridge, Massachusetts 02139		2a. REPORT SECURITY CLASSIFICATION Unclassified
		2b. GROUP NA
3. REPORT TITLE Development of a 50 KVA Laboratory Prototype Superconducting AC Generator		
4. DESCRIPTIVE NOTES (Type of report and inclusive dates) Final Report (15 Mar 65 - 31 Oct 66)		
5. AUTHOR(S) (Last name, first name, initial) Henry W. Mooncai, Hugh A. Robinson, Charles J. Oberbauer, John M. Reynolds		
6. REPORT DATE 28 Feb 67	7a. TOTAL NO. OF PAGES 114 p.	7b. NO. OF REFS 14
8a. ORIGINATOR'S REPORT NUMBER(S) Dynatech Report No. 692	8b. OTHER REPORT NO(S) (Any other numbers that may be assigned this report) TR-67-20	
10. AVAILABILITY/LIMITATION NOTICES "Qualified Requesters may obtain copies of this report from DDC" "Foreign announcement and dissemination of this report by DDC is not authorized."		
11. SUPPLEMENTARY NOTES		12. SPONSORING MILITARY ACTIVITY Air Force Aero Propulsion Laboratory Research and Technology Division A. F. Systems Command, Wright-Patterson, Ohio
13. ABSTRACT The objective of this exploratory development program was the completion of the superconducting generator investigations initiated under previous contracts,* and culminating with the fabrication and evaluation of a 50 kva laboratory model to verify the generator performance potential predicted by such investigations. The design and fabrication effort of the laboratory model superconducting generator was divided into three major areas. First, an electrical phase provided for the field and armature components from an electrical viewpoint. Second, a heat transfer phase provided for the removal of heat generated by the loss mechanisms of the generator. Third, a mechanical phase provided and maintained the environment package required by superconductors. The completed generator was tested to demonstrate a capability of power generation. A one megawatt generator design is presented based on the experience gained on the design and test of the 50 kva generator.  *Contract AF 33(547)-11062 Contract AF 33(615)-1574		

Unclassified

Security Classification

14	KEY WORDS	LINK A		LINK B		LINK C	
		ROLE	WT	ROLE	WT	ROLE	WT
Superconducting AC Generator Superconductivity AC Generator							

## INSTRUCTIONS

1. **ORIGINATING ACTIVITY:** Enter the name and address of the contractor, subcontractor, grantee, Department of Defense activity or other organization (*corporate author*) issuing the report.

2a. **REPORT SECURITY CLASSIFICATION:** Enter the overall security classification of the report. Indicate whether "Restricted Data" is included. Marking is to be in accordance with appropriate security regulations.

2b. **GROUP:** Automatic downgrading is specified in DoD Directive 5200.10 and Armed Forces Industrial Manual. Enter the group number. Also, when applicable, show that optional markings have been used for Group 3 and Group 4 as authorized.

3. **REPORT TITLE:** Enter the complete report title in all capital letters. Titles in all cases should be unclassified. If a meaningful title cannot be selected without classification, show title classification in all capitals in parenthesis immediately following the title.

4. **DESCRIPTIVE NOTES:** If appropriate, enter the type of report, e.g., interim, progress, summary, annual, or final. Give the inclusive dates when a specific reporting period is covered.

5. **AUTHOR(S):** Enter the name(s) of author(s) as shown on or in the report. Enter last name, first name, middle initial. If military, show rank and branch of service. The name of the principal author is an absolute minimum requirement.

6. **REPORT DATE:** Enter the date of the report as day, month, year, or month, year. If more than one date appears on the report, use date of publication.

7a. **TOTAL NUMBER OF PAGES:** The total page count should follow normal pagination procedures, i.e., enter the number of pages containing information.

7b. **NUMBER OF REFERENCES:** Enter the total number of references cited in the report.

8a. **CONTRACT OR GRANT NUMBER:** If appropriate, enter the applicable number of the contract or grant under which the report was written.

8b, 8c, & 8d. **PROJECT NUMBER:** Enter the appropriate military department identification, such as project number, subproject number, system numbers, task number, etc.

9a. **ORIGINATOR'S REPORT NUMBER(S):** Enter the official report number by which the document will be identified and controlled by the originating activity. This number must be unique to this report.

9b. **OTHER REPORT NUMBER(S):** If the report has been assigned any other report numbers (either by the originator or by the sponsor), also enter this number(s).

10. **AVAILABILITY/LIMITATION NOTICES:** Enter any limitations on further dissemination of the report, other than those

imposed by security classification, using standard statements such as:

- (1) "Qualified requesters may obtain copies of this report from DDC."
- (2) "Foreign announcement and dissemination of this report by DDC is not authorized."
- (3) "U. S. Government agencies may obtain copies of this report directly from DDC. Other qualified DDC users shall request through \_\_\_\_\_."
- (4) "U. S. military agencies may obtain copies of this report directly from DDC. Other qualified users shall request through \_\_\_\_\_."
- (5) "All distribution of this report is controlled. Qualified DDC users shall request through \_\_\_\_\_."

If the report has been furnished to the Office of Technical Services, Department of Commerce, for sale to the public, indicate this fact and enter the price, if known.

11. **SUPPLEMENTARY NOTES:** Use for additional explanatory notes.

12. **SPONSORING MILITARY ACTIVITY:** Enter the name of the departmental project office or laboratory sponsoring (paying for) the research and development. Include address.

13. **ABSTRACT:** Enter an abstract giving a brief and factual summary of the document indicative of the report, even though it may also appear elsewhere in the body of the technical report. If additional space is required, a continuation sheet shall be attached.

It is highly desirable that the abstract of classified reports be unclassified. Each paragraph of the abstract shall end with an indication of the military security classification of the information in the paragraph, represented as (TS), (S), (C), or (U).

There is no limitation on the length of the abstract. However, the suggested length is from 150 to 225 words.

14. **KEY WORDS:** Key words are technically meaningful terms or short phrases that characterize a report and may be used as index entries for cataloging the report. Key words must be selected so that no security classification is required. Identifiers, such as equipment model designation, trade name, military project code name, geographic location, may be used as key words but will be followed by an indication of technical context. The assignment of links, rules, and weights is optional.

Unclassified

Security Classification